Co(Salen)-Catalyzed Aerobic Oxidation of Lignin Models: Investigating the Role of Ligands Through Data Science

Mateus O. Costa[a,‡], Ariel A. Pereira[a,‡] Edson L. S. Souza,[a] Antonio C. B. Burtoloso,[b] and Marco A. B. Ferreira[a,]*

[a]Department of Chemistry, Federal University of São Carlos, 13565-905, São Carlos, SP, Brazil.

[b]Departament of Physical Chemistry, Institute of Chemistry of Sao Carlos, University of Sao Paulo, Sao Carlos, SP, Brazil

[‡]Contributed Equally

Supporting Information

Table of Contents

S1. Data Set Curation for Previously Synthesized Salen Ligands

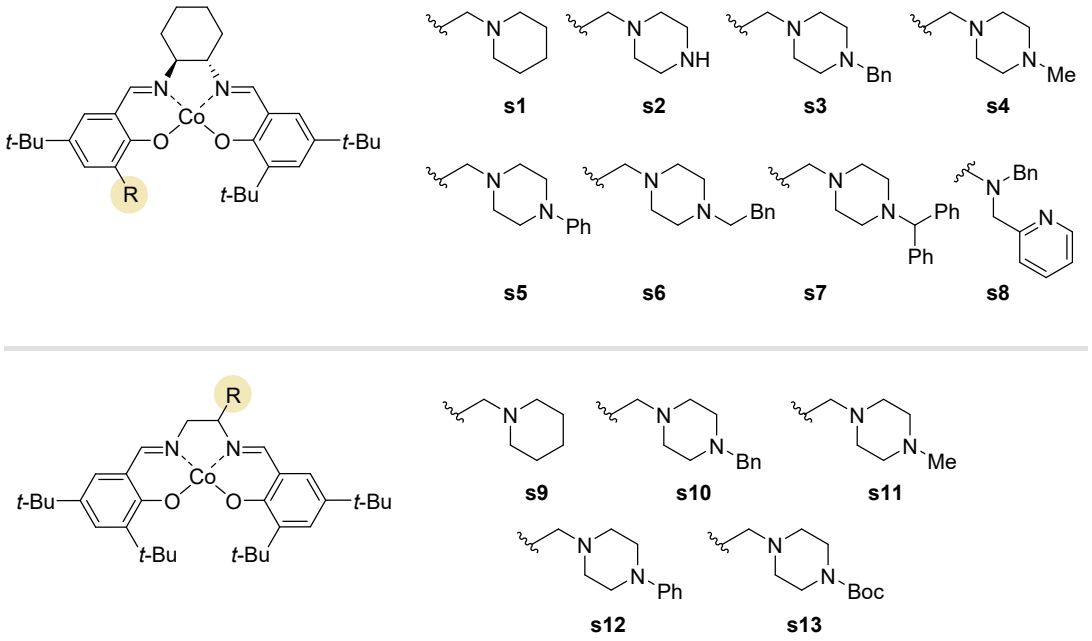

Figure S1. Previously Synthesized Salen Ligands.

Table S1. Data set curation for initial parameterization studies.

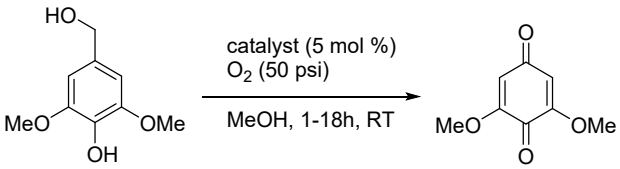

Entry	Catalyst	Time (h)	Yield (%)	Reference
1	**s1**	16	75	1
2	**s2**	5	61	1
3	**s3**	18	71	2
4	**s3**	1	75	2
5	**s3**	1	74	1
6	**s4**	16	54	1
7	**s5**	2	65	1
8	**s6**	18	80	2
9	**s6**	1	73	2

10	**s7**	18	70	2
11	**s7**	1	81	2
12	**s8**	16	46	1
13	**s9**	16	42	3
14	**s10**	16	71	3
15	**s11**	16	41	3
16	**s12**	16	51	3
17	**s13**	16	45	3

S2. Computational Details

The conformational searches were done in gas phase using the Monte Carlo (MCMM) method as implemented as implemented in MacroModel (Version 9.9).[4] The energy minimization was carried out using the Polak-Ribiere Conjugate Gradient (PRCG), and the OPLS_2005 force field, using dielectric constant-dependent electrostatics (e=1) and normal cut-off points to model the non-bonded interactions. All heavy atoms and hydrogens at heteroatoms were included in the test for redundant conformers, using the default cutoff (maximum atom deviation) of 0.5 Å. All rotatable single bonds were included in the conformational search. The energy window for saving new structures was 5 kcal mol-1 relative to the current global minimum, using a maximum number of steps of 30000 and 1000 steps per rotable bond. Each search was continued until the global energy minima were found at least 10-20 times, thus giving confidence that all the relevant conformers had been found. The resulting conformers were clustered based on structural similarity, and representative structures from each group were selected for further geometry optimization and parameter extraction via quantum mechanical calculations. All subsequent geometry optimizations and electronic property extractions were carried out using Gaussian16 (version B.01) [5] and NBO6.0. [6] Density Functional Theory (DFT) calculations were performed at the M06/def2-SVP level of theory including the ECP basis set def2-SVP for Cobalt. [7] For the studies involving intramolecular coordination (Scheme 3 in the main text), the energies were refined at the M06/def2-TZVP level of theory. Frequency calculations at 295.15 K (1 atm) ensured that the stationary points represent either minima (no imaginary frequency) on the potential-energy surface, furnishing also the zero-point vibrational energies, the thermal and entropic

correction from which the Gibbs free energies were determined. All geometries of this study were available in Salen_Regression.xyz file.

S2.1. Molecular parameters extraction

The descriptors employed in this study are summarized in Table S2, and were grouped as follows: electronic (including natural charges, NBO orbital energies, spin density, HOMO and LUMO energies, and dipole moment); steric (Sterimol parameters, buried volume, selected bond distances and angles). These parameters were selected to capture both the electronic effects introduced by substituents on the aromatic rings, transmitted through the Co–O and Co–N bonds, and the steric influence associated with the substitution pattern near the cobalt center, particularly around the diamine bridge and aromatic moieties. The atomic regions used for the calculation of the descriptors listed above, along with their corresponding color codes are shown in Table 2S. Considering the relevance of conformational sampling to the reactivity trends investigated herein,[8] descriptors were computed for representative conformers. Each parameter was extracted and classified into four categories of conformer: Boltzmann-weighted average across conformers of a given catalyst (BOLTZ); maximum (MAX) and minimum (MIN) value of parameter among conformers; and the value corresponding to the lowest-energy conformer (LEC). Descriptors are referred to using the appropriate distribution label, e.g., the cobalt spin density for the lowest-energy conformer is denoted as LEC_*Spin*_Co. The full set of extracted parameters is provided in the supplementary file Salen_Regression_Featurization.xlsx.

Table S2. Molecular descriptors and corresponding atomic regions used for their calculation.

Feature (abrev.)	Description
Electronic Energy (EE)	Total electronic energy of the optimized molecule in kcal/mol
Zero Point Energy (Zero_Point)	Zero-point vibrational energy, accounting for quantum mechanical motion of atoms at 0 K
Thermal Energy (Thermal)	Thermal corrected energy from vibrational, rotational, and translational motion at 298.15 K
Enthalpy	Thermal corrected enthalpy, from internal energy and pressure-volume work

Gibbs Free Energy (Gibbs)	Gibbs Free Energy potential at 298.15 K
HOMO	Energy of the **H**ighest **O**ccupied **M**olecular **O**rbital
LUMO	Energy of the **L**owest **U**noccupied **M**olecular **O**rbital
Dipole Moment (Dipole)	Magnitude of Molecular Dipole Moment
Electronegativity	Reactivity parameters derived from Koopman's approximation of FMO theory
Chemical Potential	
Hardness	
Softness	
Electrophilicity Index	
Nucleophilicity Index	
Mulliken Population Analisys (Mulliken)	Atomic charges, spin densities, and normalized spin fractions
Natural Population Analisys (NPA)	Atomic Charges and contributions from Core, Valence, Rydberg, and Total electron populations
Natural Bonding Orbitals (NBO)	Energies of bonding (BD), anti-bonding (BDu), lone pair (LP), and lone valence (LV) orbitals
Sterimol	Steric descriptors quantifying the axial length (L) and lateral widths (Bmax, Bmin) to account for steric effects of the hole ligand
Substituent Sterimol (SubSterimol)	Steric descriptors quantifying the axial length (L) and lateral widths (Bmax, Bmin) to account for steric effects of a specific substituent group
Burried Volume (BVol)	Percentage of a defined sphere (of radius r) around a central atom that is occupied by the ligand or substituent atoms
Distance	Distance between two atoms, reported in angstroms (Å)
Bond Angle	Angle between three atoms (A–B–C), reported in degrees (°)
Dihedral Angle	Torsional angle between two planes defined by four atoms (A–B–C–D), reported in degrees (°)

Table S3. Evaluation of the relevance of intramolecular coordination

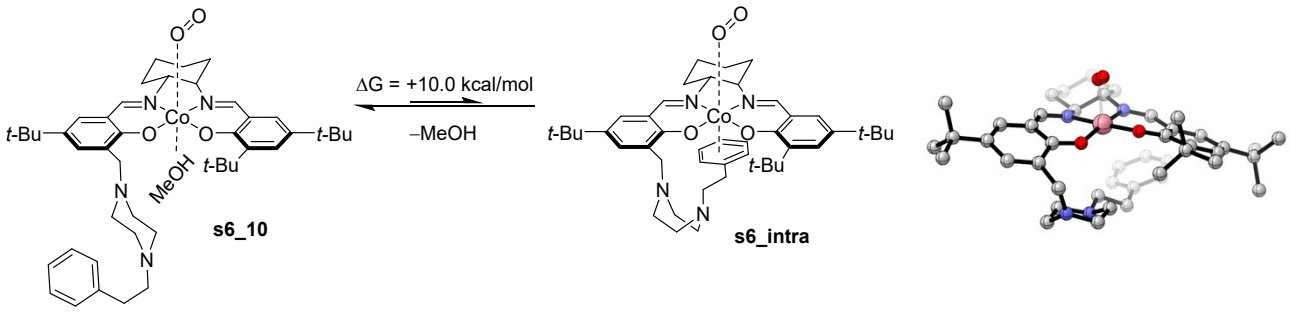

Conformer	Energy (Hartrees)	ZP energy (Hartrees)	Gibbs Free-energy (Hartrees)
MeOH	-115.560952	0.051046	-115.532619
s6_10	-3766.877461	1.047156	-3765.926510
s6_intra	-3651.287237	0.994661	-3650.377532

Table S4. Gibbs Free Energy of conformers related to complexes s1-s13

Conformer	Energy (Hartrees)	ZP energy (Hartrees)	Gibbs Free-energy (Hartrees)
s01_1	-3441.659283	0.921805	-3440.821632
s01_2	-3441.6599	0.921913	-3440.821837
s01_3	-3441.658952	0.922325	-3440.819365
s01_4	-3441.657764	0.922142	-3440.818825
s01_6	-3441.658498	0.922266	-3440.818152
s01_7	-3441.660785	0.921889	-3440.822311
s01_8	-3441.660431	0.922928	-3440.819129
s02_1	-3457.672595	0.910712	-3456.847597
s02_2	-3457.653538	0.91137	-3456.821397
s02_3	-3457.671331	0.910983	-3456.843989

s02_4	-3457.671521	0.910612	-3456.84478
s02_5	-3457.674421	0.910936	-3456.847176
s02_6	-3457.655062	0.911387	-3456.823243
s02_7	-3457.674315	0.9108	-3456.846595
s02_8	-3457.645671	0.911886	-3456.814185
s03_1	-3727.624091	1.019763	-3726.692453
s03_2	-3727.624307	1.019048	-3726.698533
s03_3	-3727.626539	1.020829	-3726.69449
s03_4	-3727.62324	1.019173	-3726.696424
s03_5	-3727.624724	1.019993	-3726.695019
s03_6	-3727.626696	1.019106	-3726.698252
s03_7	-3727.626729	1.019599	-3726.697543
s03_8	-3727.630002	1.019689	-3726.700661
s03_9	-3727.626452	1.019412	-3726.698603
s04_1	-3496.920586	0.93831	-3496.066833
s04_2	-3496.922028	0.937858	-3496.069557
s04_3	-3496.926209	0.938399	-3496.071673
s04_4	-3496.920592	0.93845	-3496.066198
s04_5	-3496.92067	0.938159	-3496.066265
s04_6	-3496.924025	0.939242	-3496.067788
s04_7	-3496.924511	0.939466	-3496.067211
s05_1	-3688.382001	0.993146	-3687.475757
s05_2	-3688.381344	0.992769	-3687.475434
s05_3	-3688.376936	0.991156	-3687.476012
s05_4	-3688.381594	0.991687	-3687.475421
s05_5	-3688.379387	0.991843	-3687.476219
s06_1	-3766.875161	1.048423	-3765.918761
s06_10	-3766.877461	1.047156	-3765.92651
s06_11	-3766.879333	1.04831	-3765.922958
s06_12	-3766.880426	1.048706	-3765.923048
s06_2	-3766.875195	1.048755	-3765.91761
s06_3	-3766.877438	1.050786	-3765.91446
s06_4	-3766.876902	1.047941	-3765.9209

s06_5	-3766.875848	1.048237	-3765.919458
s06_6	-3766.877497	1.048462	-3765.920203
s06_7	-3766.882173	1.049822	-3765.920453
s06_8	-3766.883388	1.048933	-3765.92473
s06_9	-3766.878085	1.047571	-3765.923037
s07_1	-3958.332435	1.101973	-3957.323324
s07_2	-3958.330496	1.100876	-3957.325284
s07_3	-3958.331501	1.100399	-3957.326982
s07_4	-3958.332821	1.102589	-3957.322522
s07_5	-3958.331538	1.100871	-3957.325415
s07_6	-3958.32737	1.100617	-3957.321313
s07_7	-3958.329872	1.099441	-3957.327266
s07_8	-3958.331971	1.099847	-3957.327131
s07_9	-3958.334546	1.101006	-3957.328578
s08_3	-3802.530513	1.008176	-3801.61326
s08_4	-3802.530597	1.007342	-3801.615559
s08_6	-3802.530088	1.007377	-3801.615436
s08_7	-3802.530767	1.007437	-3801.614192
s08_8	-3802.531794	1.00729	-3801.6185
s09_1	-3442.844375	0.940167	-3441.990366
s09_2	-3442.845666	0.940231	-3441.990862
s09_3	-3442.843086	0.940674	-3441.987057
s10_1	-3728.813325	1.037429	-3727.871286
s10_10	-3728.808702	1.037801	-3727.864788
s10_11	-3728.809511	1.038284	-3727.863059
s10_12	-3728.810417	1.037759	-3727.864907
s10_2	-3728.812098	1.037777	-3727.86883
s10_3	-3728.812021	1.037303	-3727.86995
s10_4	-3728.812836	1.037738	-3727.866945
s10_5	-3728.811981	1.037585	-3727.86873
s10_6	-3728.814174	1.037676	-3727.870559
s10_7	-3728.808859	1.037654	-3727.865632
s10_8	-3728.808032	1.037584	-3727.865912

s10_9	-3728.807608	1.037374	-3727.865572
s11_1	-3498.107864	0.955928	-3497.239822
s11_2	-3498.108551	0.956714	-3497.238156
s11_3	-3498.102945	0.956276	-3497.234221
s11_4	-3498.101766	0.95718	-3497.231045
s11_5	-3498.101757	0.956134	-3497.234295
s11_6	-3498.104523	0.956545	-3497.234374
s12_1	-3689.562038	1.009791	-3688.644801
s12_10	-3689.558644	1.009335	-3688.642621
s12_2	-3689.564306	1.009744	-3688.645985
s12_3	-3689.563277	1.009437	-3688.646486
s12_4	-3689.56078	1.009659	-3688.641825
s12_5	-3689.563186	1.010214	-3688.644649
s12_6	-3689.561595	1.009411	-3688.643175
s12_7	-3689.560751	1.009467	-3688.645006
s12_8	-3689.562026	1.009452	-3688.645568
s12_9	-3689.557548	1.008963	-3688.641724
s13_1	-3804.234655	1.055123	-3803.276153
s13_10	-3804.237844	1.057184	-3803.271066
s13_11	-3804.235388	1.057042	-3803.270008
s13_2	-3804.214723	1.056196	-3803.246901
s13_3	-3804.234443	1.055187	-3803.274857
s13_4	-3804.232894	1.05542	-3803.273846
s13_5	-3804.235766	1.056459	-3803.27001
s13_6	-3804.234478	1.055555	-3803.273544
s13_7	-3804.239542	1.055038	-3803.28106
s13_8	-3804.237603	1.055173	-3803.27895
s13_9	-3804.239701	1.056333	-3803.275066

S3. UMAP Plot of Salicylaldehyde Chemical Space and Clustering

S3.1. Computational Methods

S3.1.1 DFT Featurization of Salicylaldehyde Chemical Space:

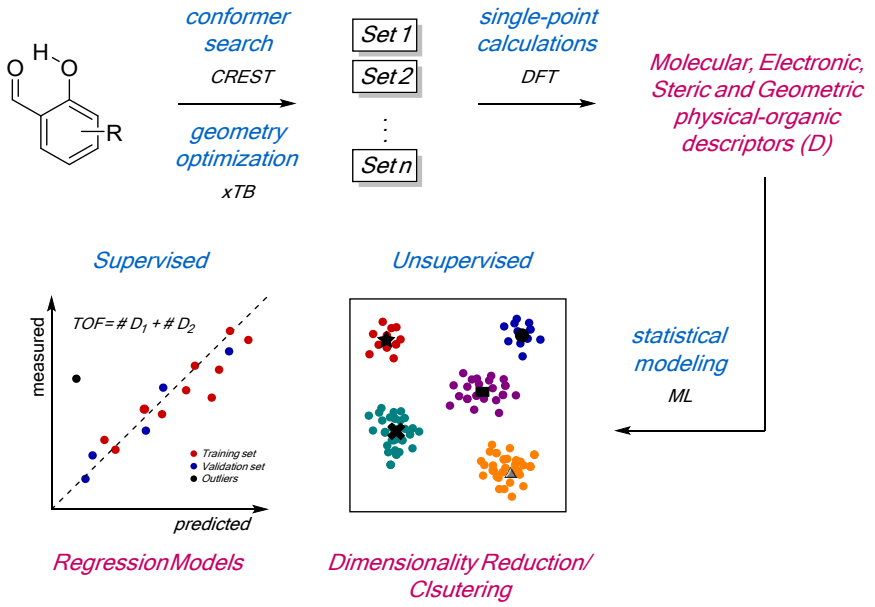

Figure S2. General workflow for salicylaldehyde molecular featurization.

Conformational Search:

Prior to the conformation search, following the best practices outlined in the program documentation, a geometry pre-optimization was conducted using the semi-empirical xTB GFN-FF method (--opt --gff --input dihedral_restriction -v). The dihedral angles associated with the carbonyl and phenol groups were constrained to force an intramolecular hydrogen bond, simulating the metal center behavior (see restrictions below). After the pre-optimization, the conformational space of all salicylaldehydes was explored using the CREST (Conformer-Rotamer Ensemble Sampling Tool) program, within a 12 kcal/mol energy window (--gff --quick -T 12 --cinp dihedral_restriction --ewin 12).

$constrain

dihedral:1,3,5,10,0

dihedral:4,11,10,5,0

force constant=1.0

$end

Geometry Optimization:

Following the conformational search, all conformers were grouped and optimized using the Screen function with the semi-empirical xTB GFN2-FF method, applying a reduced energy window of 6 kcal/mol (--screen --gfn 2 -T 8 --ewin 6). Subsequently, the Cluster function was used to group the conformers based on energy and structural similarity, allowing for the removal of redundant structures (--cregen "${job_input/ref/confs_confs}" --notopo --cluster -T 2 --ewin 6).

Electronic Single Point Calculations:

The optimized structures underwent DFT calculations in Gaussian16[2] at the M06-2X/def2-SVP[4] level of theory and population analysis using NBO6,[3] which is well-suited for analyzing delocalized and aromatic systems, such as the catalysts in this study (#p m062x def2svp nosymm int=ultrafine pop=(savenbos,nbo6)).

S3.2. Construction of Salicylaldehyde Chemical Space

The complete code and associated Jupyter notebooks supporting the results of this study are publicly available at the GitHub repository: https://github.com/ArielAraujo00/CoSalen-repo

Substructure Search:

The search for the structures was conducted on the SciFinder-n (CAS Chemical Abstracts Service) platform on March 23, 2023. On the *Substance* tab, the salicylaldehyde structure were draw as show bellow (Figure S3), using both the *Lock Atoms* tool to block undesired substitutions on the oxygens and the aldehyde carbon, and the *Lock Ring Fusion or Formation* tool to block the aromatic ring.

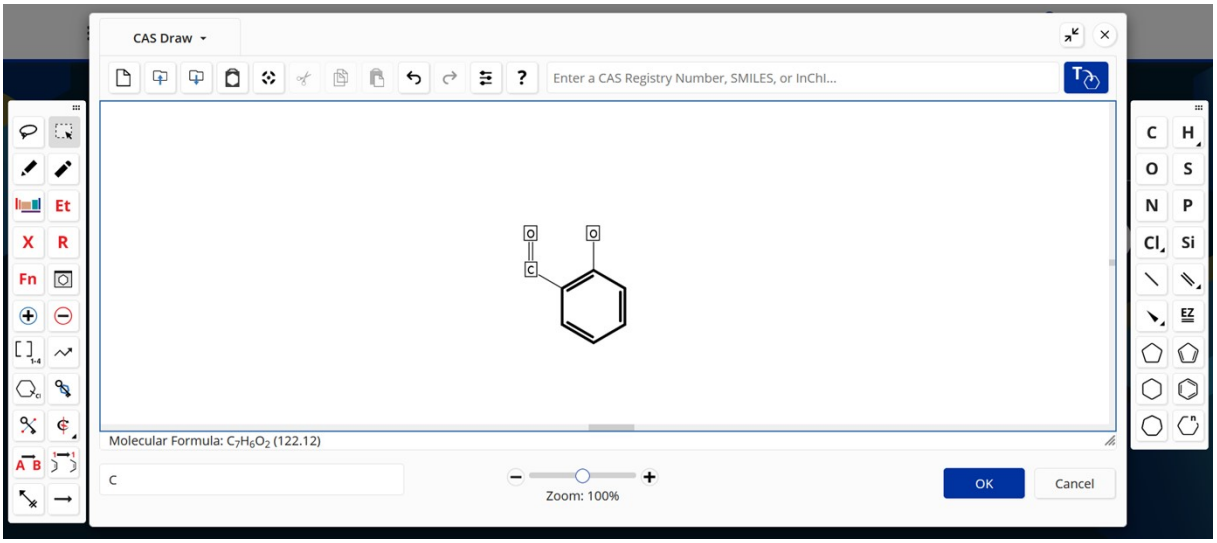

Figure S3. CAS SciFinder-n Draw tool screenshot highlighting the salicylaldehyde blocked positions.

The search was done using the *Substructure Match* option affording ~43,000 structures, from which the following filters were applied (using the *Exclude* option on *Filter Behavior*):

- Molecular Weight: 600 to No Max
- Commercial Availability: Not Available
- Metals: Containing Metals
- Isotopes: Containing Isotopes
- Element: B, P, S, Se, I
- Number of Components: 2, 3, 4, 5 or more
- Substance Class: Incompletely Defined Substance
- Reference Role: Natural Product Occurrence

After filtering the unwanted structures, the search afforded ~30,000 structures, but through some visual inspection we notice a great number of results containing the alkyne functional group (> 20,000), which could be too reactive to our system. To address this, we applied a final filter using the “Search Within Results” option (set to Exclude mode) to remove these entries from the dataset. The remaining 7,775 structures were exported as .sdf files. All export files, along with a list of smiles with the *in house* salicylaldehydes of our lab (manually added to the data set) is attached as a separate file (*Salicylaldehyde_dataset.rar*).

Recursive SMARTS Search:

To further refine the dataset to include only molecules compatible with our catalytic system, we implemented the RDKit python library for cheminformatics (*ChemSpaceSelection.ipynb*) to exclude all molecules containing the following functional groups:

- OH and NH donors
- Oxygen radicals and Phenolate anion
- C-C double bonds
- Aldehydes and Imine derivatives
- Ketal, Hemiaminal and Aminal derivatives
- Carbonate, Carbamate, Urea and Guanidine derivatives
- Aliphatic chains with 6 carbons or more
- Epoxides and Aziridines
- Hexoses
- Alkyl and Acyl Halides
- α-Haloketones and 1,3-diketo derivatives
- Diazo derivatives
- Anhydrides
- Nitrate and Nitroso derivatives
- Quinones

All SMARTS fragments are available in the smiles_filters.py file for verification. Each filter was printed and individually verified to ensure proper functionality. The final set of 2,815 filtered molecules was then converted to 3D structures and pre-optimized using RDKit's built-in force field optimization function, AllChem.MMFFOptimizeMolecule(), before being saved as .xyz files. An additional step was taken to standardize the numbering of core atoms (Figure S4) in the coordinate files, streamlining the featurization process.

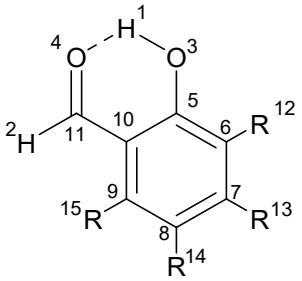

Figure S4. Salicylaldehyde reference core atoms.

Molecular Featurization:

As demonstrated by Doyle[9] and coworkers, the information contained in Molecular Fingerprints and Mordred descriptors, such as structural patterns, functional groups, connectivity graphs, and molecular topology, fails to isolate the electronic and steric properties necessary to capture reactivity trends in organic systems. Building on their work, we opted to proceed directly with DFT featurization (as detailed in the computational methods section).

Using an *in house* script (see *Featurization.ipynb*) a total of 257 numeric descriptors were gathered from the DFT calculations. The molecular, electronic and geometric properties were obtained directly from the single-point files, the steric parameters calculated using the *Morfeus*[10] module by Jorner *et al* (Table S4), and the reactivity parameters (see below) using the formulas derived from the Koopmans[11] theorem of FMO.

(1) $$\mu = \frac{(E_{Lumo} + E_{Homo})}{2}$$

(2) $$\chi = -\mu$$

(3) $$\eta = \frac{(E_{Lumo} - E_{Homo})}{2}$$

(4) $$S = \eta^{-1}$$

(5) $$\omega = \frac{\mu^2}{2\eta}$$

(6) $$N_{index} = \omega^{-1}$$

Dimensionality Reduction and Clustering:

To construct the salicylaldehyde chemical space from the assembled high-dimensional dataset, we selected a manifold learning algorithm capable of handling the inherent complex, non-linear relationships in chemical systems. We opted for UMAP (**U**niform

Manifold **A**pproximation and **P**rojection), a state-of-the-art, projection-based dimensionality reduction algorithm, which has been validated in similar studies by Sigman[12], Doyle[1], and others. For clustering, the HDBSCAN (Hierarchical Density-Based Spatial Clustering of Applications with Noise) algorithm was chosen due to its density-based nature, accommodating variance in cluster shape, and its hierarchical approach, which maximizes cluster dissimilarity. Although we initially explored PCA for dimensionality reduction, its performance across all subsequent steps was inferior to that of the UMAP algorithm, yielding a maximum silhouette score of only 0.41 for three clusters.

Prior to model training, we cleaned the dataset to remove irrelevant and redundant features, aiming to avoid multicollinearity and overfitting, as it can lead to unstable models, impaired interpretability, or obscure the true significance of variables. We first excluded columns with missing values (e.g., some delocalized aromatic NBO's) and zero-variance features, allowing the conformer distributions to be properly calculated according to the following naming convention: Boltzmann-weighted average across conformers (BOLTZ); maximum (MAX) and minimum (MIN) feature value among conformers; and the value corresponding to the **L**owest-**E**nergy **C**onformer (LEC).

Afterward, redundant data were addressed by eliminating linearly dependent columns through QR decomposition, and those with correlations above 95%. The data were then normalized using a standard scaler. Initial tests indicated that models trained exclusively with the BOLTZ distribution descriptors performed better, yielding more coherent clusters. Thus, we further reduced the dataset from 272 descriptors to 143 derived from this distribution.

Since unsupervised learning algorithms lack a response vector, extrinsic evaluation metrics must be used to assess clustering quality within itself and their spatial distributions. One common metric is the silhouette score, which measures the similarity of points within a cluster and the separation between different clusters. According to sklearn documentation, the silhouette coefficient for a sample is calculated as follows:

$$s = \frac{b - a}{max(a,b)}$$

a: The mean distance between a sample and all other points in the same class.
b: The mean distance between a sample and all other points in the *next nearest cluster*.

This score is bounded between -1 and 1, where negative values indicate poor cluster separation, and higher positive values suggest well-defined cluster partition. To optimize the algorithms hyperparameters, we performed a brute-force search over various value ranges, calculating the silhouette score for each scenario (see tuning section in *ModelTraining.ipynb*). After evaluating over 11,000 iterations, the final validation step involved assigning chemical significance to the labels generated by the optimal model (with the best silhouette score).

<Model Hyperparameters>
UMAP(n_components=5, n_neighbors=20,
    min_dist=0.05, random_state=0)
HDBSCAN(cluster_selection_epsilon=1.0)

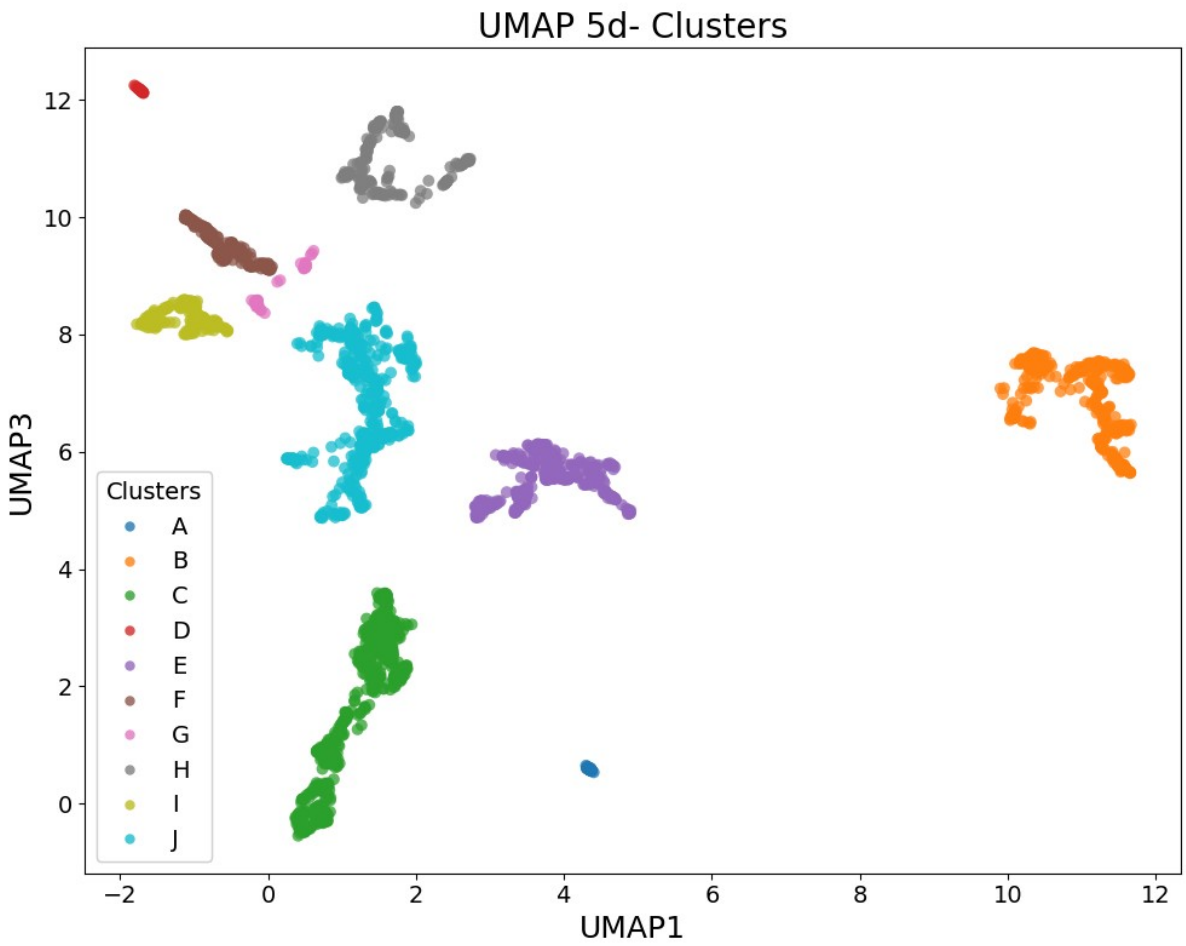

Figure S5. UMAP Plot of Salicylaldehyde Chemical Space Embedding with HDBSCAN Clustering Results Highlighted.

Cluster Evaluation and Scope Selection:

After selecting the model with the best silhouette performance, we proceeded to search for chemical meaning within the clusters, so we looked for rationalizable structural patters:

Cluster A (41 molecules): *meta*1-secondary amines

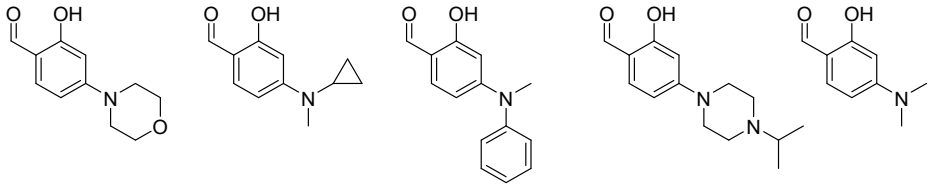

Cluster B (410 molecules): *para*-diverse substitutions

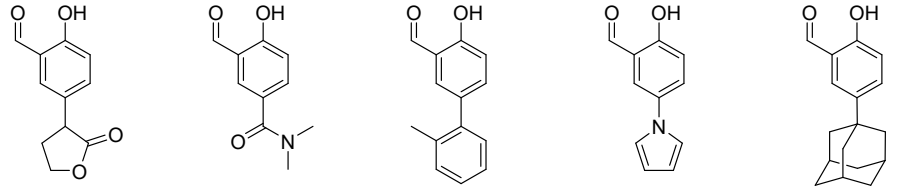

Cluster C (649 molecules): *meta2*-diverse substitutions

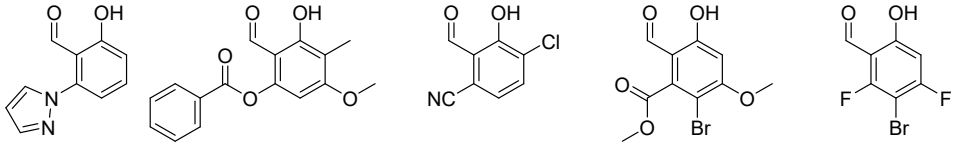

Cluster D (22 molecules): *ortho*-substituted chroman-4-one derivatives

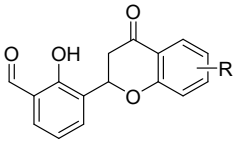

R = *o*-Me, *m*-Me, *p*-Me,
o-F, *m*-F, *m*-OMe, *m*-CN...

Cluster E (490 molecules): *meta1*-diverse substitutions

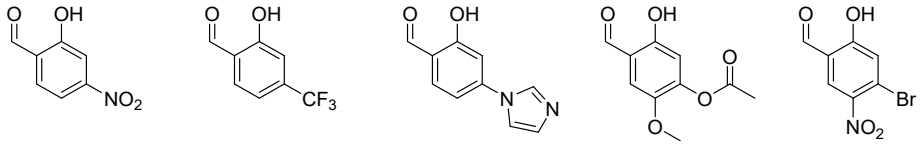

Cluster F (249 molecules): *ortho*-substituted bulky aryl/alkyl

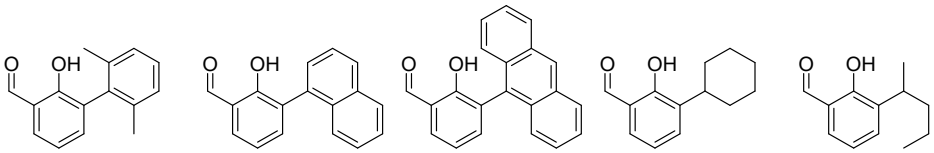

Cluster G (47 molecules): *ortho*-substituted electron-donating groups

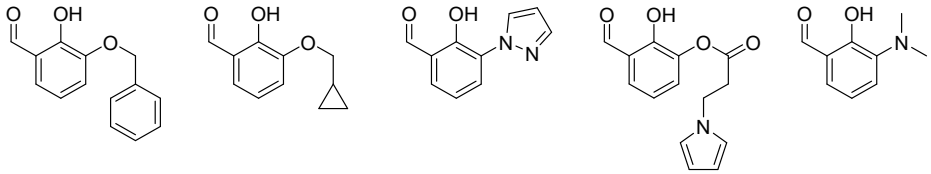

Cluster H (216 molecules): *ortho/para* bulky substitutions

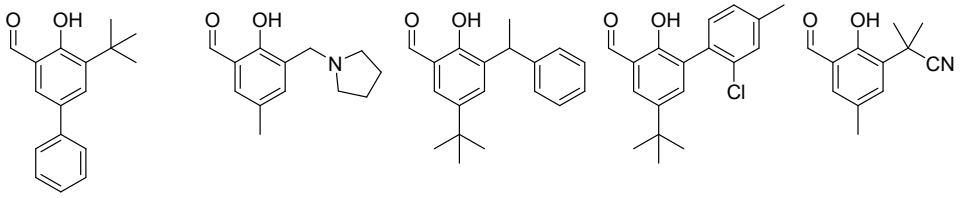

Cluster I (155 molecules): *ortho*-substituted ethers with para variations

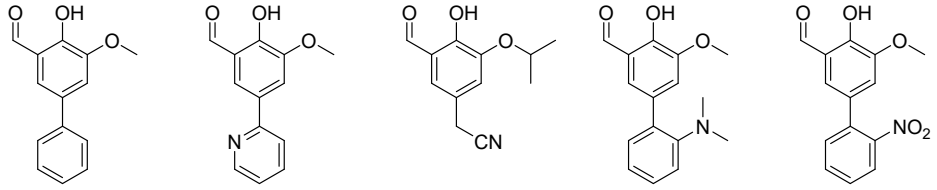

Cluster J (536 molecules): *ortho*-substituted electron-withdrawing

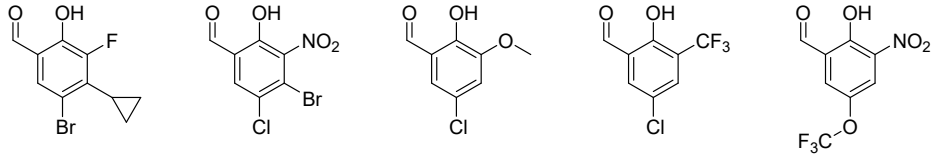

Cluster A: This cluster is a small subset of the *meta1*-only substitution pattern, featuring only secondary amines in this position. Due to the strong electron-donating nature of this group, which is directly conjugated with the carbonyl, these molecules are expected to exhibit special stability, which differs from the rest of the dataset.

Cluster B: This cluster contains all *para*-only substituted molecules, and aside from 3 outliers, it exclusively presents this substitution pattern, showcasing a wide range of electronic and steric effects.

Cluster C: At first, this cluster might appear complex, as it has 8 different structural combinations. However, upon closer inspection, it contains almost all *meta2*-substituted molecules (98.8%, with only 8 outliers out of 657 entries). Since the *meta2* position has negligible impact on our system, **we opted to exclude this group from the analysis**.

Cluster D: Interestingly, the algorithm collected a specific fragment of chroman-4-one derivatives substituted at the *ortho* position and placed all together in this cluster. Due to being a small and specific cluster of molecules and the literature-supported observation that high steric demand near the reactive center negatively affects the reaction outcome, **we opted to exclude this group from the analysis**.

Cluster E: This cluster contains 58.6% *meta1*-only substitutions and 40.0% *meta1-para* substitutions. Apart from cluster 1 (which presents a special subclass of *meta1* substitutions), this is the only other cluster that shows the *meta1*-only pattern, exhibiting significant electronic diversity. The cluster also contains 99.0% of all *meta1-para* pattern (with only 2 outliers), suggesting that these two patterns were somehow logically grouped by the algorithm.

Cluster F: Composed of 97.6% *ortho*-only substitutions, this cluster contains bulky, sterically demanding groups, predominantly aryl in nature. With limited examples of heteroatoms directly bonded to the salicylaldehyde ring, the electronic effects within the cluster are mainly limited to conjugation across the bis-aryl system.

Cluster G: This small cluster predominantly features *ortho* substitutions (89.4%), primarily with electron-donating groups. Since clusters F through J all involve *ortho* substitutions as their main structural feature, we conducted a pairwise silhouette analysis to assess the separation and similarity among these clusters. Interestingly, clusters G and J had the lowest silhouette score (0.39), indicating poor separation (with the mean silhouette value among all clusters being 0.79 ± 0.12). This may suggest, since the main effect on both clusters is electronic, that whether the substituent is an electron-donating or electron-withdrawing group at the *ortho* position has minimal impact on overall catalyst reactivity.

Cluster H: This cluster also features sterically demanding groups at the *ortho* position, though it primarily presents the *ortho-para* substitution pattern (99.1%). While some aryl groups are found at the *para* position, most of the substituents are alkyl or linked by saturated systems, significantly limiting electronic effects.

Cluster I: This final cluster consists exclusively of ortho-para substitutions, with a combination of electronic and steric effects. The *ortho* position is primarily occupied by ether groups, while the para position features bulky aryl moieties. Given that the initial scope candidates were selected from in-house salicylaldehydes with ether groups at *ortho* or bulky groups at para, **we opted to exclude this group from the analysis**.

Cluster J: This cluster is primarily composed of *ortho*-substituted molecules with electron-withdrawing groups, though it also includes some electron-donating groups, particularly ethers. The presence of both types of substituents may account for the relatively low silhouette score when compared to cluster G.

The scope was then selected based on synthetic accessibility and the availability of in-house chemicals, with the examples highlighted on Scheme 4 of main text.

S4. Experimental details

S4.1. General Procedure for the Oxidation of Phenols to Benzoquinones

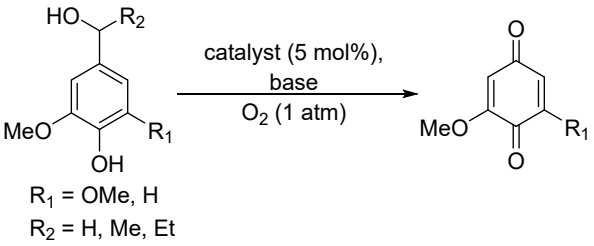

The lignin model substrate (0.20 mmol), catalyst (0.010 mmol), and base (0–0.10 mmol) were combined in MeOH (1 mL) in a 5 mL reaction vial. The vial was connected to a balloon filled with O_2, and the mixture was stirred for the indicated time (5 or 30 min). The solvent was removed under reduced pressure at room temperature. An analytical sample was purified by flash column chromatography (eluent: 40% EtOAc/CH_2Cl_2) to afford the corresponding quinone product.

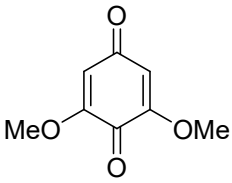

2,6-Dimethoxybenzoquinone (6):[13] Yellow solid. Rf = 0.6 (DCM/EtOAc 6:4); ^{1}H NMR (400 MHz, $CDCl_3$) δ 5.79 (s, 2H), 3.76 (s, 6H); ^{13}C NMR (101 MHz, $CDCl_3$) δ 186.8, 176.6, 157.3, 107.4, 56.4.

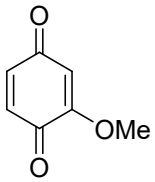

2-Methoxybenzoquinone (8):[1] Orange solid. Rf = 0.7 (DCM/EtOAc 7:3); ^{1}H NMR (400 MHz, $CDCl_3$) δ 6.67 (s, 2H), 5.88 (s, 1H), 3.81 (s, 3H).

For the lignin model **12** the conversion >99% and yield of 78% was determined from crude ^{1}H-NMR in comparison with quinone standard. Since it was added 1.0 equivalent of internal standard (in relation to starting material, lignin model) after the completion of the reaction, the yield could be obtained directly from the integration of the crude spectrum.

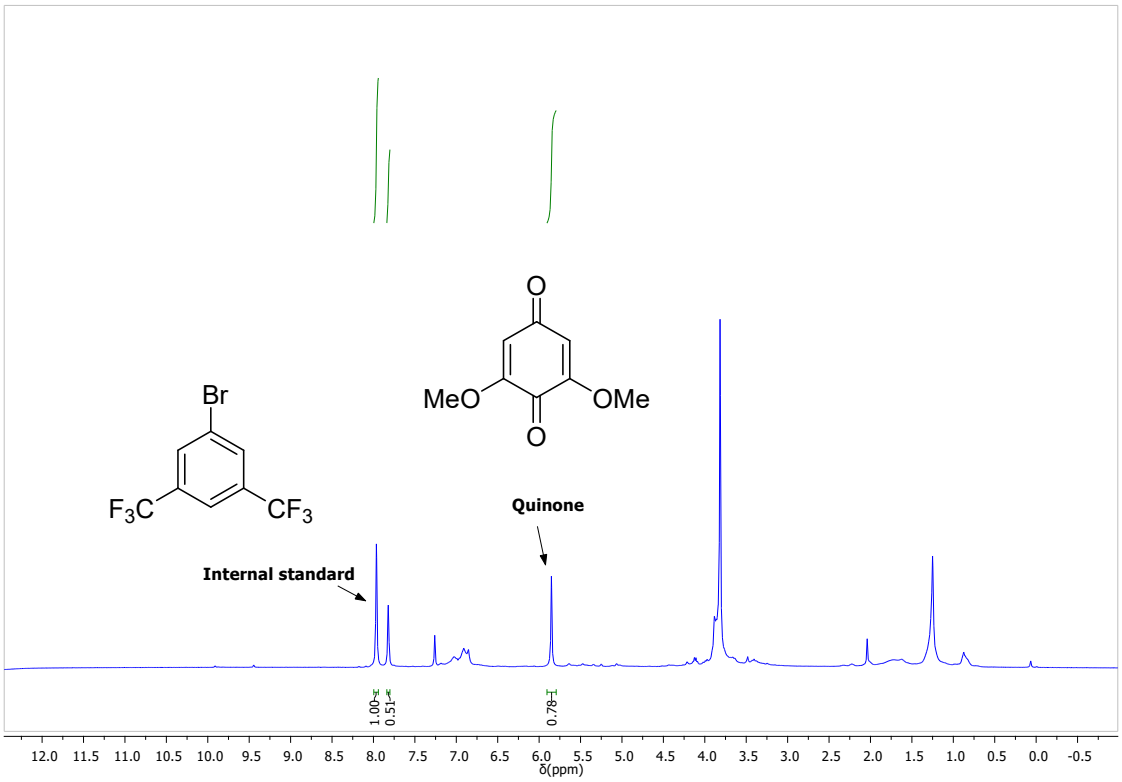

Crude reaction ^{1}H-NMR spectrum.

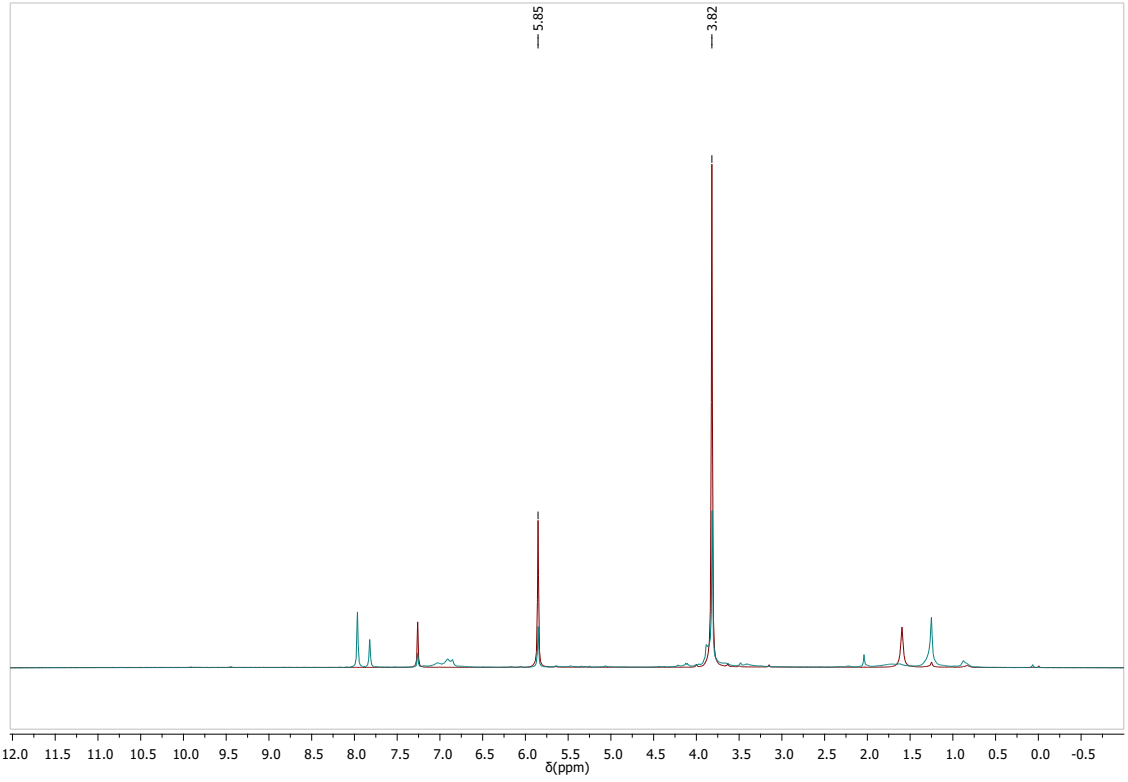

Overlapped quinone (red) and crude reaction (green) ^{1}H-NMR spectra.

S4.2. General Procedure for the Oxidation of Lignin

Powdered sugarcane lignin (100 mg) and catalyst **4b** (10 mg; 19.2 μmol) were mixed in a 1:1 mixture of MeOH/acetone (2 mL) in a pressure-resistant glass vessel. The vessel was flushed three times with O_2 and then pressurized with O_2 to 50 psi. The reaction mixture was vigorously stirred at 25 °C for 48 h. After completion, the mixture was concentrated under reduced pressure, dissolved in CH_2Cl_2 (20 mL), and filtered. The filtrate was combined with H_2O (50 mL) and extracted with CH_2Cl_2 (2 × 20 mL). The organic layers were dried over Na_2SO_4 and concentrated under reduced pressure to give a brown solid (4.8 mg, 4.8% mass recovery). GC–MS analysis of this solid indicated the presence of compounds **6**, vanillin **13**, **8** and **7** in a relative ratio of 13:10:5:1, respectively.

S4.3. Synthesis of Precursors of Salicylaldehydes 1d and 1h

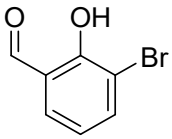

3-Bromo-2-hydroxybenzaldehyde (0d):[14] To a solution of salicylaldehyde (8.0 mmol) in CH_2Cl_2 (10 mL), N,N-diisopropylamine (0.80 mmol) was added, followed by dropwise addition of a solution of N-bromosuccinimide (8.0 mmol) in CH_2Cl_2 (60 mL) over 1 h 40 min using a syringe pump (36 mL h^{-1}). The reaction mixture was stirred at room temperature for 3 h and then acidified to pH 1 with 1.0 M HCl. The resulting mixture was washed with H_2O (20 mL), dried over Na_2SO_4, and concentrated under reduced pressure. The crude product was purified by flash column chromatography to afford the brominated salicylaldehyde in 20% yield. Rf = 0.80 (hexane/EtOAc 9.5:0.5). ^{1}H NMR (400 MHz, $CDCl_3$) δ 11.54 (s, 1H), 9.79 (s, 1H), 7.71 (d, *J* = 7.7 Hz, 1H), 7.48 (d, *J* = 7.7 Hz, 1H), 6.93 – 6.83 (m, 1H); ^{13}C NMR (101 MHz, $CDCl_3$) δ 196.1, 158.1, 140.0, 133.0, 121.4, 120.8, 111.2.

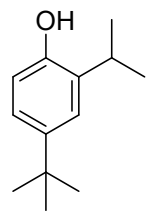

4-(Tert-butyl)-2-isopropylphenol (0h):[15] In a 100 mL flask, CH_2Cl_2 (40 mL), 4-(tert-butyl)phenol (3.85 g, 20.0 mmol), and tert-butyl alcohol (4.82 g, 65.0 mmol) were combined, followed by the slow addition of H_2SO_4 (1.5 mL) under constant stirring. The reaction mixture was stirred at room temperature for 48 h, then quenched with a CH_2Cl_2/H_2O mixture. The organic phase was separated, dried over Na_2SO_4, and concentrated under reduced pressure to afford a yellowish oil in 38% yield (1.04 g, 5.38 mmol). The yield was estimated based on the ratio of aromatic signals in the ^{1}H NMR spectrum. Rf = 0.6 (100% hexane). ^{1}H NMR (60 MHz, $CDCl_3$) δ: 11.62 (s, 1H), 9.85 (s, 1H), 7.59 (d, *J* = 2.5 Hz, 1H), 7.33 (d, *J* = 2.4 Hz, 1H), 3.43 (s, 1H), 1.42 (s, 9H), 1.32 (s, 6H).

S4.4. Synthesis of Salicylaldehyde 1d

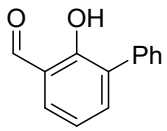

2-Hydroxy-[1,1'-biphenyl]-3-carbaldehyde (1d):[16] A mixture of 2-bromosalicylaldehyde (100.5 mg, 0.50 mmol), phenylboronic acid (182.9 mg, 1.50 mmol), KOH (1.0 M, 3.0 mL, 6.0 equiv), and Pd/C (10 wt %, 5.3 mg, 1.0 mol %) in H_2O (1.5 mL) was placed in a sealed microwave tube. The reaction mixture was heated at 120 °C for 30 min under microwave irradiation. After cooling to room temperature, the mixture was filtered through a Celite pad, the aqueous phase acidified with 1.0 M HCl, and the aqueous phase was extracted with Et_2O, washed with brine, dried over Na_2SO_4, filtered, and concentrated under reduced pressure. The crude product was purified by flash column chromatography to afford 2-phenylsalicylaldehyde in 29% yield. Rf = 0.40 (hexane/EtOAc 9:1). ^{1}H NMR (400 MHz, $CDCl_3$) δ 11.45 (s, 1H), 9.86 (s, 1H), 7.56 – 7.43 (m, 4H), 7.41 – 7.32 (m, 2H), 7.31 – 7.26 (m, 1H), 7.06 – 6.95 (m, 1H); ^{13}C NMR (101 MHz, $CDCl_3$) δ 197.0, 159.0, 137.9, 136.4, 133.3, 130.6, 129.4, 128.4, 127.8, 121.0, 120.0.

S4.5. Synthesis of Salicylaldehyde 1h and 1l

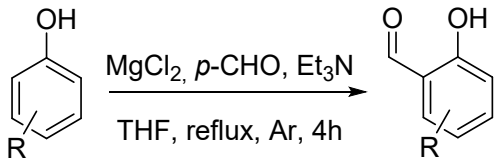

1h, 1l

In a two-neck flask containing THF (15 mL), phenol (5.0 mmol), $MgCl_2$ (0.953 g, 10,0 mmol), and paraformaldehyde (0.450 g, 15,0 mmol) were combined and stirred under an Ar atmosphere. Triethylamine (1.5 mL, 10 mmol) was added dropwise, during which the solution turned green. The mixture was heated at mild reflux for 4 h, then quenched with saturated NH_4Cl solution and transferred to a separatory funnel. The organic layer was dried over Na_2SO_4, filtered, and concentrated under reduced pressure. The crude product was purified by flash column chromatography to afford the corresponding hydroxymethylated phenol derivative.

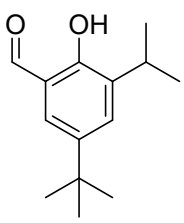

5-(Tert-butyl)-2-hydroxy-3-isopropylbenzaldehyde (**1h**):[17] White solid, yield of 31%. Rf = 0.5 (Hexane/EtOAc 9:1). ^{1}H NMR (400 MHz, $CDCl_3$) δ: 9.78 (s, 1H), 7.63 (d, *J* = 2.0 Hz, 1H), 7.58 (d, *J* = 2.0 Hz, 1H), 5.78 (s, 1H), 3.02 (sept, *J* = 6.8 Hz, 1H), 1.38 (s, 9H), 1.25 (d, *J* = 6.8 Hz, 6H). ^{13}C NMR (101 MHz, $CDCl_3$) δ: 191.9, 157.6, 136.4, 134.3, 129.2, 127.5, 126.1, 34.7, 29.6, 26.8, 22.6.

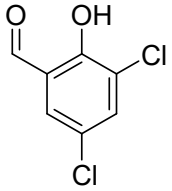

3,5-Dichloro-2-hydroxybenzaldehyde (**1l**):[18] Pale yellow solid, yield of 35%; Rf = 0.6 (hexane/EtOAc 9:1); ^{1}H NMR (400 MHz, $CDCl_3$) δ 11.31 (s, 1H), 9.79 (s, 1H), 7.55 (d, *J* = 2.5 Hz, 1H), 7.43 (d, *J* = 2.5 Hz, 1H); ^{13}C NMR (101 MHz, $CDCl_3$) δ 195.1, 155.9, 136.5, 131.1, 124.7, 123.4, 121.4.

S4.6. General Procedure for the Synthesis of Catalysts 4a-m

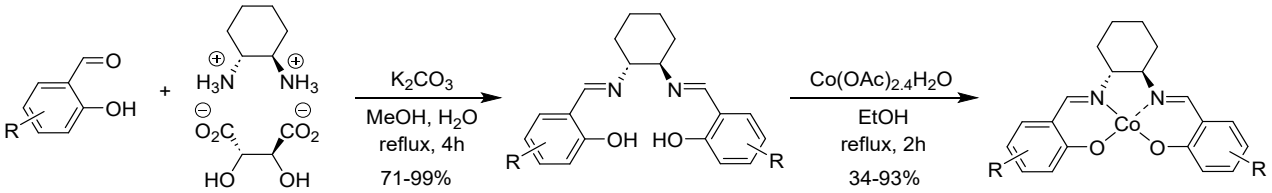

A solution of the (1*R*,2*R*)-(+)-1,2-diaminocyclohexane L-tartrate (0.317 g, 1.20 mmol) and K_2CO_3 (0.166 g, 1.20 mmol) in H_2O (0.8 mL) was prepared. MeOH (20 mL) was added, and the mixture was heated to reflux. A solution of the corresponding salicylaldehyde (2.40 mmol) in MeOH (3 mL) was added dropwise to the refluxing mixture. The reaction was maintained under reflux for 2 h. After cooling to room temperature, the solvent was removed under reduced pressure. The residue was extracted with EtOAc (3 × 15 mL) and H_2O (50 mL), and the crude product was purified by flash column chromatography to afford the corresponding salen ligands (**3a–3m**).

A flask containing anhydrous, degassed EtOH (12 mL) was charged with the corresponding salen ligand (1.0 mmol) and stirred under an inert atmosphere. In a separate flask, $Co(OAc)_2{\cdot}4H_2O$ (0.249 g, 1.00 mmol) was dissolved in hot EtOH (4 mL). This solution was transferred via cannula to the stirred ligand solution. After 1 h at room temperature, the reaction mixture was filtered through a Büchner funnel, and the resulting solid was washed with cold EtOH and dried under vacuum to afford the cobalt(II) salen complexes (**4a–4m**).

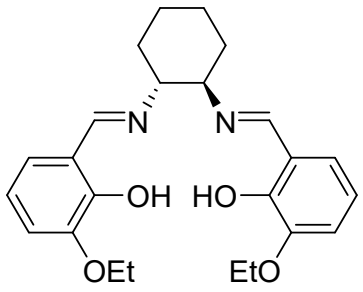

(*R*,*R*)-*N*,*N*′-Bis(3-ethoxysalicylidene)-1,2-cyclohexanediamine (3a):[19] Yellow solid, yield: 96% (0.402 g, 0.865 mmol); Rf = 0.7 (hexane/EtOAc 6:4); ^{1}H NMR (400 MHz, $CDCl_3$) δ 13.86 (s, 2H), 8.16 (s, 2H), 6.78 (dd, *J* = 7.8, 1.6 Hz, 2H), 6.70 (dd, *J* = 7.8, 1.6 Hz, 2H), 6.63 (t, *J* = 7.8 Hz, 2H), 3.99 (q, *J* = 7.0 Hz, 4H), 3.28–3.16 (m, 2H), 1.91–1.81 (m, 2H), 1.82–

1.75 (m, 2H), 1.65–1.56 (m, 2H), 1.44–1.36 (m, 8H); ^{13}C NMR (101 MHz, $CDCl_3$) δ 164.7, 151.6, 147.5, 123.1, 118.4, 117.8, 114.9, 77.3, 72.4, 64.2, 33.0, 24.0, 14.9.

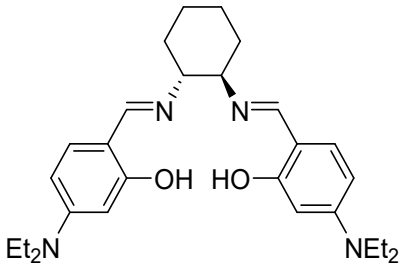

(*R*,*R*)-*N*,*N*′-Bis(4-diethylaminosalicylidene)-1,2-cyclohexanediamine (3b):[20] Yellow solid, yield: 96% (0.442 g, 0.951 mmol); Rf = 0.7 (hexane/EtOAc 6:4); ^{1}H NMR (400 MHz, $CDCl_3$) δ 13.86 (s, 2H), 8.16 (s, 2H), 6.78 (dd, *J* = 7.8, 1.6 Hz, 2H), 6.70 (dd, *J* = 7.8, 1.6 Hz, 2H), 6.63 (t, *J* = 7.8 Hz, 2H), 3.99 (q, *J* = 7.0 Hz, 4H), 3.28–3.16 (m, 2H), 1.91–1.81 (m, 2H), 1.82–1.75 (m, 2H), 1.65–1.56 (m, 2H), 1.44–1.36 (m, 8H); ^{13}C NMR (101 MHz, $CDCl_3$) δ 164.7, 151.6, 147.5, 123.1, 118.4, 117.8, 114.9, 77.3, 72.4, 64.2, 33.0, 24.0, 14.9.

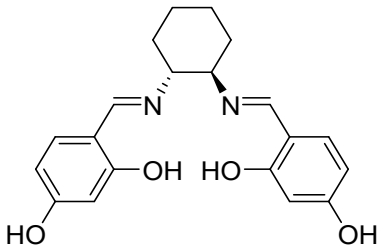

(*R*,*R*)-*N*,*N*′-Bis(4-hydroxysalicylidene)-1,2-cyclohexanediamine (3c):[8] Yellow solid, yield: 98% (0.4133 g, 1.166 mmol); Rf = 0.5 (hexane/EtOAc 6:4); ^{1}H NMR (400 MHz, DMSO-d_6) δ 13.66 (s, 2H), 8.26 (s, 2H), 7.09 (d, *J* = 8.4 Hz, 2H), 6.22 (d, *J* = 8.5 Hz, 2H), 6.12 (s, 2H), 3.29–3.23 (m, 2H), 1.85 (d, *J* = 12.5 Hz, 2H), 1.77 (d, *J* = 8.0 Hz, 2H), 1.62–1.49 (m, 2H), 1.42 (t, *J* = 9.0 Hz, 2H); ^{13}C NMR (101 MHz, DMSO) δ 164.5, 164.2, 162.0, 133.6, 111.5, 107.3, 102.8, 70.9, 33.2, 24.2.

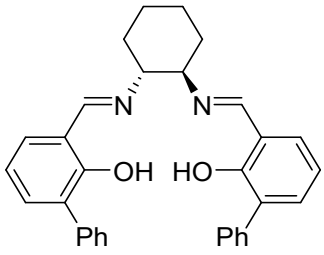

(*R*,*R*)-*N*,*N*′-Bis(3-phenylsalicylidene)-1,2-cyclohexanediamine (3d)[21] Yellow solid, yield 99% (0.1117 g, 0.223 mmol); Rf = 0.8 (hexano/EtOAc 1:1); ^{1}H NMR (400 MHz, $CDCl_3$) δ 8.34 (s, 2H), 7.67 – 7.58 (m, 4H), 7.46 (t, *J* = 7.5 Hz, 4H), 7.39 – 7.33 (m, 4H), 7.19 (dd, *J* = 7.6, 1.7 Hz, 2H), 6.91 (t, *J* = 7.6 Hz, 2H), 3.42 – 3.27 (m, 2H), 2.01 – 1.86 (m, 4H), 1.79 – 1.66 (m, 2H), 1.52 – 1.42 (m, 2H); ^{13}C NMR (101 MHz, $CDCl_3$) δ 164.9, 158.4, 137.8, 133.2, 130.9, 129.6, 129.3, 128.1, 127.0, 118.7, 118.5, 72.5, 60.3, 33.1, 29.7, 24.1, 21.0, 14.2.

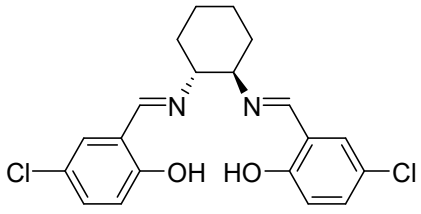

(*R*,*R*)-*N*,*N*′-Bis(5-chlorosalicylidene)-1,2-cyclohexanediamine (3e):[22] Yellow solid, yield: 95% (0.4424 g, 1.131 mmol); Rf = 0.8 (hexane/EtOAc 6:4); ^{1}H NMR (400 MHz, $CDCl_3$) δ 13.15 (s, 2H), 8.11 (s, 2H), 7.12 (dd, *J* = 8.8, 2.6 Hz, 2H), 7.05 (d, *J* = 2.6 Hz, 2H), 6.77 (d, *J* = 8.8 Hz, 2H), 3.31–3.19 (m, 2H), 1.84 (tt, *J* = 12.0, 3.0 Hz, 4H), 1.64 (dd, *J* = 16.5, 8.2 Hz, 2H), 1.40 (ddd, *J* = 12.0, 8.2,

3.0 Hz, 2H); ^{13}C NMR (101 MHz, $CDCl_3$) δ 163.5, 159.5, 132.1, 130.5, 123.2, 119.2, 118.4, 72.6, 32.9, 24.0.

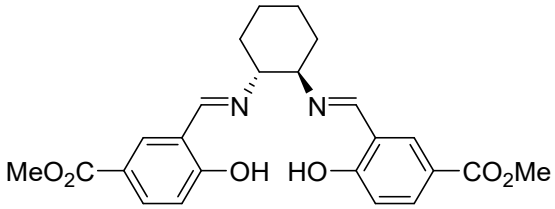

(*R*,*R*)-*N*,*N*′-Bis(5-carbomethoxysalicylidene)-1,2-cyclohexanediamine (3f):[23] Yellow solid, yield: 99% (0.5300 g, 1.209 mmol); Rf = 0.6 (hexane/EtOAc 6:4); ^{1}H NMR (400 MHz, $CDCl_3$) δ 13.97 (s, 2H), 8.31 (s, 2H), 7.94 (dd, *J* = 8.6, 2.1 Hz, 2H), 7.91 (d, *J* = 2.1 Hz, 2H), 6.92 (d, *J* = 8.6 Hz, 2H), 3.87 (s, 6H), 3.44–3.33 (m, 2H), 1.99 (d, *J* = 14.6 Hz, 2H), 1.93 (d, *J* = 9.8 Hz, 2H), 1.81–1.70 (m, 2H), 1.51 (t, *J* = 9.8 Hz, 2H); ^{13}C NMR (101 MHz, $CDCl_3$) δ 166.3, 165.4, 164.3, 133.8, 133.7, 120.6, 117.8, 117.2, 72.3, 51.9, 32.9, 24.0.

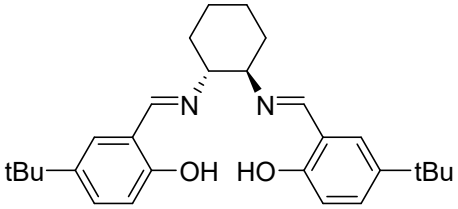

(*R*,*R*)-*N*,*N*′-Bis(5-tert-butylsalicylidene)-1,2-cyclohexanediamine (3g):[9] Yellow solid, yield: 86% (0.2986 g, 0.6871 mmol); Rf = 0.8 (hexane/EtOAc 6:4); ^{1}H NMR (400 MHz, $CDCl_3$) δ 13.14 (s, 2H), 8.26 (s, 2H), 7.28 (dd, *J* = 8.6, 2.4 Hz, 2H), 7.12 (d, *J* = 2.4 Hz, 2H), 6.83 (d, *J* = 8.6 Hz, 2H), 3.35–3.24 (m, 2H), 1.92–1.85 (m, 4H), 1.77–1.66 (m, 2H), 1.46 (t, *J* = 9.9 Hz, 2H), 1.23 (s, 18H); ^{13}C NMR (101 MHz, $CDCl_3$) δ 165.0, 158.6, 141.2, 129.4, 127.9, 117.9, 116.2, 72.8, 33.9, 33.2, 31.4, 24.2.

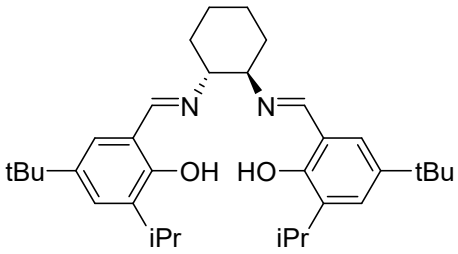

(*R*,*R*)-*N*,*N*′-Bis(3-*iso*-propyl,5-*tert*-butylsalicylidene)-1,2-cyclohexanediamine (3h):[24] Yellow solid, yield: 78% (1.0091 g, 1.9451 mmol); Rf = 0.8 (hexane/EtOAc 6:4); ^{1}H NMR (400 MHz, $CDCl_3$) δ 13.74 (s, 2H), 8.34 (s, 2H), 7.34 (s, 2H), 7.02 (s, 2H), 3.41–3.31 (m, 2H), 1.98 (d, *J* = 13.8 Hz, 2H), 1.91 (d, *J* = 9.0 Hz, 2H), 1.83–1.72 (m, 2H), 1.53–1.48 (m, 2H), 1.44 (s, 18H), 1.27 (s, 12H); ^{13}C NMR (101 MHz, $CDCl_3$) δ 165.8, 158.0, 139.9, 136.3, 126.8, 126.0, 117.8, 72.3, 34.9, 34.0, 33.2, 31.4, 29.4, 24.3.

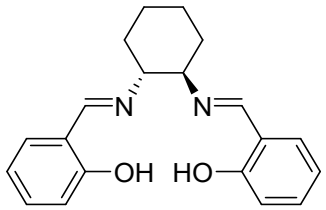

(*R*,*R*)-*N*,*N*′-Bis(salicylidene)-1,2-cyclohexanediamine (3i):[9] Yellow solid, yield: 97% (0.3952 g, 1.226 mmol); Rf = 0.8 (hexane/EtOAc 6:4); ^{1}H NMR (400 MHz, $CDCl_3$) δ 13.26 (s, 2H), 8.18 (s, 2H), 7.21–7.12 (m, 2H), 7.07 (dd, *J* = 7.6, 1.5 Hz, 2H), 6.81 (d, *J* = 8.3 Hz, 2H), 6.72 (t, *J* = 7.6 Hz, 2H), 3.30–3.19 (m, 2H), 1.91–1.83 (m, 2H), 1.84–1.77 (m, 2H), 1.72–1.59 (m, 2H), 1.40 (t, *J* = 9.7 Hz, 2H); ^{13}C NMR (101 MHz, $CDCl_3$) δ 164.7, 160.9, 132.1, 131.4, 118.6, 116.7, 72.6, 33.1, 24.1.

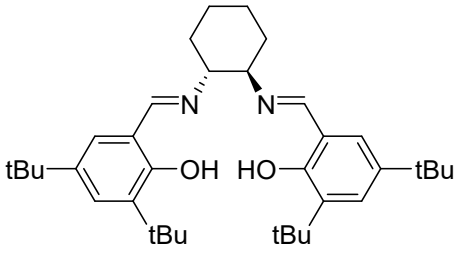

(*R*,*R*)-*N*,*N*′-Bis(3,5-di-tertbutylsalicylidene)-1,2-cyclohexanediamine (3j):[9] Yellow solid, yield: 90% (0.6880 g, 1.258 mmol) after purification by flash chromatography; Rf = 0.8 (hexane/EtOAc 6:4); ^{1}H NMR (400 MHz, $CDCl_3$) δ 13.76 (s, 2H), 8.33 (s, 2H), 7.33 (d, *J* = 2.4 Hz, 2H), 7.01 (d, *J* = 2.4 Hz, 2H), 3.39–3.30 (m, 2H), 1.97 (d, *J* = 14.4 Hz, 2H), 1.90 (d, *J* = 9.7 Hz, 2H), 1.82–1.70 (m, 2H), 1.49 (t, *J* = 9.7 Hz, 2H), 1.44 (s, 18H), 1.26 (s, 18H); ^{13}C NMR (101 MHz, $CDCl_3$) δ 165.8, 158.0, 139.8, 136.3, 126.7, 126.0, 117.8, 72.4, 34.9, 34.0, 33.3, 31.4, 29.4, 24.3.

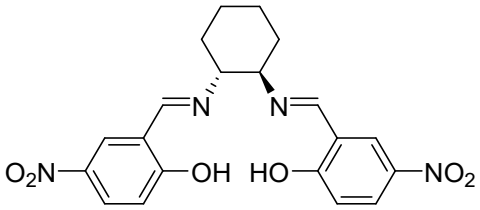

(*R*,*R*)-*N*,*N*′-Bis(5-nitrosalicylidene)-1,2-cyclohexanediamine (3k):[9] Yellow solid, yield: 60% (0.1970 g, 0.4777 mmol); Rf = 0.7 (hexane/EtOAc 6:4); ^{1}H NMR (400 MHz, $CDCl_3$) δ 14.26 (s, 2H), 8.29 (s, 2H), 8.09–8.03 (m, 4H), 6.86 (d, *J* = 9.0 Hz, 2H), 3.47–3.35 (m, 2H), 2.00–1.91 (m, 2H), 1.91–1.82 (m, 2H), 1.76–1.62 (m, 2H), 1.49–1.40 (m, 2H); ^{13}C NMR (101 MHz, $CDCl_3$) δ 167.6, 163.7, 139.3, 128.1, 128.0, 118.4, 117.0, 71.7, 32.6, 23.9.

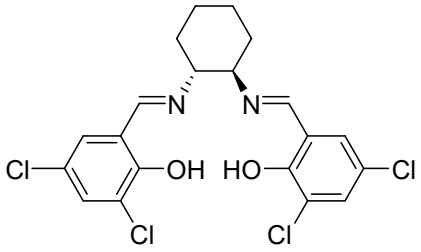

(*R*,*R*)-*N*,*N*′-Bis(3,5-di-chlorosalicylidene)-1,2-cyclohexanediamine (3l):[9] Yellow solid, yield: 51% (0.1884 g; 0.4094 mmol); Rf = 0.3 (hexane/EtOAc 9:1); ^{1}H NMR (400 MHz, $CDCl_3$) δ 14.13 (s, 2H), 8.11 (s, 2H), 7.29 (d, J = 2.5 Hz, 2H), 7.01 (d, *J* = 2.5 Hz, 2H), 3.35–3.24 (m, 2H), 1.93–1.79 (m, 4H), 1.64 (q, *J* = 11.2 Hz, 2H), 1.46–1.35 (m, 2H); ^{13}C NMR (101 MHz, $CDCl_3$) δ 163.4, 156.3, 132.3, 129.2, 122.9, 122.6, 119.2, 72.1, 32.8, 23.9.

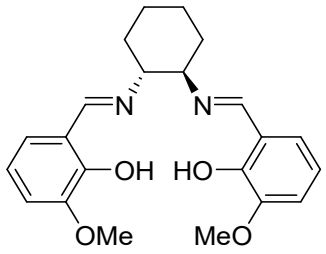

(*R*,*R*)-*N*,*N*′-Bis(3-methoxysalicylidene)-1,2-cyclohexanediamine (3m):[7] Yellow solid, yield: 96% (0.5001 g; 1.307 mmol); Rf = 0.6 (hexane/EtOAc 6:4); ^{1}H NMR (400 MHz, $CDCl_3$) δ 13.79 (s, 2H), 8.17 (s, 2H), 6.78 (dd, *J* = 7.8, 1.6 Hz, 2H), 6.72 (dd, *J* = 7.8, 1.6 Hz, 2H), 6.65 (t, *J* = 7.8 Hz, 2H), 3.80 (s, 6H), 3.29–3.20 (m, 2H), 1.89–1.79 (m, 4H), 1.64 (q, J = 11.2 Hz, 2H), 1.41 (t, J = 10.6 Hz, 2H); ^{13}C NMR (101 MHz, $CDCl_3$) δ 164.7, 151.5, 148.2, 123.1, 118.3, 117.8, 113.7, 72.4, 56.0, 33.0, 24.0.

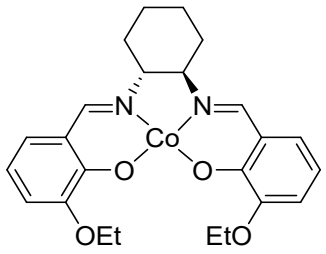

(*R*,*R*)-*N*,*N*′-Bis(3-ethoxysalicylidene)-1,2-cyclohexanediamino cobalt(II) (4a):[17] Brown solid, 66% yield (0.1441 g; 0.3083 mmol).

HRMS (ESI) m/z: [M+Na]+ Calculated for $C_{24}H_{28}CoN_2O_4Na^+$: 490.1279; Found: 490.1292. IR (KBr, cm^{-1}): 3430, 3052, 2978, 2933, 2864, 2367, 1637, 1601, 1469, 1390, 1323, 1224, 1177, 1083, 1037, 905, 851, 734, 679, 565, 458.

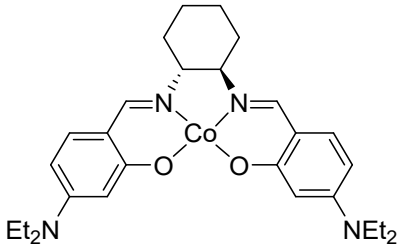

(*R*,*R*)-*N*,*N*′-Bis(4-diethylaminosalicylidene)-1,2-cyclohexanediamino cobalt(II) (4b):[25] Orange solid, 71% yield (0.1930 g; 0.3703 mmol). mp 297 °C. HRMS (ESI) m/z: [M]+ Calculated for $C_{28}H_{38}CoN_4O_2$: 521.2321; Found: 521.2316. IR (KBr, cm^{-1}): 3430, 2967, 2929, 2863, 2363, 1590, 1506, 1353, 1248, 1135, 1076, 1014, 822, 774, 714, 443.

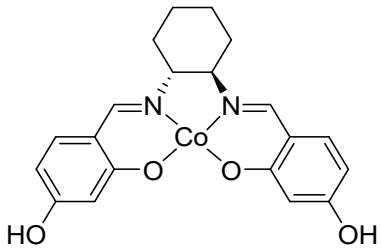

(*R*,*R*)-*N*,*N*′-Bis(4-hydroxysalicylidene)-1,2-cyclohexanediamino cobalt(II) (4c): Brown solid, 46% yield (0.7780 g; 0.1892 mmol). HRMS (ESI) m/z: [M]+ Calculated for $C_{20}H_{20}CoN_2O_4$: 411.0749; Found: 411.0749. IR (KBr, cm^{-1}): 3449, 3200, 2937, 2862, 2365, 1607, 1449, 1342, 1230, 1183, 1127, 1042, 988, 848, 800, 760, 645, 548, 465.

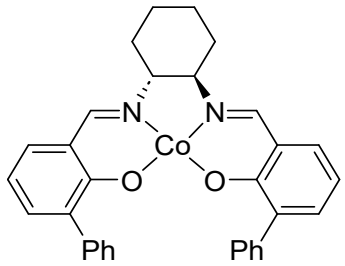

(*R*,*R*)-*N*,*N*′-Bis(3-phenylsalicylidene)-1,2-cyclohexanediamino cobalt(II) (4d):[26] Red solid, 73% yield (0.7320 g; HRMS (ESI) m/z [M+] Calculated for $C_{32}H_{28}CoN_2O_2$: 531.1483; Found: 531.1483. IR (KBr, cm^{-1}): 3054, 3022, 2930, 2857, 1764, 1692, 1590, 1538, 1447, 1412, 1382, 1324, 1284, 1227, 1195, 1155, 1110, 1072, 1032, 941.2, 851.7, 798.5, 746.2, 695.9, 617.5, 570.4, 477.3, 447.1, 425.

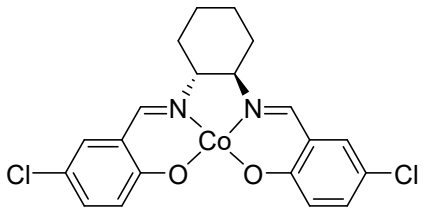

(*R*,*R*)-*N*,*N*′-Bis(5-chlorosalicylidene)-1,2-cyclohexanediamino cobalt(II) (4e):[27] Orange solid, 84% yield (0.1683 g; 0.3755 mmol). mp 389 °C. HRMS (ESI) m/z: [M+Na]+ Calculated for $C_{20}H_{18}Cl_2CoN_2O_2Na^+$: 469.9969; Found: 469.9951. IR (KBr, cm^{-1}): 3551, 3449, 2931, 2855, 1721, 1605, 1536, 1479, 1432, 1354, 1279, 1232, 1191, 1107, 1044, 940, 842, 771, 720, 658, 584, 537, 442.

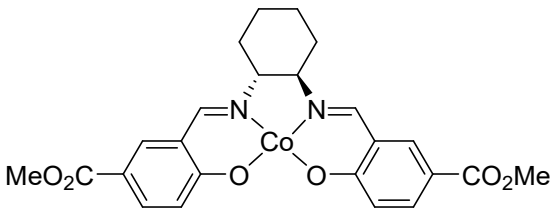

(*R*,*R*)-*N*,*N*′-Bis(5-carbomethoxysalicylidene)-1,2-cyclohexanediamino cobalt(II) (4f): Brown

solid, 85% yield (0.2085 g; 0.4209 mmol). mp 376 °C. HRMS (ESI) m/z: $[M]^+$ Calculated for $C_{24}H_{24}CoN_2O_6$: 495.0960; Found: 495.0948. IR (KBr, cm^{-1}): 3429, 3054, 2936, 2856, 2363, 1876, 1601, 1521, 1447, 1374, 1315, 1245, 1184, 1130, 1083, 1040, 926, 823, 736, 667, 585, 535, 444, 341.

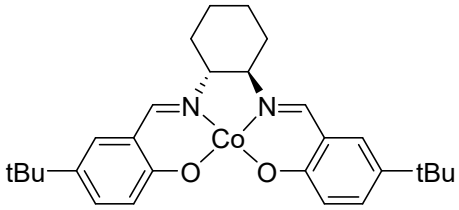

(*R*,*R*)-*N*,*N*′-Bis(5-tert-butylsalicylidene)-1,2-cyclohexanediamino cobalt(II) (4g):[28] Red solid, 70% yield (0.1689 g; 0.3436 mmol). mp 336–342 °C. HRMS (ESI) m/z: $[M]^+$ Calculated for $C_{28}H_{36}CoN_2O_2$: 491.2103; Found: 491.2092. IR (KBr, cm^{-1}): 3431, 3050, 3018, 2929, 2855, 2363, 1602, 1530, 1444, 1389, 1319, 1201, 1147, 1025, 908, 846, 808, 755, 569, 516, 443.

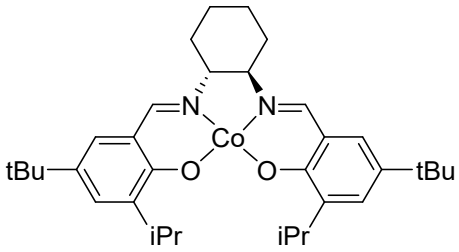

(*R*,*R*)-*N*,*N*′-Bis(3-*iso*-propyl,5-*tert*-butylsalicylidene)-1,2-cyclohexanediamino cobalt(II) (4h): Orange solid, 69% yield (0.5753 g; 0.9993 mmol). mp 380–392 °C. HRMS (ESI) m/z: $[M+K]^+$ Calculated for $C_{34}H_{48}CoN_2O_2K^+$: 614.2679; Found: 614.2635. IR (KBr, cm^{-1}): 2954, 2865, 1596, 1525, 1463, 1427, 1358, 1319, 1253, 1174, 1131, 1047, 934, 868, 835, 785, 746, 641, 571.

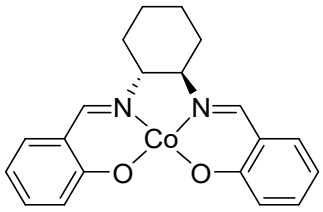

(*R*,*R*)-*N*,*N*′-Bis(salicylidene)-1,2-cyclohexanediamino cobalt(II) (4i):[18] Red solid, 65% yield (0.3790 g; 0.9992 mmol). mp 365 °C. HRMS (ESI) m/z: $[M+Na]^+$ Calculated for $C_{20}H_{20}CoN_2O_2Na^+$: 402.0749; Found: 402.0750. IR (KBr, cm^{-1}): 3427, 2951, 2862, 2363, 1612, 1527, 1466, 1316, 1257, 1183, 1039, 935, 831, 735, 672, 615, 552, 452, 360.

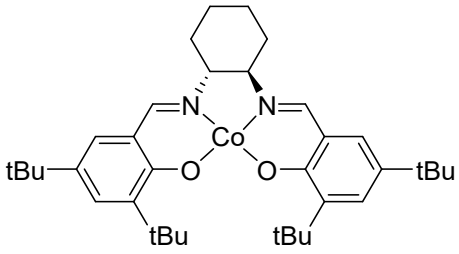

(*R*,*R*)-*N*,*N*′-Bis(3,5-di-tertbutylsalicylidene)-1,2-cyclohexanediamino cobalt(II) (4j):[29] Orange solid, 93% yield (0.3388 g; 0.5611 mmol). HRMS (ESI) m/z: $[M]^+$ Calculated for $C_{36}H_{52}CoN_2O_2$: 603.3355; Found: 603.3346. IR (KBr, cm^{-1}): 3430, 2952, 2865, 2375, 1595, 1525, 1460, 1427, 1359, 1320, 1253, 1175, 1130, 1046, 936, 868, 835, 786, 636, 572, 302.

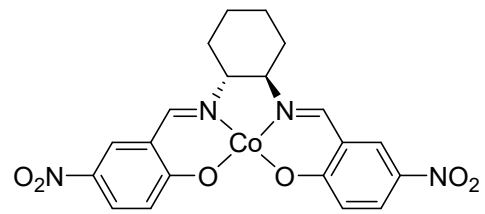

(*R*,*R*)-*N*,*N*′-Bis(5-nitrosalicylidene)-1,2-cyclohexanediamino cobalt(II) (4k):[30] Brown solid, 40% yield (0.8810 g; 0.1877 mmol). HRMS (ESI) m/z:

[M]$^+$ Calculated for $C_{20}H_{18}CoN_4O_6$: 469.0552; Found: 469.0539. IR (KBr, cm^{-1}): 3433, 2938, 2862, 2413, 1641, 1599, 1549, 1493, 1441, 1386, 1332, 1305, 1246, 1198, 1153, 1131, 1100, 1042, 946, 835, 755, 728, 660, 539, 442.

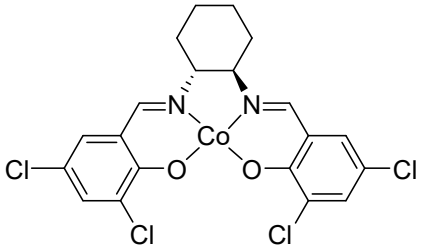

(*R*,*R*)-*N*,*N*′-Bis(3,5-di-chlorosalicylidene)-1,2-cyclohexanediamino cobalt(II) (4l):[31] Red solid, 85% yield (0.5149 g; 0.9957 mmol). HRMS (ESI) m/z: [M+Na]$^+$ Calculated for $C_{20}H_{16}Cl_4CoN_2O_2Na^+$: 537.9190; Found: 537.9167. IR (KBr, cm^{-1}): 3433, 2935, 2860, 1602, 1560, 1436, 1325, 1212, 1177, 1103, 1033, 971, 928, 864, 765, 675, 615, 587, 556, 481, 447.

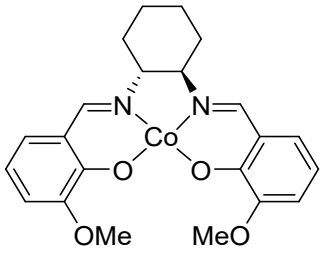

(*R*,*R*)-*N*,*N*′-Bis(3-methoxysalicylidene)-1,2-cyclohexanediamino cobalt(II) (4m):[31] Brown solid, 88% yield (0.1698 g; 0.3864 mmol). HRMS (ESI) m/z: [M]$^+$ Calculated for $C_{28}H_{38}CoN_4O_2$: 439.1063; Found: 439.1066. IR (KBr, cm^{-1}): 3430, 3271, 3055, 2938, 2862, 1719, 1640, 1604, 1474, 1448, 1375, 1326, 1223, 1171, 1083, 1039, 979, 925, 865, 822, 729, 677, 646, 566, 490, 461, 377, 352.

S5.7. Synthesis of lignin models

S5.7.1. Primary alcohol

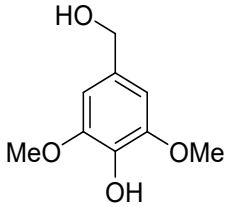

Syringyl Alcohol (5):[32] In a 100 mL flask, 50 mL of methanol and syringyl aldehyde (2.00 g; 0.0110 mol) were added and stirred in an ice bath for 5 minutes. Then, small portions of $NaBH_4$ were added until a total of 1.25 g (0.033 mol) was reached. The mixture was then removed from the ice bath and stirred for 30 minutes at room temperature. After this period, 30 mL of a saturated NH_4Cl solution was added, and the mixture was stirred for another 30 minutes. At the end of the reaction, the methanol was evaporated, and the product was extracted with ethyl acetate and purified by flash chromatography, yielding 92% (1.86g; 10.1 mmol) of a white solid. Rf = 0.6 (Hexane/AcOEt/MeOH 4:4:2). ^{1}H NMR (400 MHz, $CDCl_3$) δ 6.63 (s, 2H); 5.55 (s, 1H); 4.63 (s, 2H); 3.92 (s, 6H). ^{13}C NMR (101 MHz, $CDCl_3$) δ 147.1; 134.1; 132.0; 103.8; 65.7; 56.3.

S5.7.2. General procedure for the synthesis of secondary alcohols

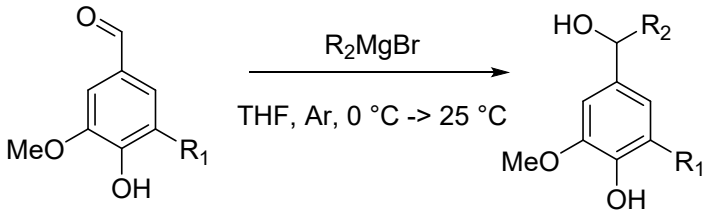

R_1 = H, R_2 = Et (22), 60%
R_1 = OMe, R_2 = Me (23), 52%

In a 50 mL round-bottom flask, correspondent aldehyde (5 mmol) was dissolved in THF (25 mL) and stirred at 0°C. The corresponding alkyl magnesium bromide (5 mL; 15 mmol; 3 M) was added dropwise, and the mixture was stirred for 1 hour. Subsequently, 5 mL of a 10% HCl solution and 30 mL of water were added. The organic phase was then extracted with DCM, concentrated using a rotary evaporator, and purified by flash chromatography.

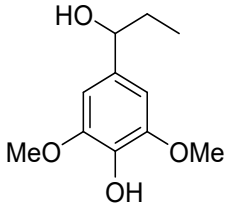

4-(1-Hydroxypropyl)-2,6-dimethoxyphenol (9): [33] White solid, 60% yield (0.580 g; 2.73 mmol). Rf 0.4 (hexane/AcOEt 1:1). ^{1}H NMR (400 MHz, $CDCl_3$) δ 6.60 (d, J = 3.7 Hz, 2H), 5.53 (d, J = 10.5 Hz, 1H), 4.53 (q, J = 6.2, 5.3 Hz, 1H), 3.91 (d, J = 4.0 Hz, 6H), 1.87-1.68 (m, 2H), 0.93 (td, J = 7.4, 2.9 Hz, 3H). ^{13}C NMR (101 MHz, $CDCl_3$) δ 146.9, 135.9, 133.9, 102.5, 76.3, 56.2, 31.9, 10.3.

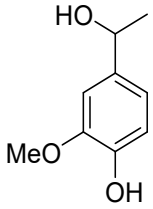

4-(1-Hydroxyethyl)-2-methoxyphenol (10): [33] White solid, 52% yield (0.526 g, 3.12 mmol). Rf 0.4 (hexane/AcOEt 1:1). ^{1}H NMR (400 MHz, $CDCl_3$) δ 6.85 (d, J = 1.8 Hz, 1H), 6.80 (d, J = 8.1 Hz, 1H), 6.75 (dd, J = 8.1, 1.9 Hz, 1H), 5.62 (s, 1H), 4.76 (q, J = 6.4 Hz, 1H), 3.82 (s, 3H), 1.88 (s, 1H), 1.40 (d, J = 6.4 Hz, 3H). ^{13}C NMR (101 MHz, $CDCl_3$) δ 146.6, 144.9, 137.9, 118.3, 114.1, 107.9, 70.3, 55.9, 25.1.

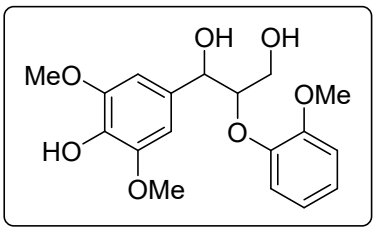

1-(4-Hydroxy-3,5-dimethoxyphenyl)-2-(2-methoxyphenoxy)propane-1,3-diol (12): The lignin model selected was prepared according to the synthesis reported by Burtoloso and coworkers (*Org. Biomol. Chem.*, **2020**, *18*, 4815).

^{1}H-NMR (400 MHz, $CDCl_3$) δ 7.06 (t, *J* = 7.6 Hz, 1H), 6.98 – 6.86 (m, 3H), 6.62 (s, 2H), 4.95 (d, *J* = 4.7 Hz, 1H), 4.14 (dd, *J* = 9.0, 4.9 Hz, 1H), 3.93 (d, *J* = 5.9 Hz, 1H), 3.88 (s, 3H), 3.86 (s, 6H), 3.66 (dd, *J* = 12.2, 3.2 Hz, 1H), 2.66 (s, 1H).

^{13}C-NMR (101 MHz, $CDCl_3$) δ 151.7, 147.2, 146.9, 134.2, 131.1, 124.4, 121.8, 121.0, 112.3, 102.9, 87.4, 73.0, 60.9, 56.5, 56.0.

S6. Quantitative data from GC-MS experiments

Table S5. Oxidation reaction without the use of pyridine additive

	0.0 py in 5 min			Average			0.0 py in 30min			Average		
Cat.	**6 (%)**	**Conv (%)**	**7 (%)**	**6 (%)**	**Conv (%)**	**7 (%)**	**6 (%)**	**Conv (%)**	**7 (%)**	**6 (%)**	**Conv (%)**	**7 (%)**
4a	3.9	28.2	14.9	2.2 ± 2.4	22.6 ± 7.9	10.0 ± 7.0	26.4	64.5	18.3	18.4 ± 7.3	57.6 ± 6.0	17.8 ± 0.5
	0.5	17.0	5.0				16.9	54.7	17.8			
							12.1	53.5	17.4			
4b	28.0	64.0	4.5	20.8 ± 10.2	48.2 ± 22.3	5.2 ± 1.0	55.7	97.6	11.9	51.4 ± 6.1	91.6 ± 8.5	17.8 ± 4.9
	13.6	32.5	5.9				47.1	85.6	18.8			
4c	1.1	11.7	3.5	0.6 ± 0.7	14.5 ± 3.9	4.4 ± 1.3	23.4	33.1	4.6	12.2 ± 10.4	35.3 ± 5.1	8.8 ± 3.7
	0.1	17.2	5.3				10.1	41.1	11.5			
							3.0	31.7	10.4			
4d	0.0	4.0	1.0	0.0 ± 0.0	4.5 ± 0.7	0.8 ± 0.3	0.5	10.6	1.7	1.3 ± 1.1	10.3 ± 0.4	1.8 ± 0.1
	0.0	5.0	0.6				2.0	10.1	1.9			
4e	0.1	3.7	0.5	0.1 ± 0.1	5.5 ± 2.6	0.4 ± 0.1	7.5	34.3	11.7	4.0 ± 3.5	32.4 ± 7.1	10.5 ± 2.1
	0.2	7.4	0.3				0.6	24.5	8.0			
							3.8	38.3	11.7			
4f	1.6	15.6	8.4	0.8 ± 1.1	11.3 ± 6.2	5.8 ± 3.7	31.9	77.4	24.2	22.1 ± 10.7	73.3 ± 7.5	26.5 ± 9.5
	0.0	6.9	3.2				23.8	77.8	36.9			
							10.7	64.7	18.4			
4g	9.9	24.3	11.9	13.5 ± 5.2	40.5 ± 23.0	11.6 ± 0.4	41.0	83.9	23.2	32.5 ± 12.0	84.6 ± 1.0	20.4 ± 4.0
	17.2	56.8	11.4				24.1	85.3	17.6			
4h	0.3	2.6	0.4	0.4 ± 0.1	9.8 ± 10.1	0.4 ± 0.0	25.4	47.4	9.9	15.4 ± 14.1	39.7 ± 10.8	9.0 ± 1.3
	0.5	16.9	0.4				5.5	32.1	8.1			

4i	14.4	44.0	13.3	8.6 ± 8.1	38.1 ± 8.4	12.2 ± 0.0	55.3	88.2	18.8	41.5 ± 14.6	87.7 ± 2.9	24.7 ± 5.1
	2.9	32.1	11.2				42.9	90.4	27.8			
							26.3	84.6	27.5			
4j	0.0	1.0	0.0	0.0 ± 0.0	1.4 ± 0.5	0.0 ± 0.0	9.1	40.9	8.7	8.6 ± 6.0	25.7 ± 13.9	4.1 ± 4.1
	0.0	1.7	0.0				14.3	22.7	2.3			
							2.4	13.5	1.2			
4k	0.0	1.4	0.0	0.0 ± 0.0	1.5 ± 0.1	0.0 ± 0.0	0.0	15.6	0.0	0.0 ± 0.0	15.4 ± 0.4	0.0 ± 0.0
	0.0	1.5	0.0				0.0	15.1	0.0			
4l	0.0	5.2	0.0	0.0 ± 0.0	4.1 ± 1.6	0.0 ± 0.0	0.0	8.2	0.0	0.0 ± 0.0	8.4 ± 0.3	0.0 ± 0.0
	0.0	2.9	0.0				0.0	8.6	0.0			
4m	12.3	41.5	29.7	10.3 ± 2.8	43.1 ± 2.3	24.1 ± 7.8	16.7	66.0	25.3	15.6 ± 1.6	64.7 ± 1.9	24.1 ± 1.7
	8.3	44.7	18.6				14.5	63.3	22.9			

Table S6. Oxidation reaction with the use of pyridine additive.

	0.5 py in 5 min			**Average**			**0.5 py in 30min**			**Average**		
Cat.	**6 (%)**	**Conv (%)**	**7 (%)**	**6 (%)**	**Conv (%)**	**7 (%)**	**6 (%)**	**Conv (%)**	**7 (%)**	**6 (%)**	**Conv (%)**	**7 (%)**
4a	0.4	4.4	1.3	0.9 ± 0.7	4.0 ± 0.5	1.8 ± 0.8	7.4	23.1	2.7	7.1 ± 0.4	24.2 ± 1.6	1.9 ± 1.2
	1.4	3.7	2.4				6.9	25.3	1.0			
4b	31.3	52.4	0.6	33.6 ± 3.3	52.5 ± 0.1	0.6 ± 0.1	100.0	100.0	0	100.0 ± 0.0	100.0 ± 0.0	0.0 ± 0.0
	35.9	52.5	0.7				100.0	100.0	0			
4d	0.9	6.4	2.1	1.1 ± 0.2	5.3 ± 3.4	1.9 ± 0.4	6.2	20.6	3.3	5.9 ± 0.4	19.8 ± 1.1	3.2 ± 0.2
	1.2	1.6	1.6				5.6	19.0	3.0			
4c	2.8	13.8	4.3	1.5 ± 1.8	8.5 ± 7.4	3.4 ± 1.3	6.5	27.7	8.5	5.6 ± 1.3	26.1 ± 2.3	5.9 ± 3.6
	0.2	3.3	2.5				4.6	24.4	3.4			
4e	32.9	41.4	0.8	40.6 ± 10.9	41.5 ± 0.1	0.9 ± 0.1	90.0	92.2	0.7	90.8 ± 1.0	92.6 ± 0.6	1.1 ± 0.6

	48.3	41.5	1.0				91.4	93.1	1.5			
4f	13.8	49.4	8.2	13.6 ± 0.2	48.4 ± 0.7	8.2 ± 0.0	88.8	94.6	2.9	87.9 ± 1.3	93.1 ± 2.1	2.7 ± 0.2
	13.5	48.4	8.2				86.9	91.6	2.6			
4g	47.4	52.4	0.4	46.9 ± 0.7	51.6 ± 0.8	0.4 ± 0.0	100.0	100.0	0	100.0 ± 0.0	100.0 ± 0.0	0.0 ± 0.0
	46.4	51.3	0.4				100.0	100.0	0			
4h	0.0	13.1	0.0	0.0 ± 0.0	12.9 ± 0.2	0.6 ± 0.8	2.4	28.2	2.0	2.4 ± 0.0	27.8 ± 0.6	2.0 ± 0.0
	0.0	12.8	1.1				2.4	27.4	2.0			
4i	37.0	48.3	2.5	40.0 ± 4.2	47.4 ± 1.3	2.2 ± 0.5	100.0	100.0	0	100.0 ± 0.0	100.0 ± 0.0	0.0 ± 0.0
	43.0	46.5	1.8				100.0	100.0	0			
4j	0.4	5.5	0.3	0.4 ± 0.0	5.0 ± 0.7	0.4 ± 0.1	13.7	27.8	0.7	10.1 ± 5.1	21.4 ± 9.1	0.5 ± 0.3
	0.4	4.5	0.4				6.5	15.0	0.3			
4k	0.0	1.5	0.0	0.0 ± 0.0	1.5 ± 0.1	0.0 ± 0.0	0.0	15.9	0.9	0.0 ± 0.0	15.6 ± 0.4	0.5 ± 0.6
	0.0	1.4	0.0				0.0	15.3	0.0			
4l	0.0	35.9	0.0	0.0 ± 0.0	36.6 ± 1.1	0.0 ± 0.0	0.0	52.8	0.0	0.0 ± 0.0	52.9 ± 0.1	0.0 ± 0.0
	0.0	37.4	0.0				0.0	52.9	0.0			
4m	0.0	2.9	0.1	8.6 ± 0.0	4.4 ± 2.1	0.1 ± 0.0	0.0	12.5	0.4	0.0 ± 0.0	11.3 ± 1.7	0.3 ± 0.1
	0.0	5.8	0.1				0.0	10.1	0.2			

S7. Green and efficiency metrics

TableS7. Metrics for Model S oxidation

	1st Gen	2nd Gen	3rd Gen	This work		
Catalyst (loading)	Co(salen) (10 mol%)	s3 (5 mol%)	s10 (5 mol%)	4b (5 mol%)	4b (0.5 mol%)	4b (0.05 mol%)
Base (equiv.)	Pyridine (1.0)	—	—	K_3PO_4 (0.5)	K_3PO_4 (0.5)	K_3PO_4 (0.5)
Yield	99%	74%	71%	99%	93%	70%
PMI	25.6	33.6	35.0	**25.5**	27.2	36.1
E-factor	24.6	32.6	34.0	**24.6**	26.2	35.1
TON	9.9	14.8	14.2	20	186	**1400**

S8. Effect of pyridine: quantitative comparison of ligand-dependent trends with and without pyridine (4a-m)

To evaluate whether pyridine merely enhances overall activity or fundamentally changes ligand-dependent trends in the newly developed catalyst set (**4a–4m**), we performed correlation analyses comparing outcomes obtained under otherwise identical conditions with and without pyridine. For each catalyst, we compared (i) yield of product **6**, (ii) conversion of the starting material, and (iii) yield of product **7**, at 5 min (0 versus 0.5 equiv of pyridine) and 30 min (0 versus 0.5 equiv of pyridine). Pearson correlations (r) probe linear association of absolute values, while Spearman rank correlations (r_s) test whether the ordering of catalyst performance is preserved (monotonic relationship), which is the key question when assessing whether ligand structure still governs relative trends after adding pyridine.

The results show moderate-to-strong positive correlations for yield of **6** and conversion at both 5 and 30 min, indicating that catalysts that perform better without pyridine generally remain among the better performers with pyridine. This supports the interpretation that pyridine acts primarily as a global activity promoter by affecting the electronics of Co (raising conversion/yield for most ligands), while ligand structure still controls relative performance within the **4a-m** series. In contrast, the yield of side product 7 shows weak or inconsistent correlations, consistent with 7 being more sensitive to competing pathways.

Table S8. Pearson and Spearman correlations between conditions without pyridine and with pyridine for the same catalyst set (4a–4m).

		Pearson		Spearman	
Time	**Metric**	***r***	***r*²**	r_s	r_s^2
5 min	Yield of **6** (%)	0.63	0.40	0.65	0.42
5 min	Conversion (%)	0.41	0.17	0.42	0.17
5 min	Yield of **7** (%)	-0.02	0.00	0.36	0.13
30 min	Yield of **6** (%)	0.71	0.50	0.72	0.52
30 min	Conversion (%)	0.63	0.40	0.54	0.29
30 min	Yield of **7** (%)	-0.23	0.05	-0.18	0.03

S9. Two-parameter threshold analysis on 4a-m: steric boundary condition and electronic gating for activity.

We first splitting the **4a-m** dataset into training and validation subsets (Figure S6). The training set contains 21 entries and the validation set contains 5 entries.

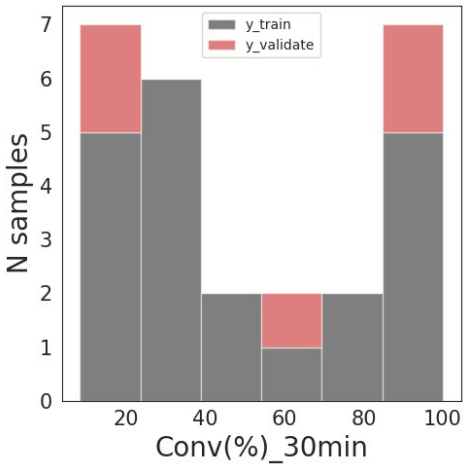

Figure S6: Train/validation split used for the threshold analysis on the **4a-m** dataset. Training set (n = 21): [[4a_py, 4c_py, 4d, 4d_py, 4e, 4e_py, 4f, 4f_py, 4g, 4g_py, 4h, 4h_py, 4i, 4i_py, 4j, 4j_py, 4k, 4k_py, 4l_py, 4m, 4m_py]. Validation set (n = 5): [4a, 4b, 4b_py, 4c, 4l]. Training set mean conversion: 49.681; validation set mean conversion: 53.580.

Catalysts were then classified into two activity classes using an operational conversion criterion (inactive: conversion ≤ 35%; active: conversion > 35%). Using the training set, we

searched for a compact and chemically interpretable two-threshold decision rule combining one electronic descriptor and one steric descriptor. The optimal model (Figure S7) uses the following thresholds: BOLTZ_BD1_N1_C1 > −0.675 and BOLTZ_BVol_2.25_O2 < 0.930.

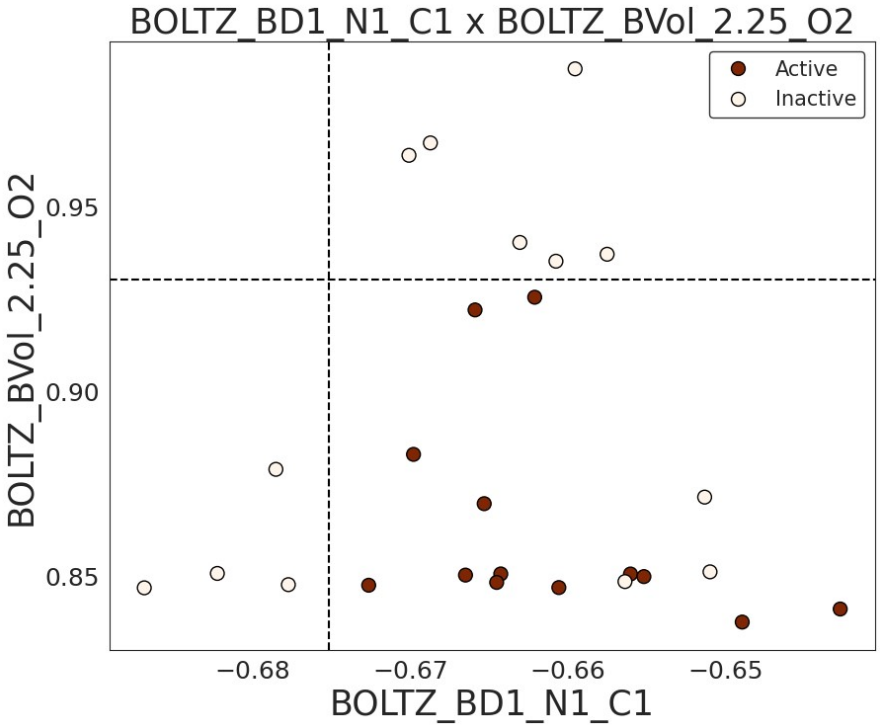

Figure S7. Two-parameter threshold classifier for activity in the **4a-m** dataset. Catalysts are classified as inactive (conversion ≤ 35%) or active (conversion > 35%). Total accuracy with 2 thresholds: 0.885. Initial accuracy with no thresholds: 0.500. Thresholds: BOLTZ_BD1_N1_C1 > -0.675 with Added accuracy of 0.154; BOLTZ_BVol_2.25_O2 < 0.930 with Added accuracy of 0.231. Accuracy/ Weighted Accuracy (all 0.885; train 0.905; validation 0.800). F1/ Weighted F1 (all 0.897; train 0.909; validation 0.857).

S10. NMR spectra

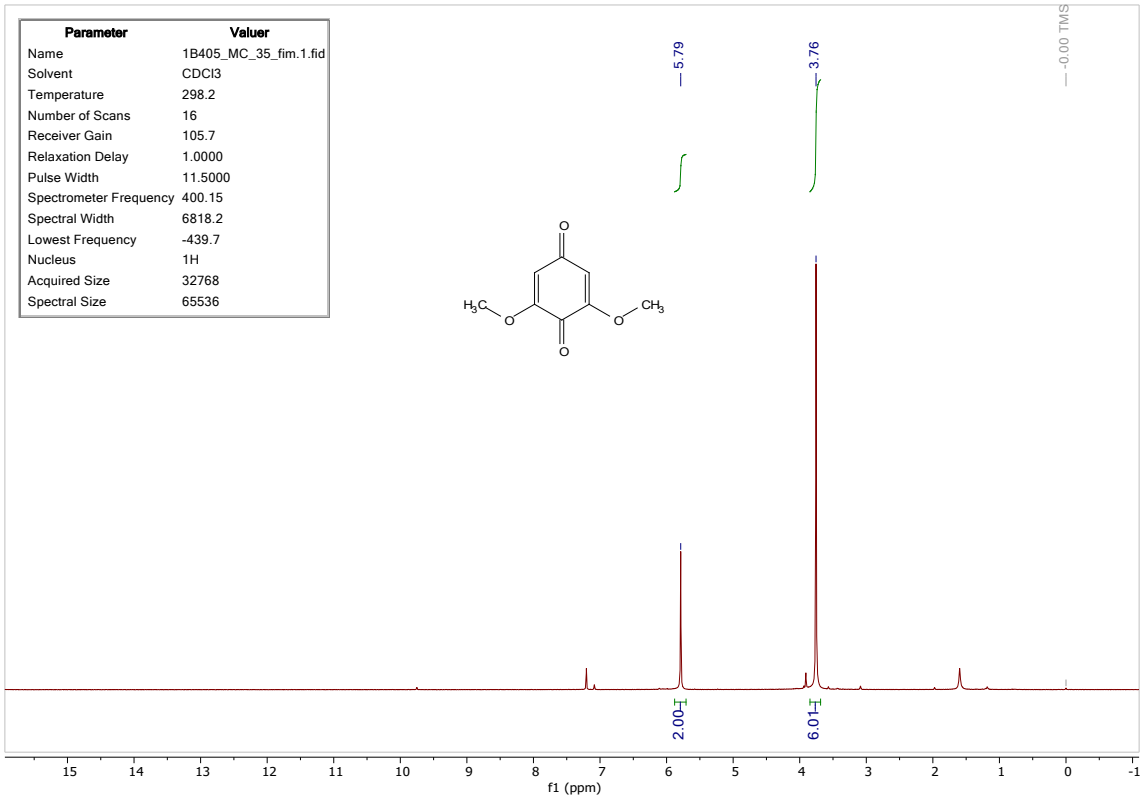

^{1}H NMR NMR spectrum of **2,6-dimethoxybenzoquinone (6)** (400 MHz, $CDCl_3$)

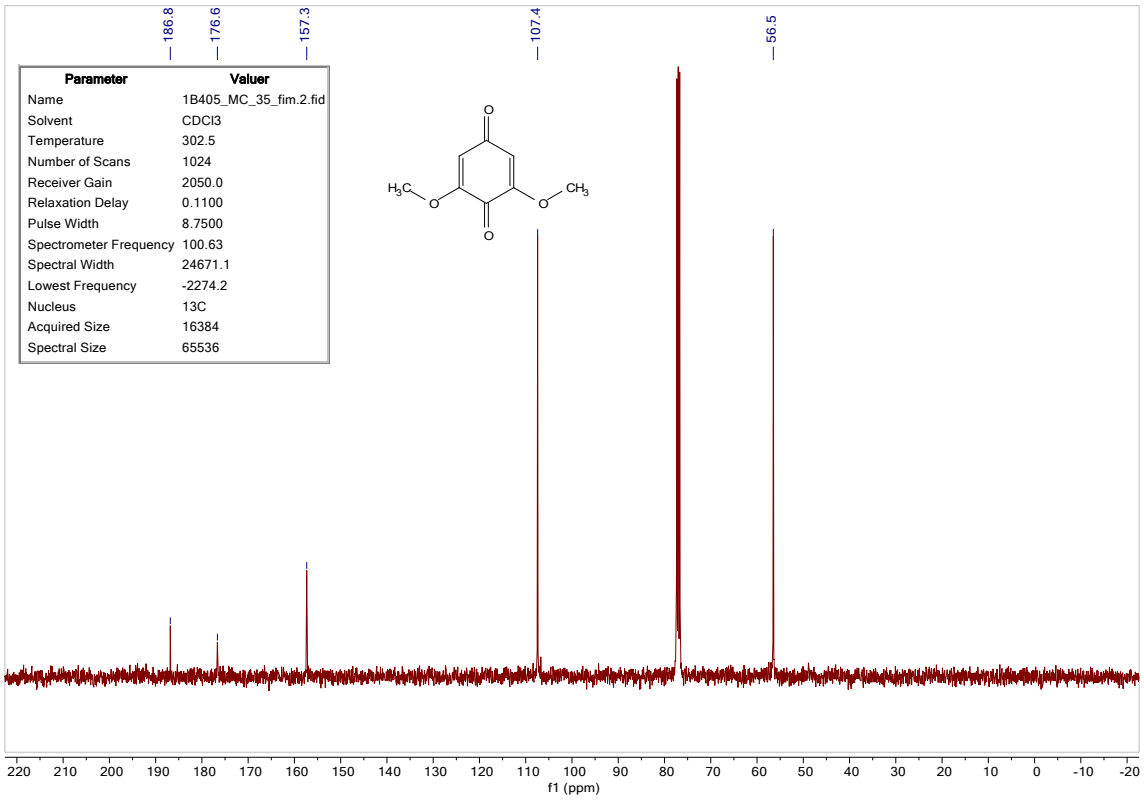

^{13}C NMR spectrum of **2-methoxybenzoquinone (6)** (101 MHz, $CDCl_3$)

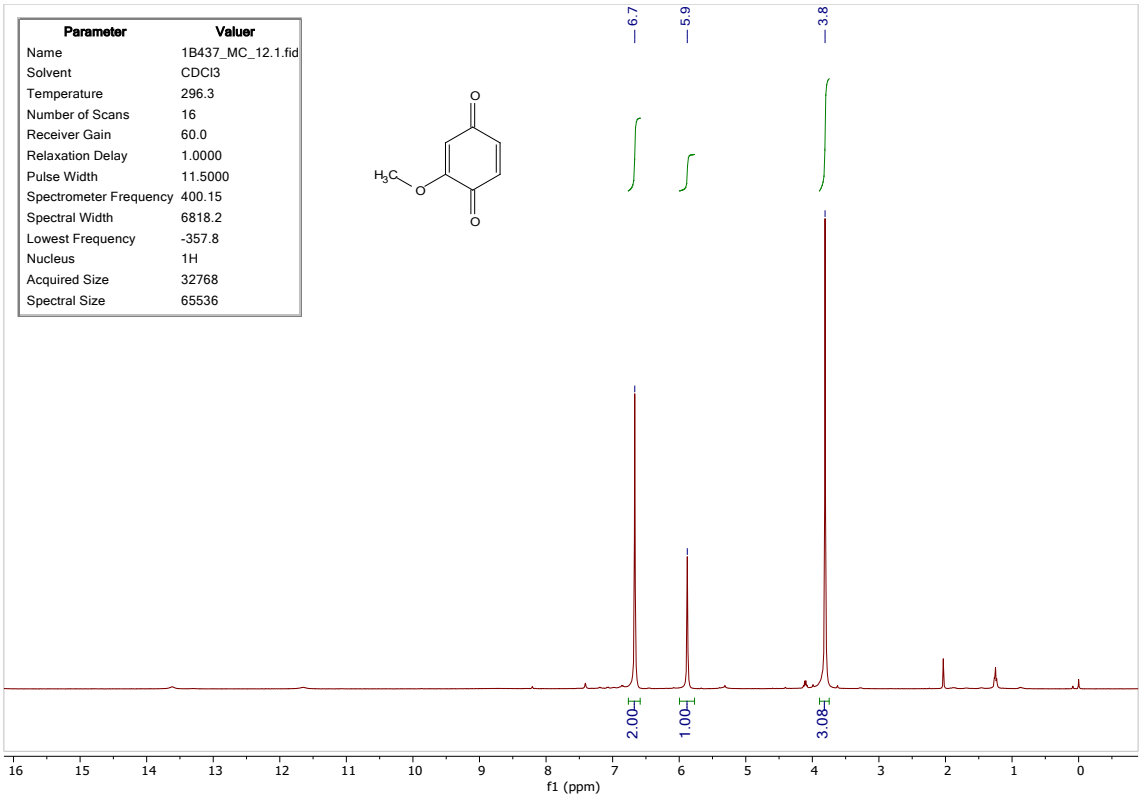

^{1}H NMR spectrum of **2-methoxybenzoquinone (8)** (400 MHz, $CDCl_3$)

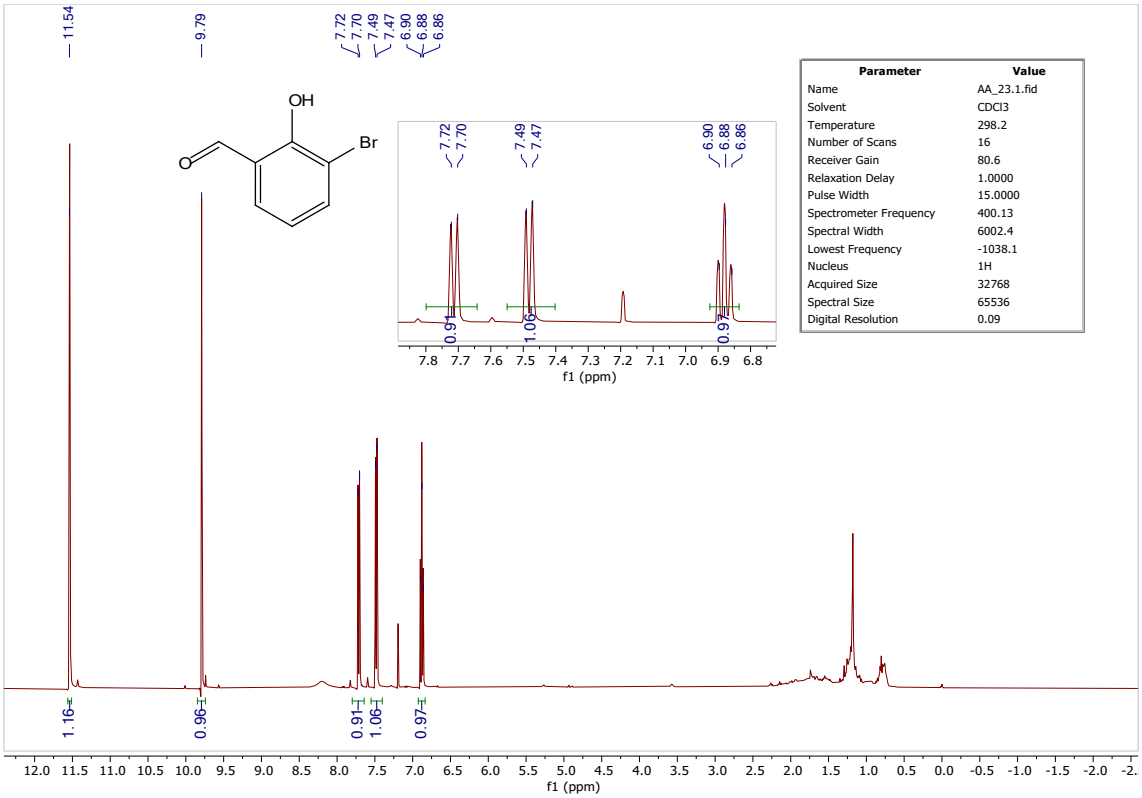

^{1}H NMR spectrum of 0**d** (400 MHz, $CDCl_3$)

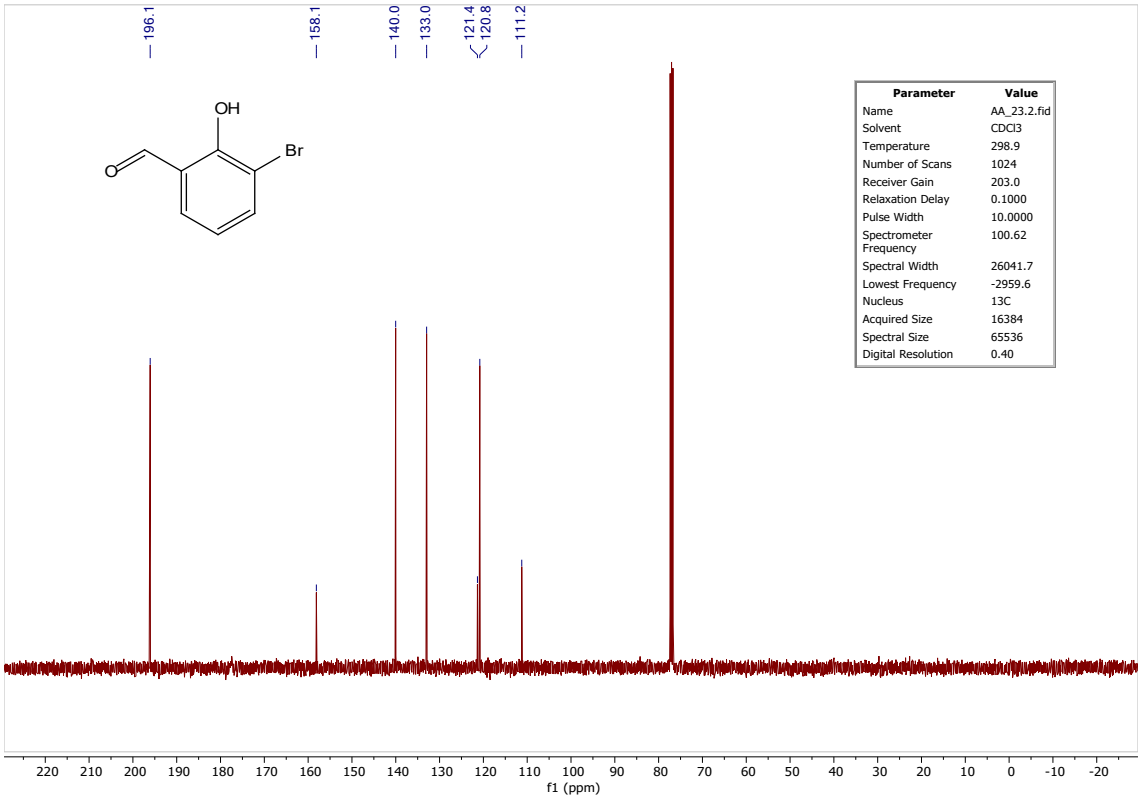

^{13}C NMR spectrum of 0**d** (101 MHz, $CDCl_3$)

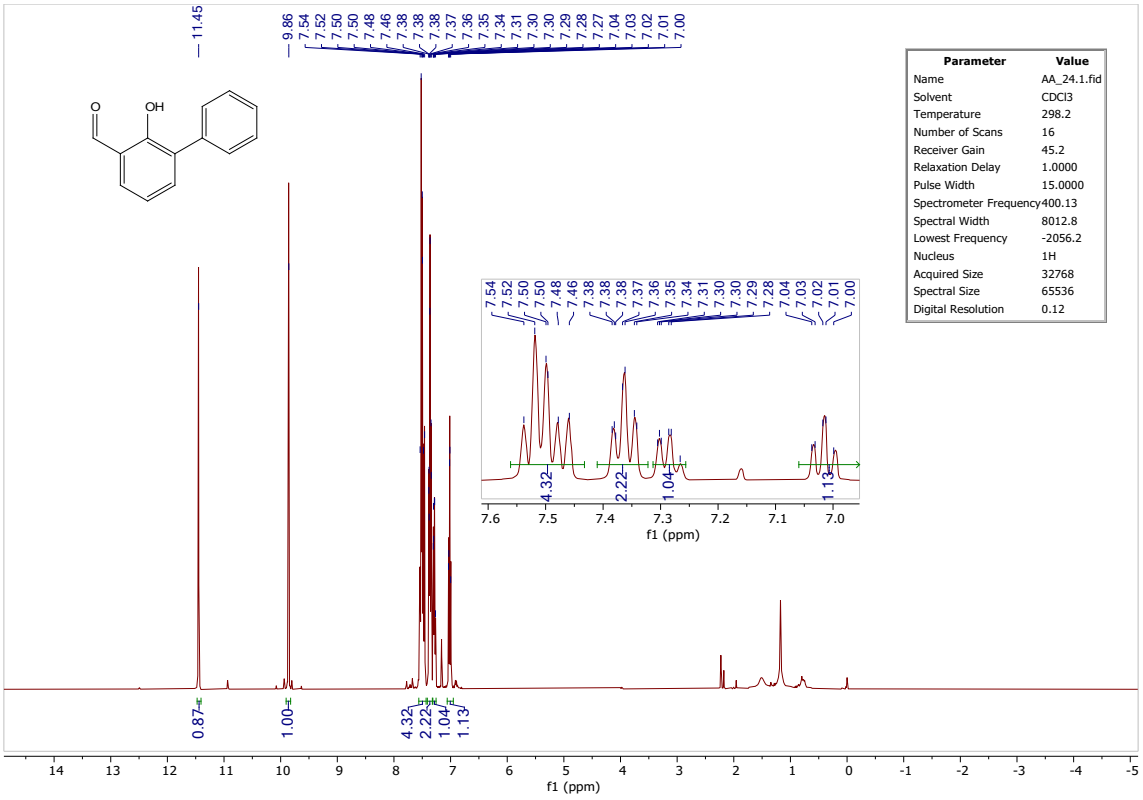

^{1}H NMR spectrum of 1**d** (400 MHz, $CDCl_3$)

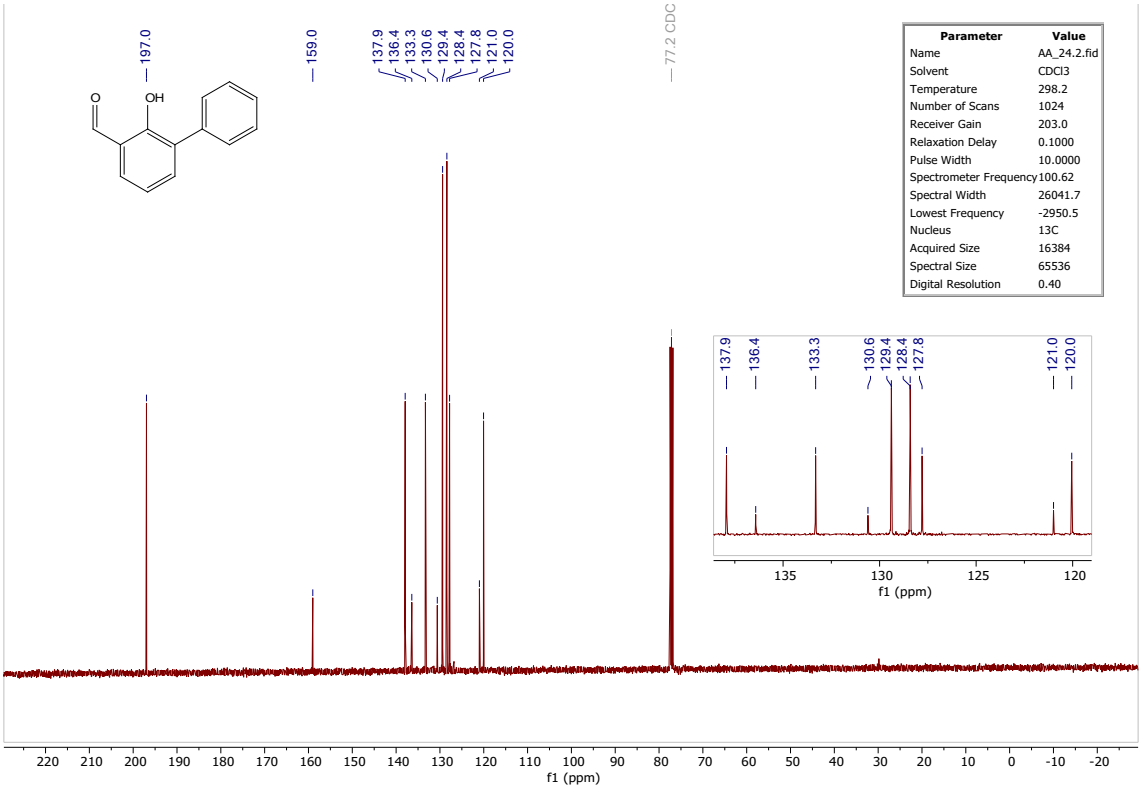

^{13}C NMR spectrum of 1**d** (101 MHz, $CDCl_3$)

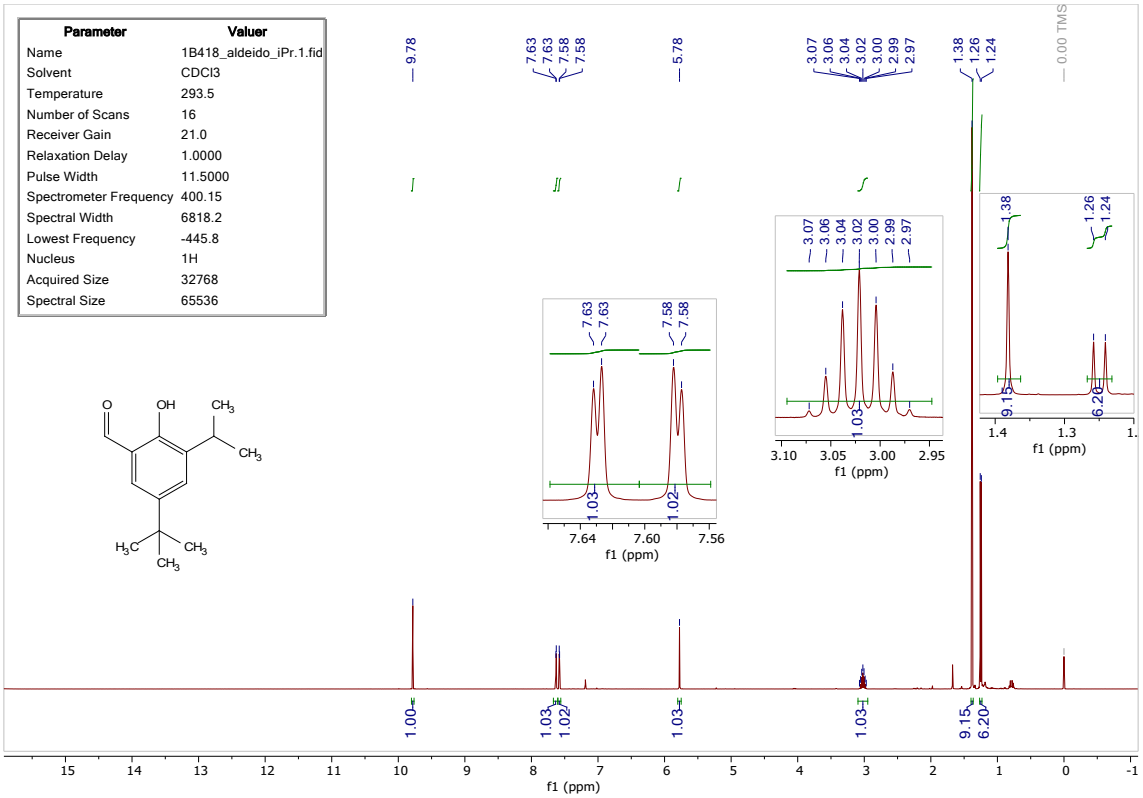

^{1}H NMR spectrum of **1h** (400 MHz, $CDCl_3$)

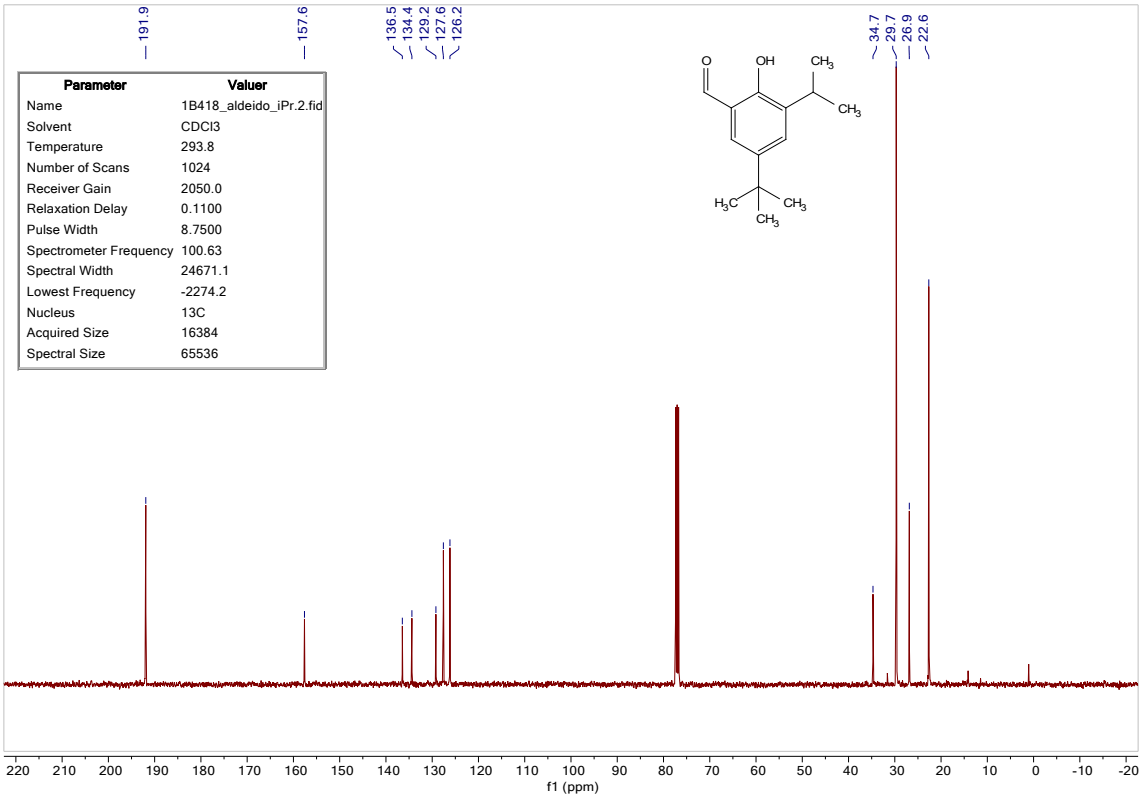

^{13}C NMR spectrum of **1h** (101 MHz, $CDCl_3$)

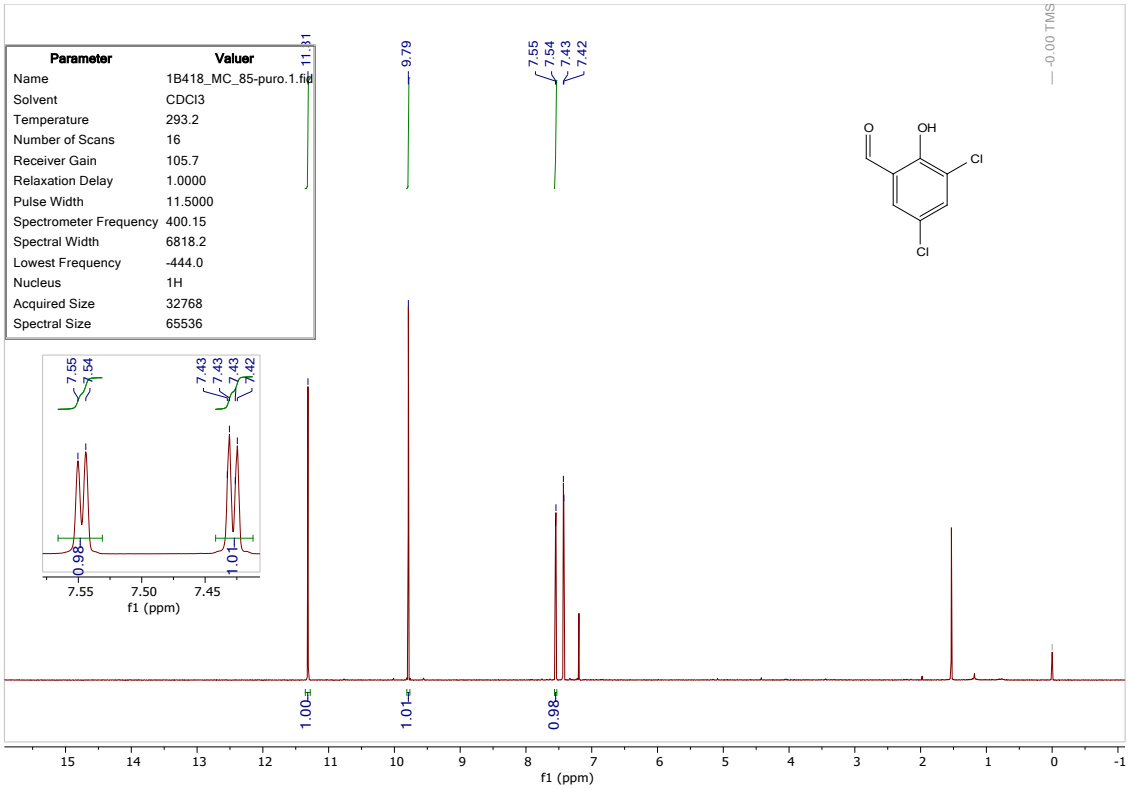

^{1}H NMR spectrum of **1l** (400 MHz, $CDCl_3$)

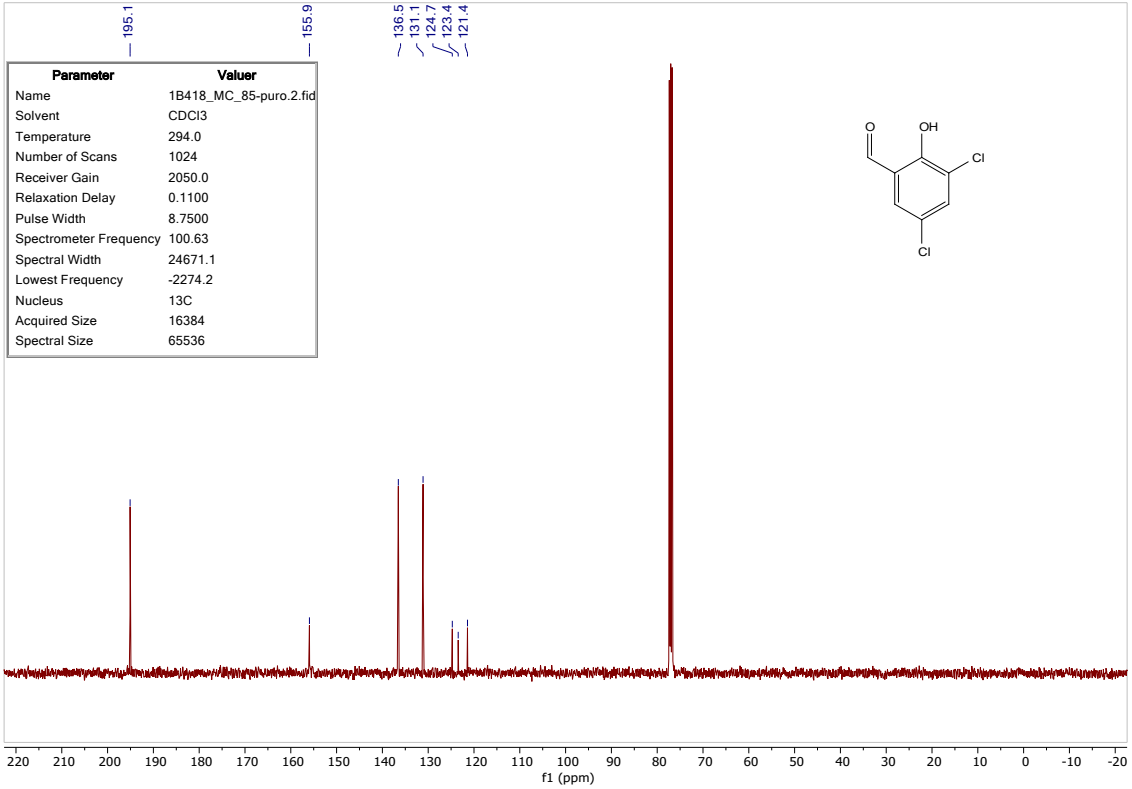

^{13}C NMR spectrum of **1l** (101 MHz, $CDCl_3$)

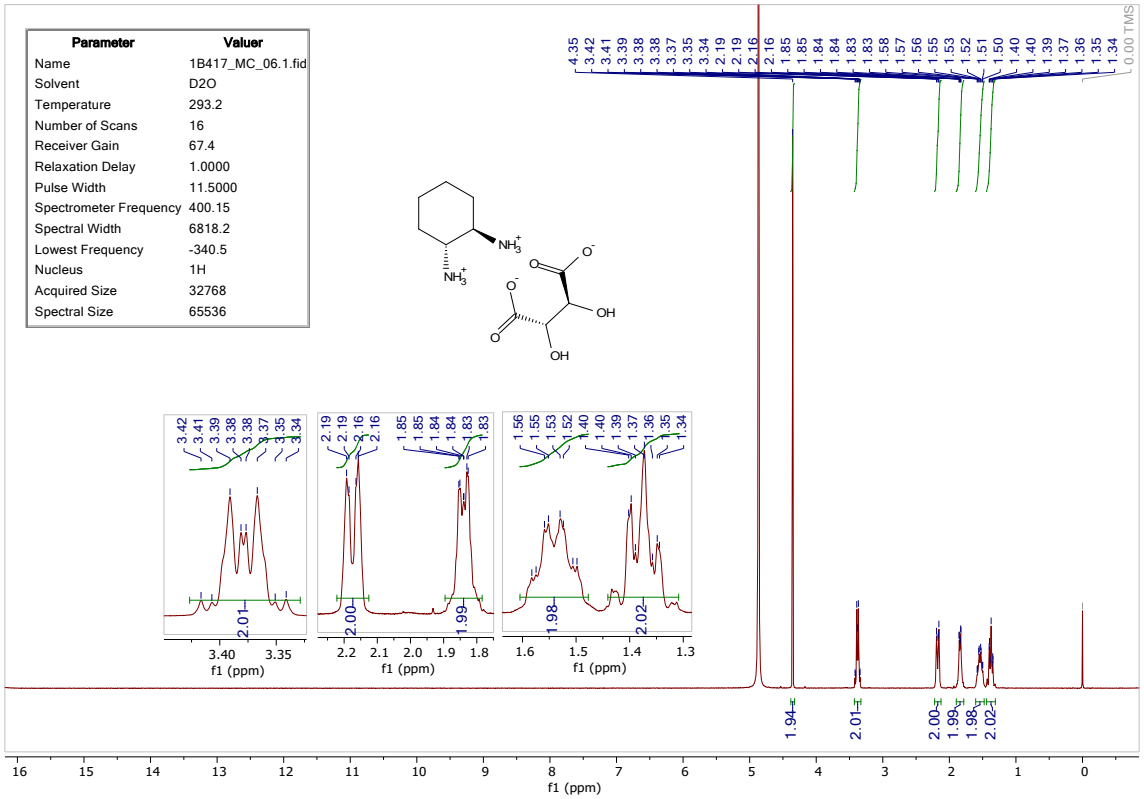

^{1}H NMR spectrum of **2** (400 MHz, D_2O)

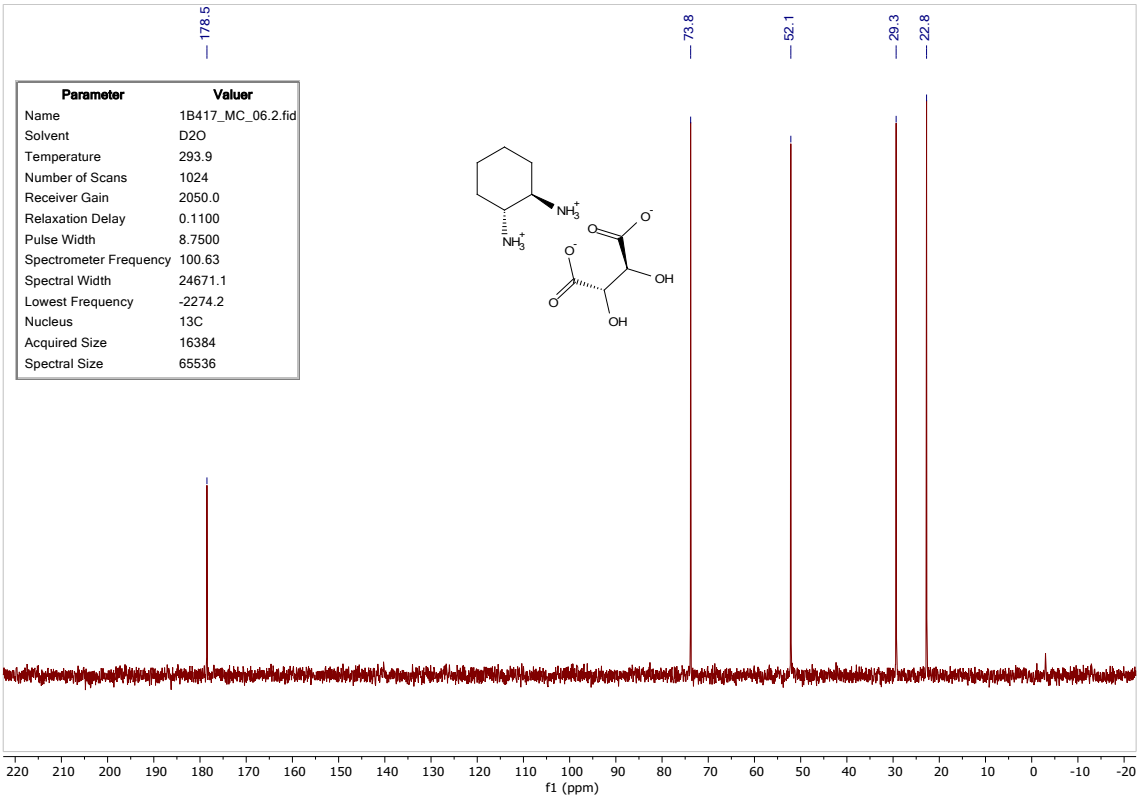

^{13}C NMR spectrum of **2** (101 MHz, D_2O)

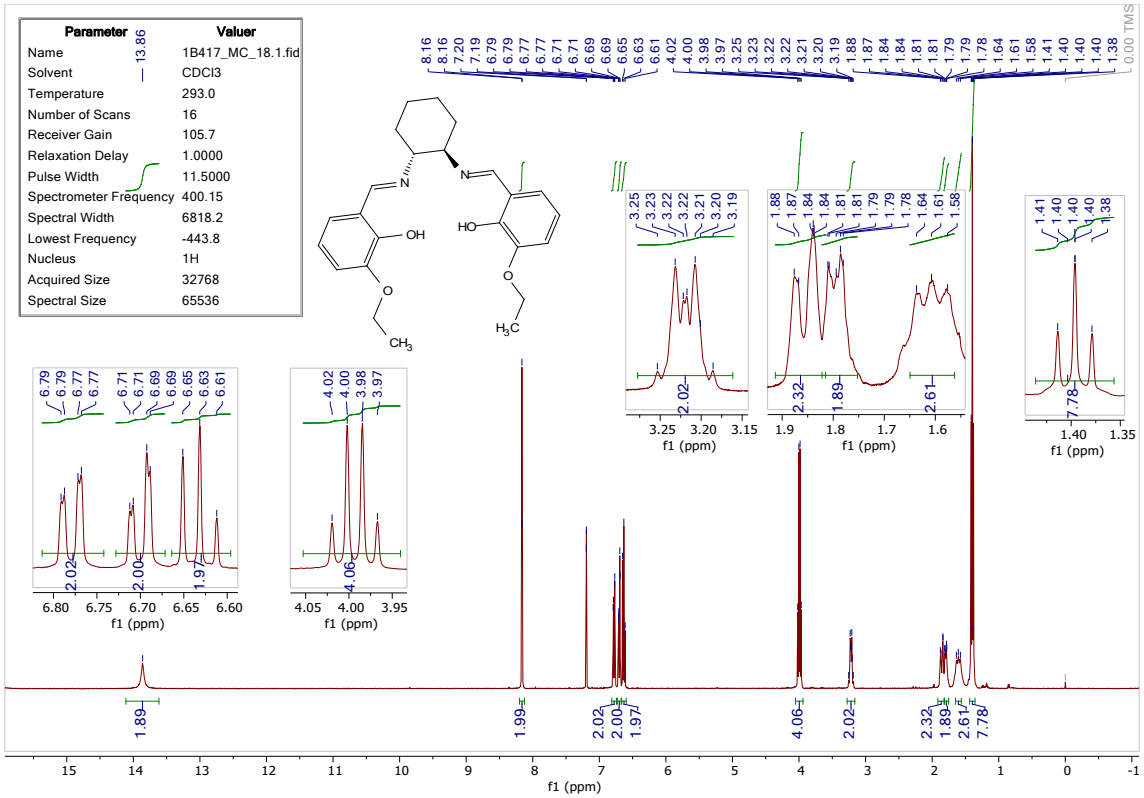

^{1}H NMR spectrum of **3a** (400 MHz, $CDCl_3$)

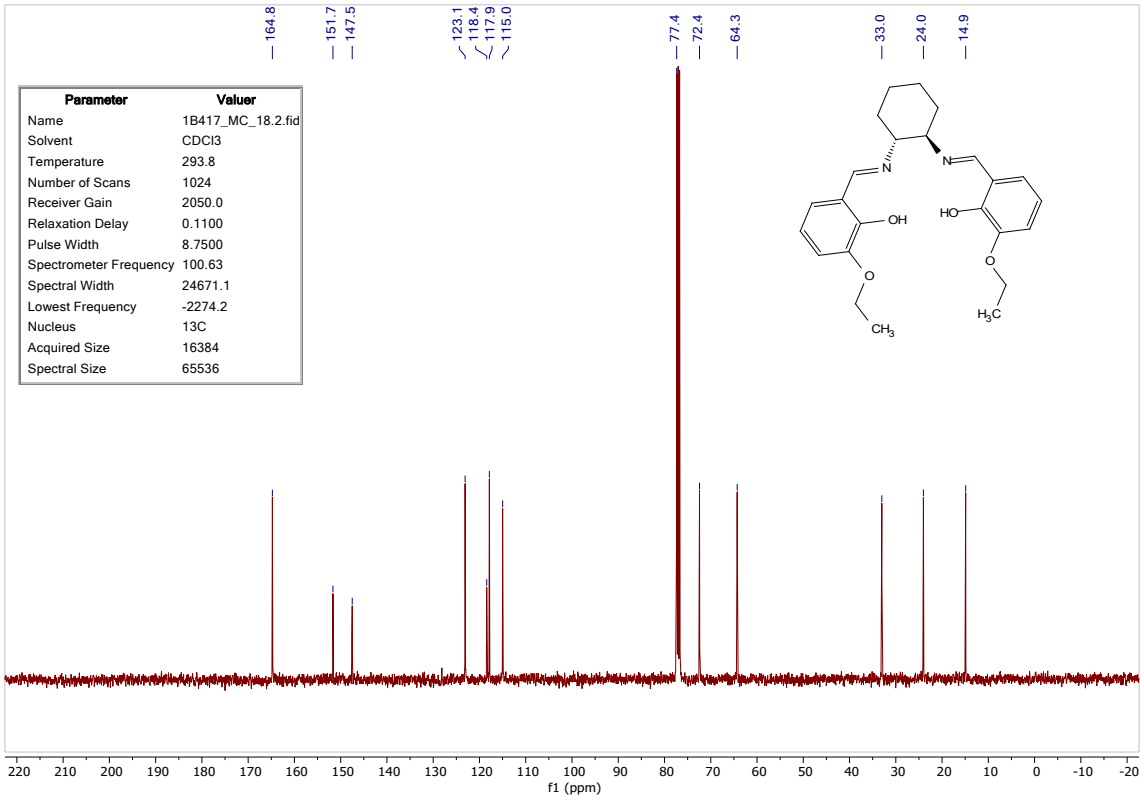

^{13}C NMR spectrum of **3a** (101 MHz, $CDCl_3$)

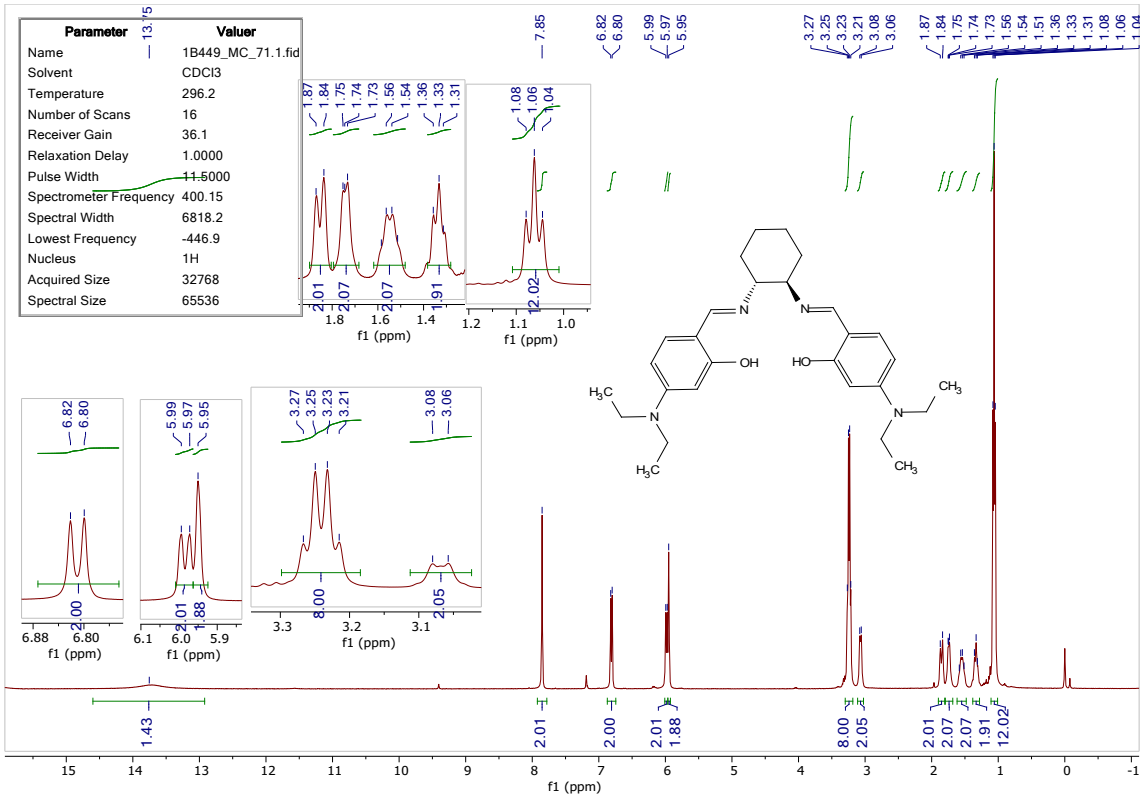

^{1}H NMR spectrum of **3b** (400 MHz, $CDCl_3$)

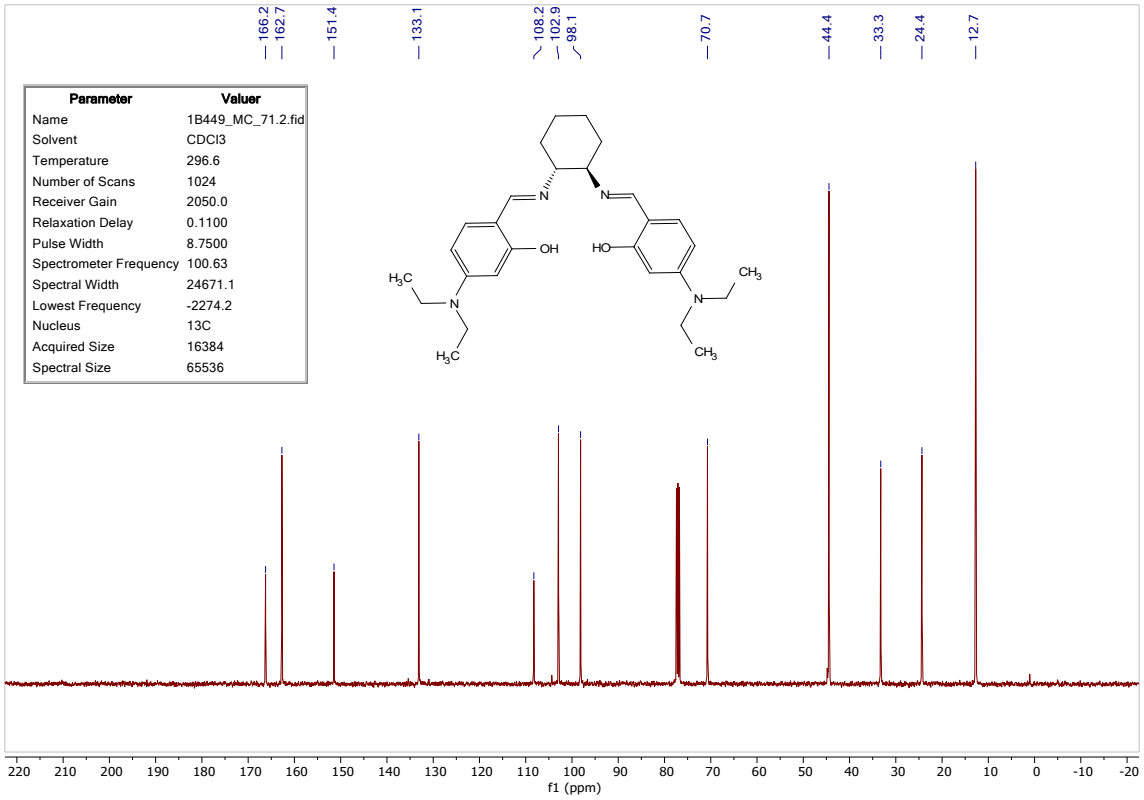

^{13}C NMR spectrum of **3b** (101 MHz, $CDCl_3$)

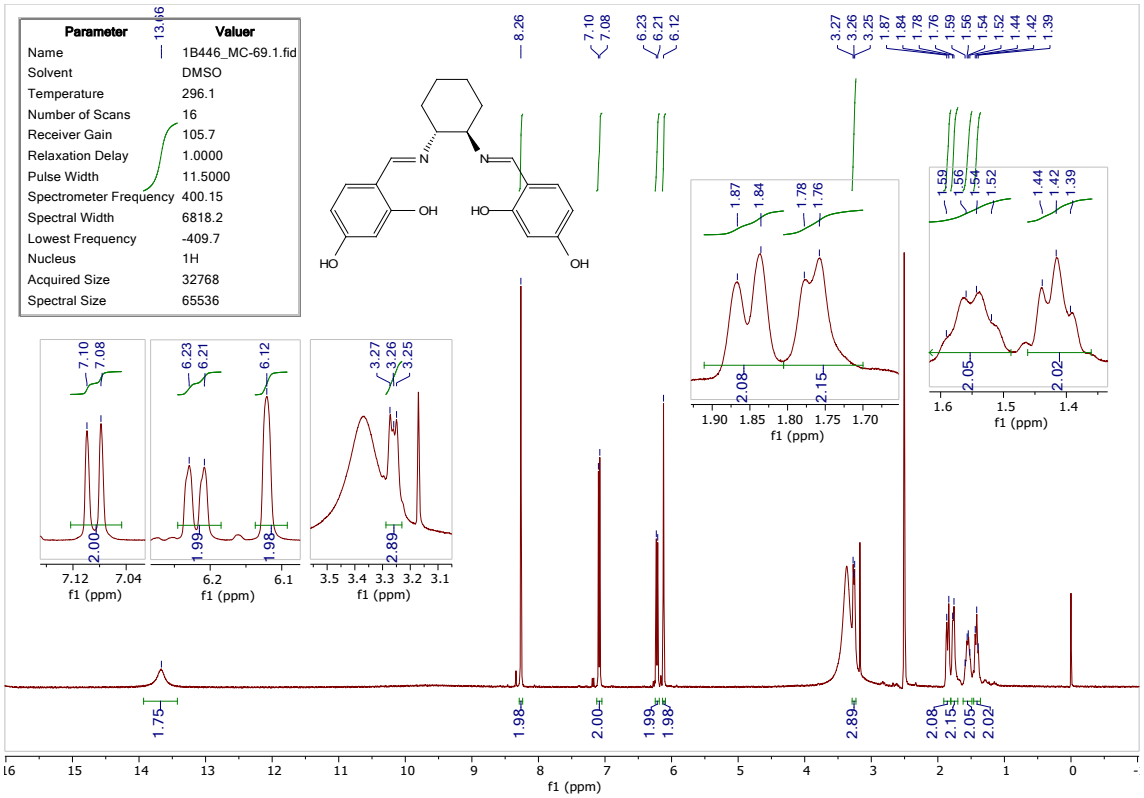

^{1}H NMR spectrum of **3c** (400 MHz, DMSO-*d6*)

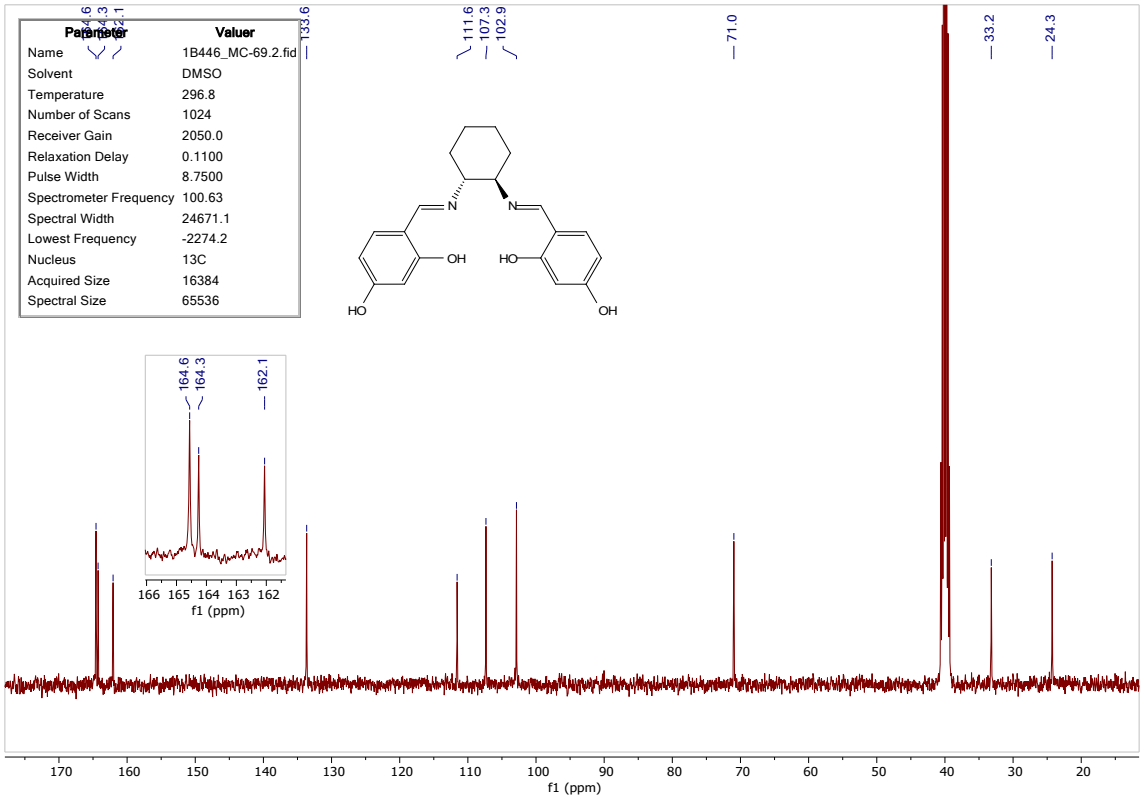

^{13}C NMR spectrum of **3c** (101 MHz, DMSO-*d6*)

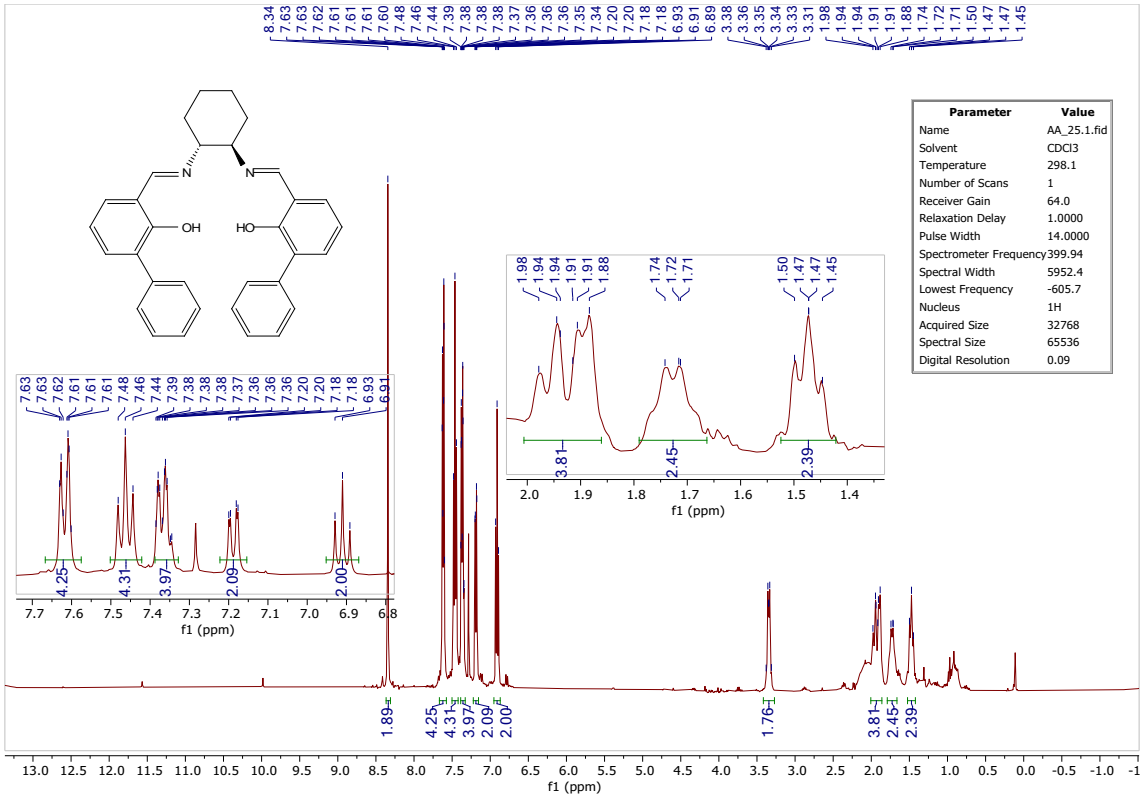

^{1}H NMR spectrum of **3d** (400 MHz, $CDCl_3$)

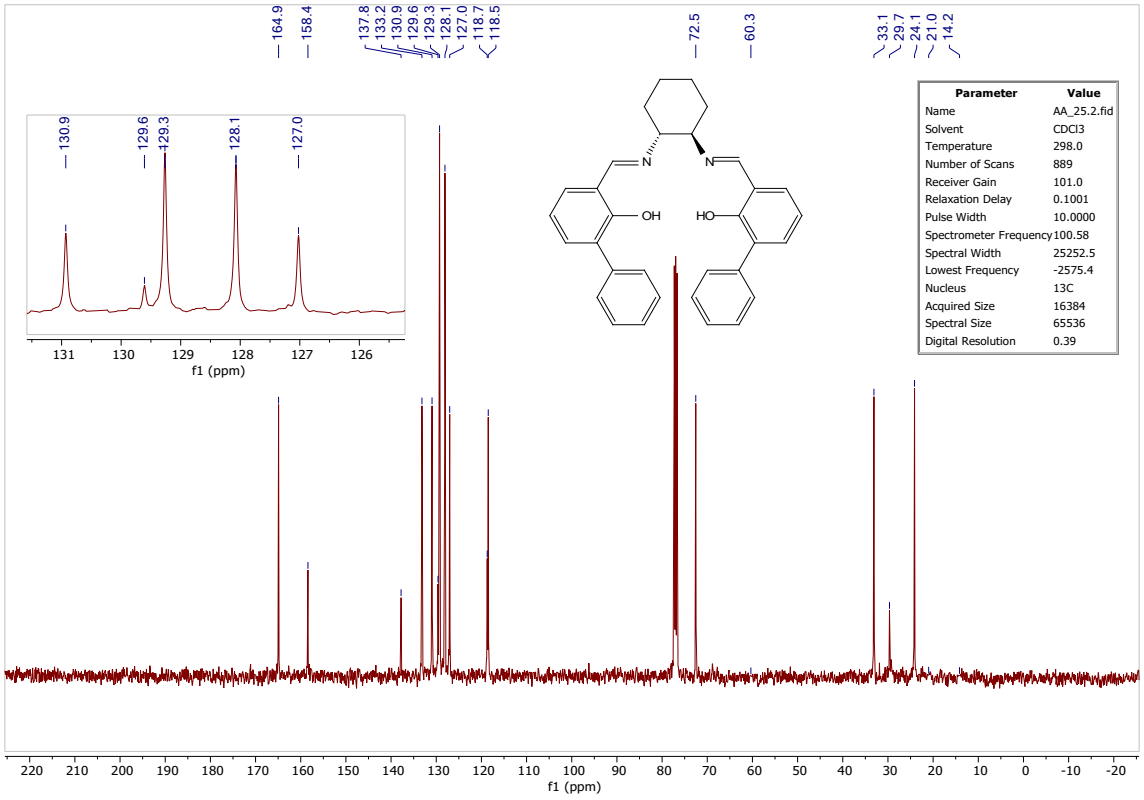

^{13}C NMR spectrum of **3d** (101 MHz, $CDCl_3$)

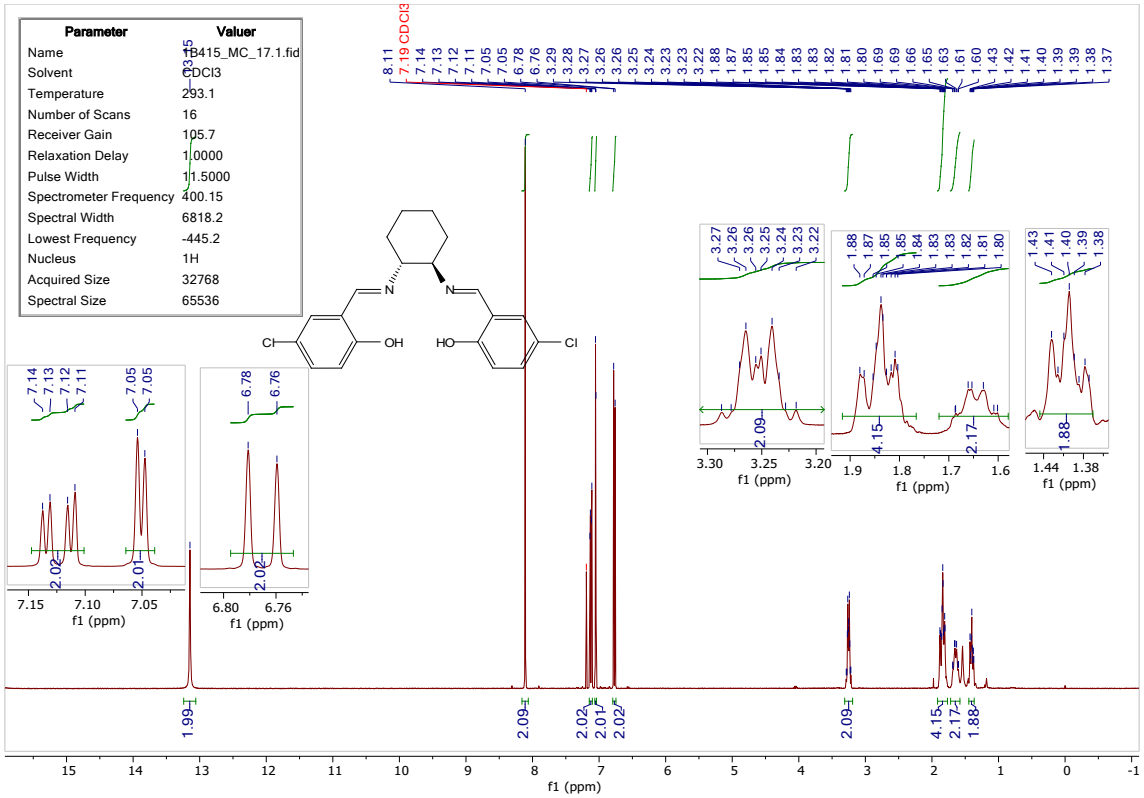

^{1}H NMR spectrum of **3e** (400 MHz, $CDCl_3$)

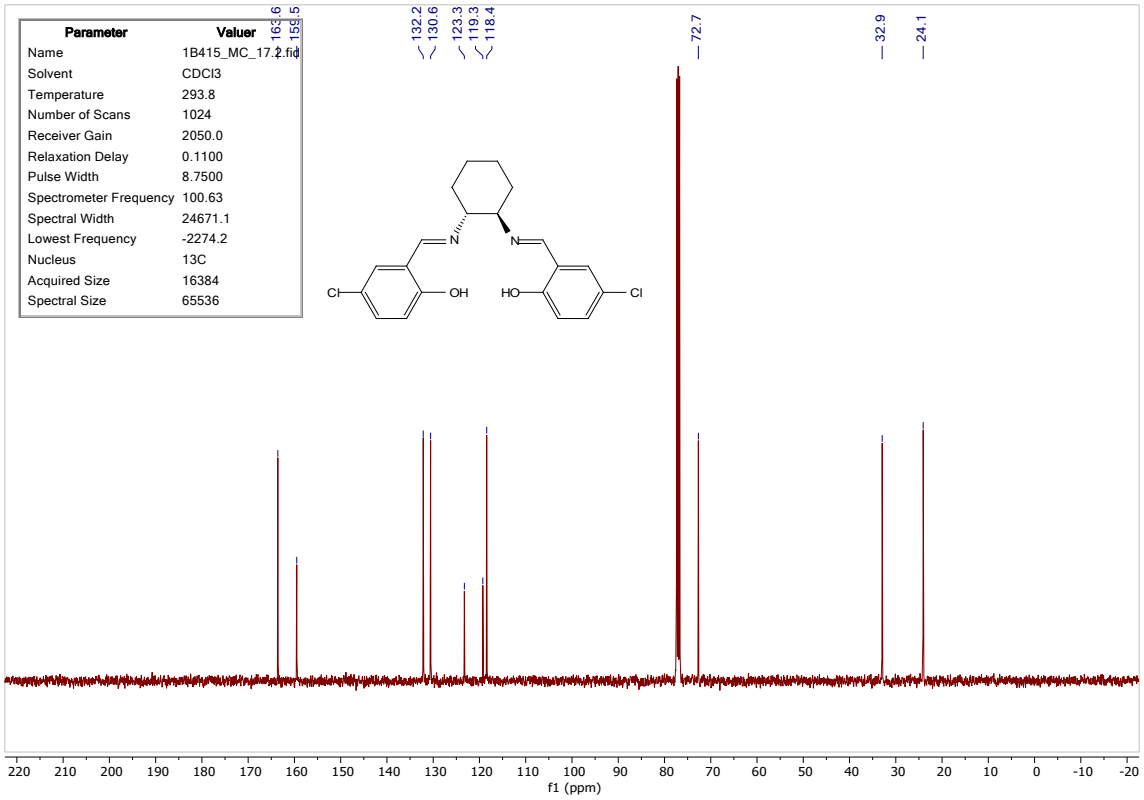

^{13}C NMR spectrum of **3e** (101 MHz, $CDCl_3$)

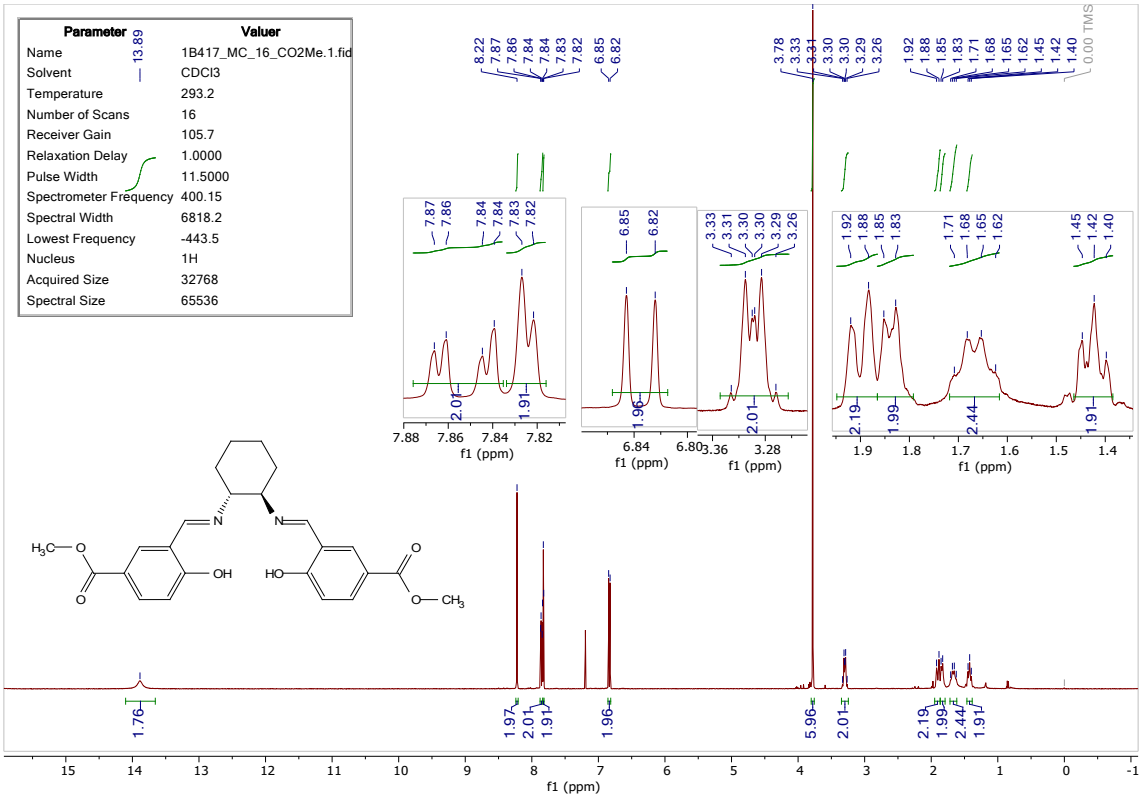

^{1}H NMR spectrum of **3f** (400 MHz, $CDCl_3$)

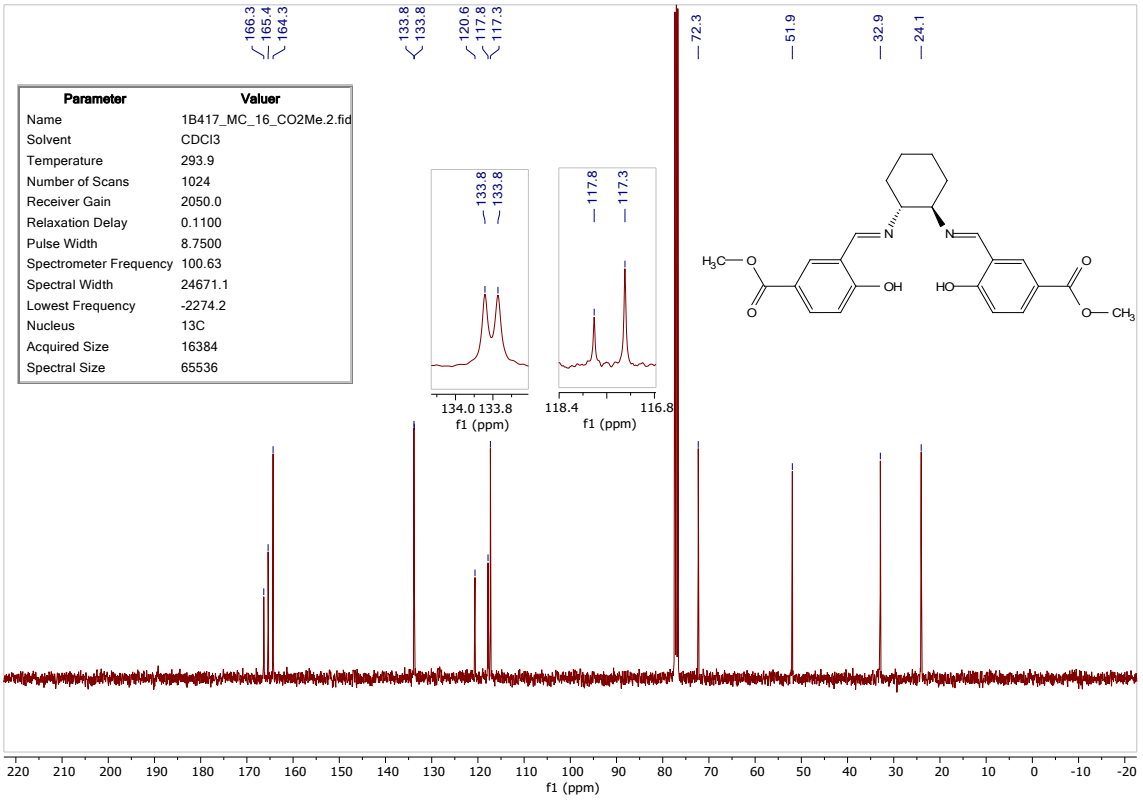

^{13}C NMR spectrum of **3f** (101 MHz, $CDCl_3$)

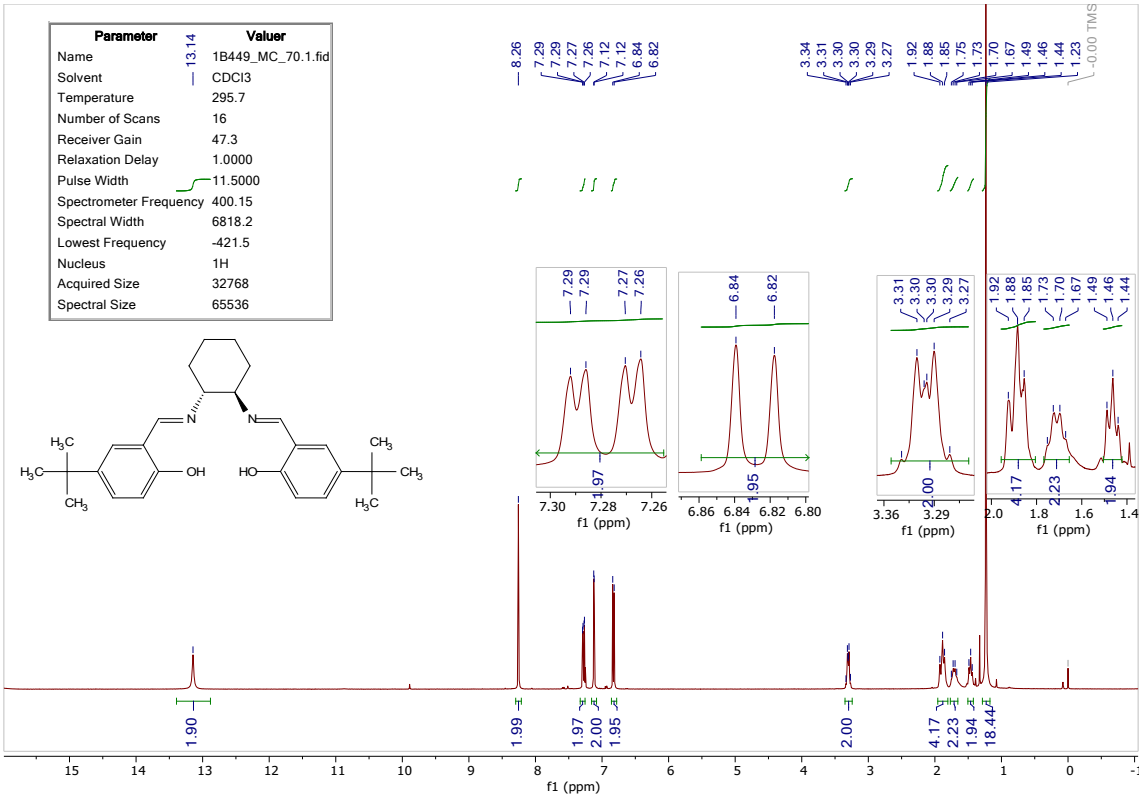

^{1}H NMR spectrum of **3g** (400 MHz, $CDCl_3$)

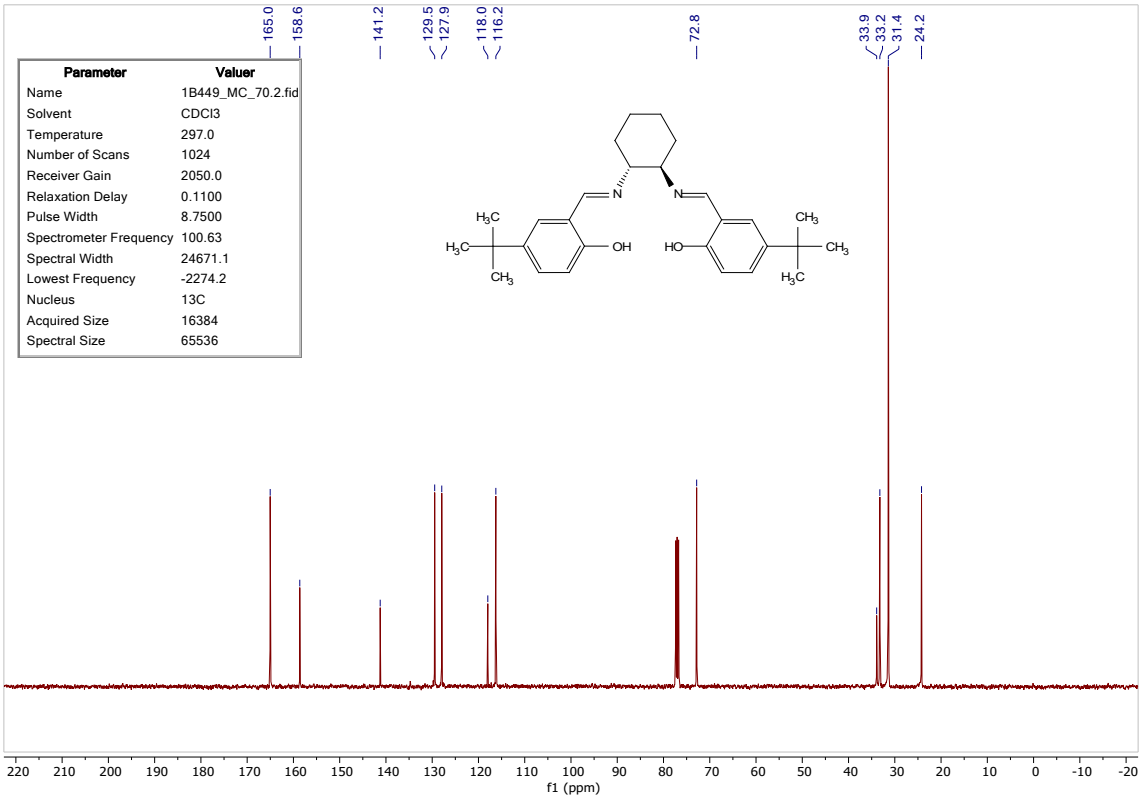

^{13}C NMR spectrum of **3g** (101 MHz, $CDCl_3$)

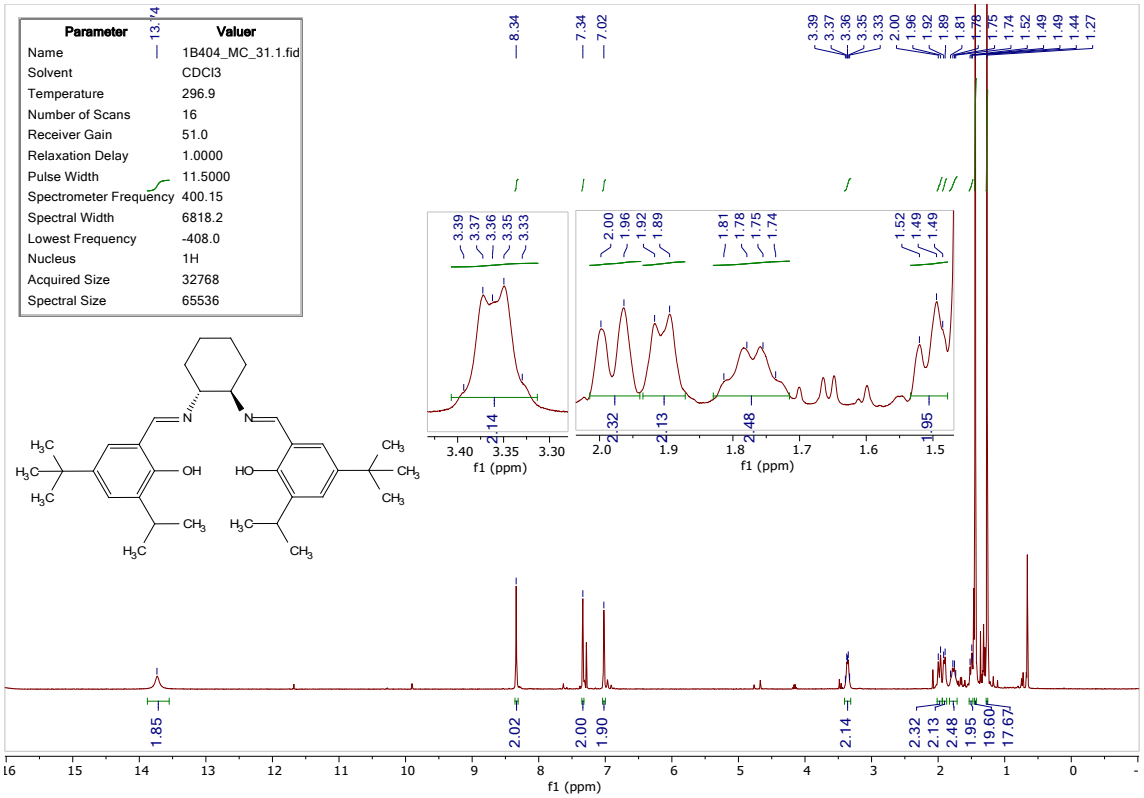

^{1}H NMR spectrum of **3h** (400 MHz, $CDCl_3$)

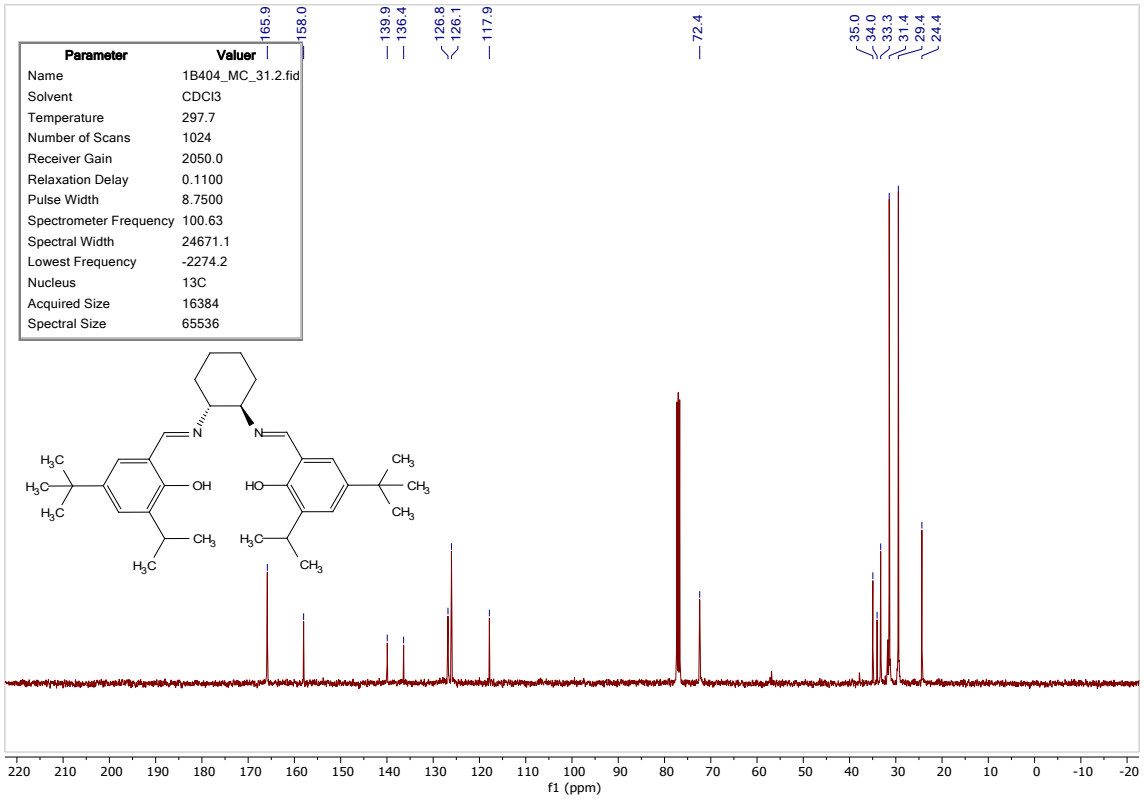

^{13}C NMR spectrum of **3h** (101 MHz, $CDCl_3$)

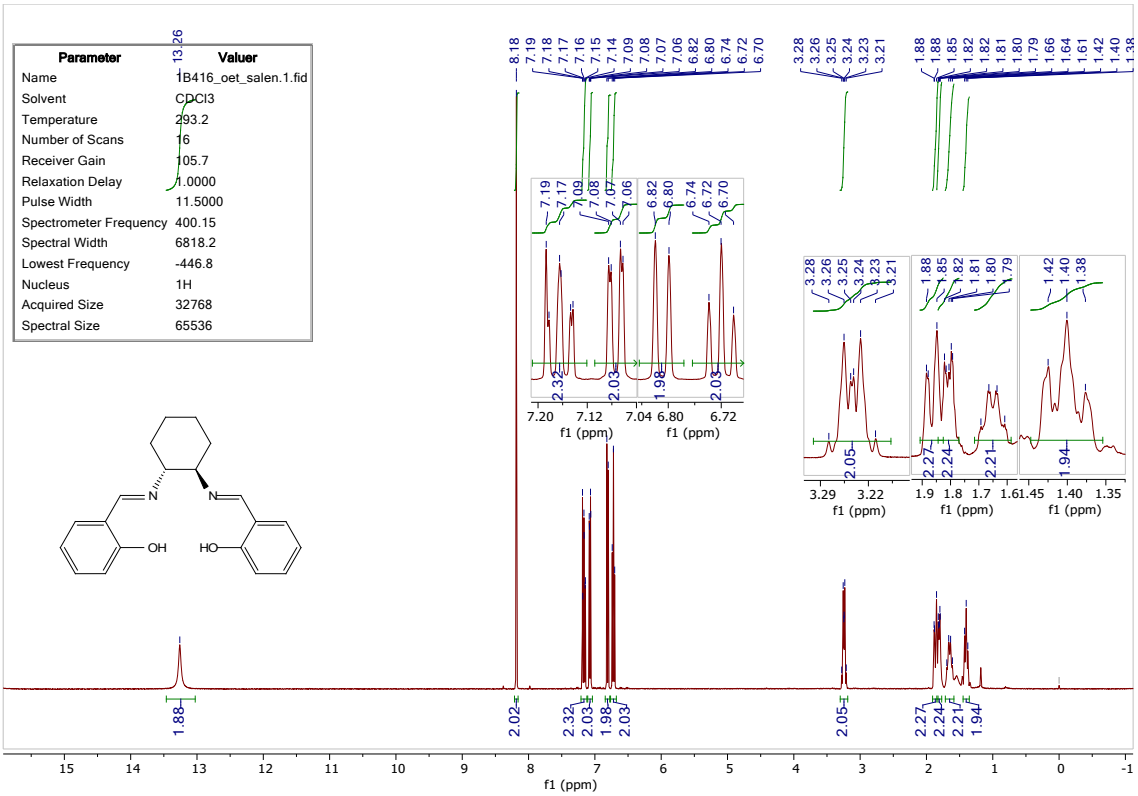

^{1}H NMR spectrum of **3i** (400 MHz, $CDCl_3$)

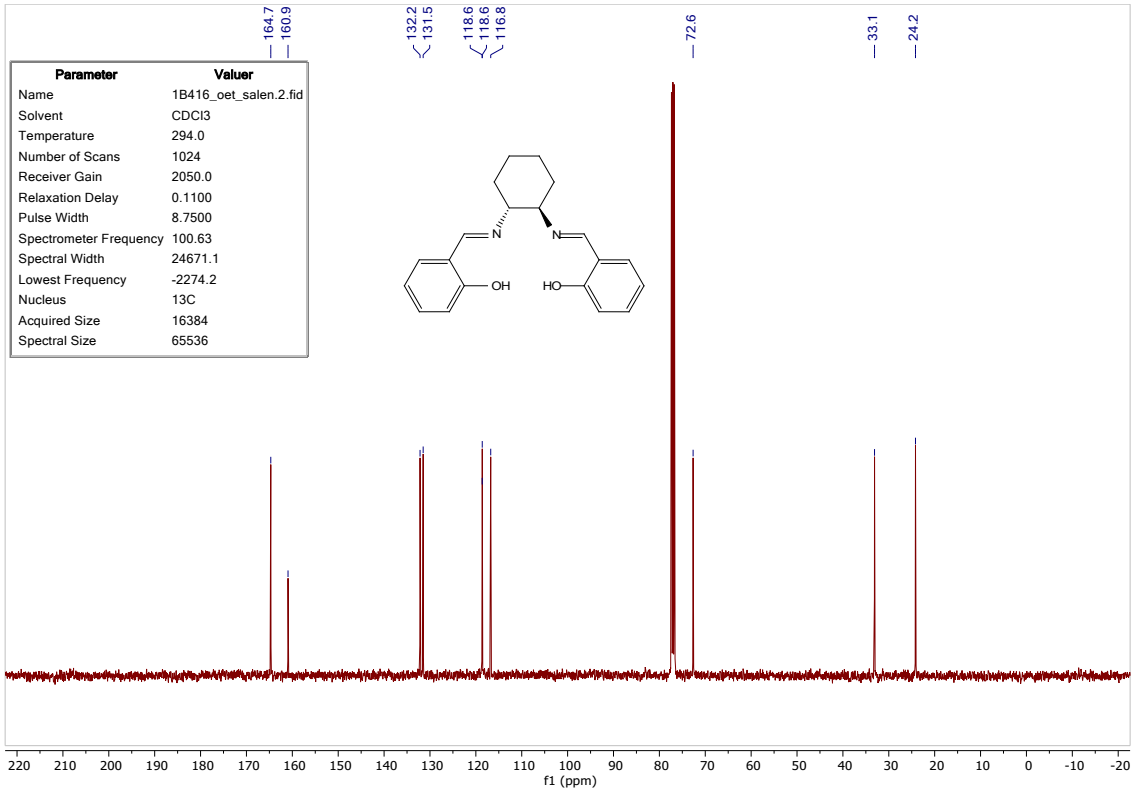

^{13}C NMR spectrum of **3i** (101 MHz, $CDCl_3$)

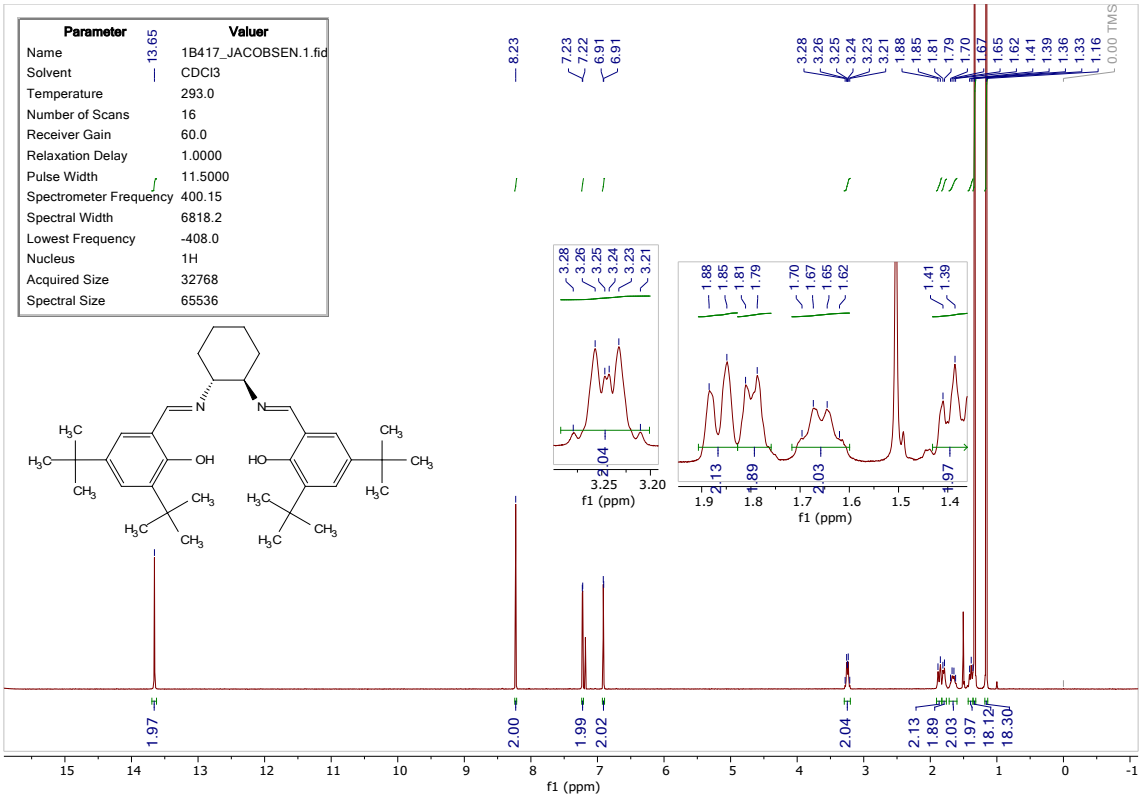

^{1}H NMR spectrum of **3j** (400 MHz, $CDCl_3$)

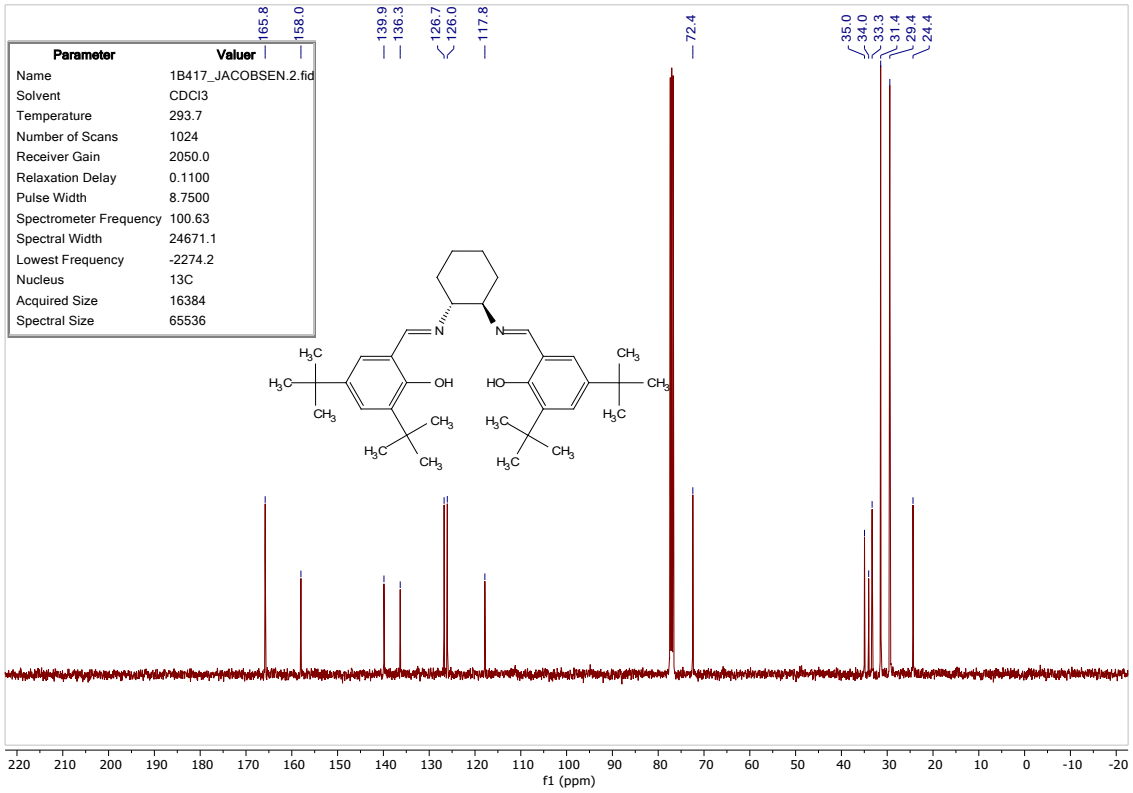

^{13}C NMR spectrum of **3j** (101 MHz, $CDCl_3$)

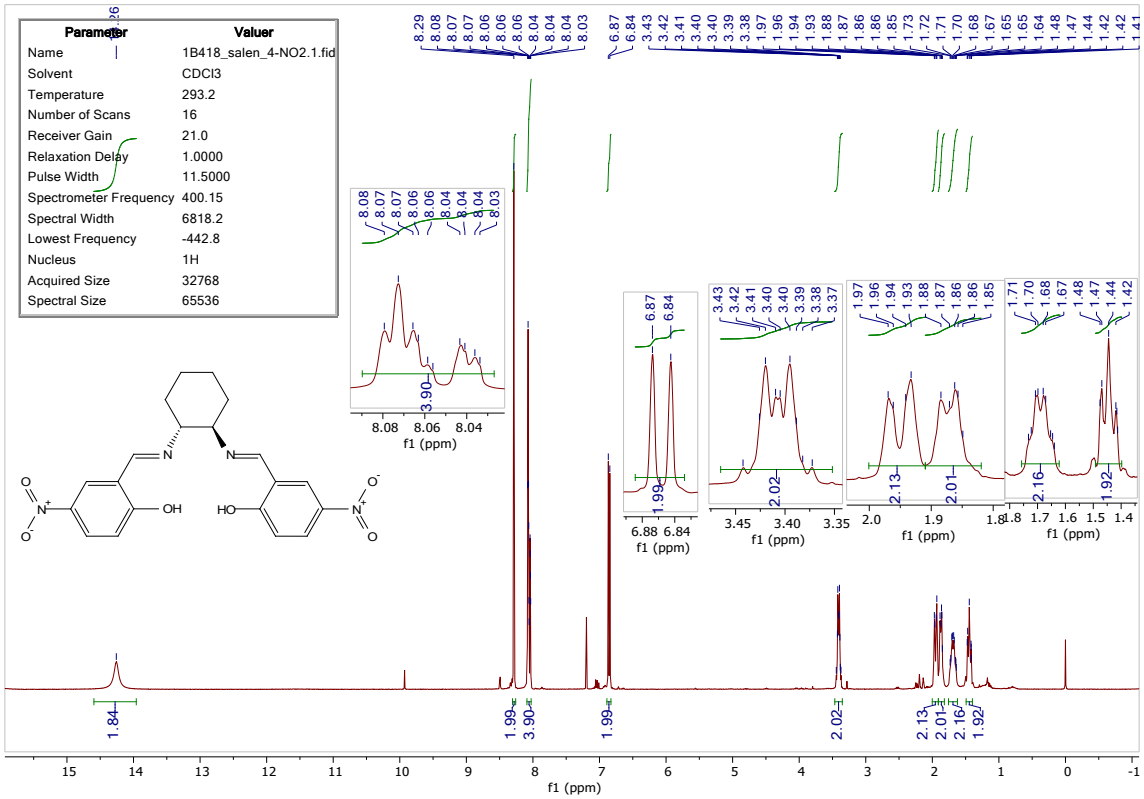

^{1}H NMR spectrum of **3k** (400 MHz, $CDCl_3$)

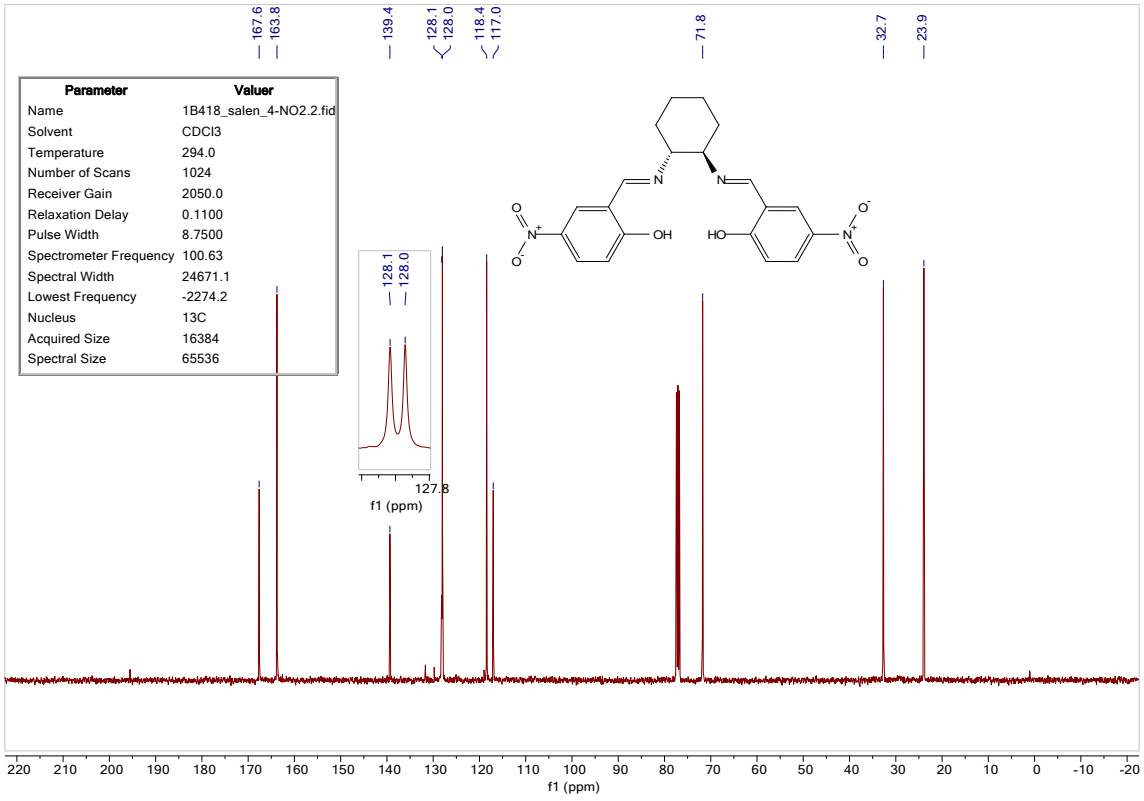

^{13}C NMR spectrum of **3k** (101 MHz, $CDCl_3$)

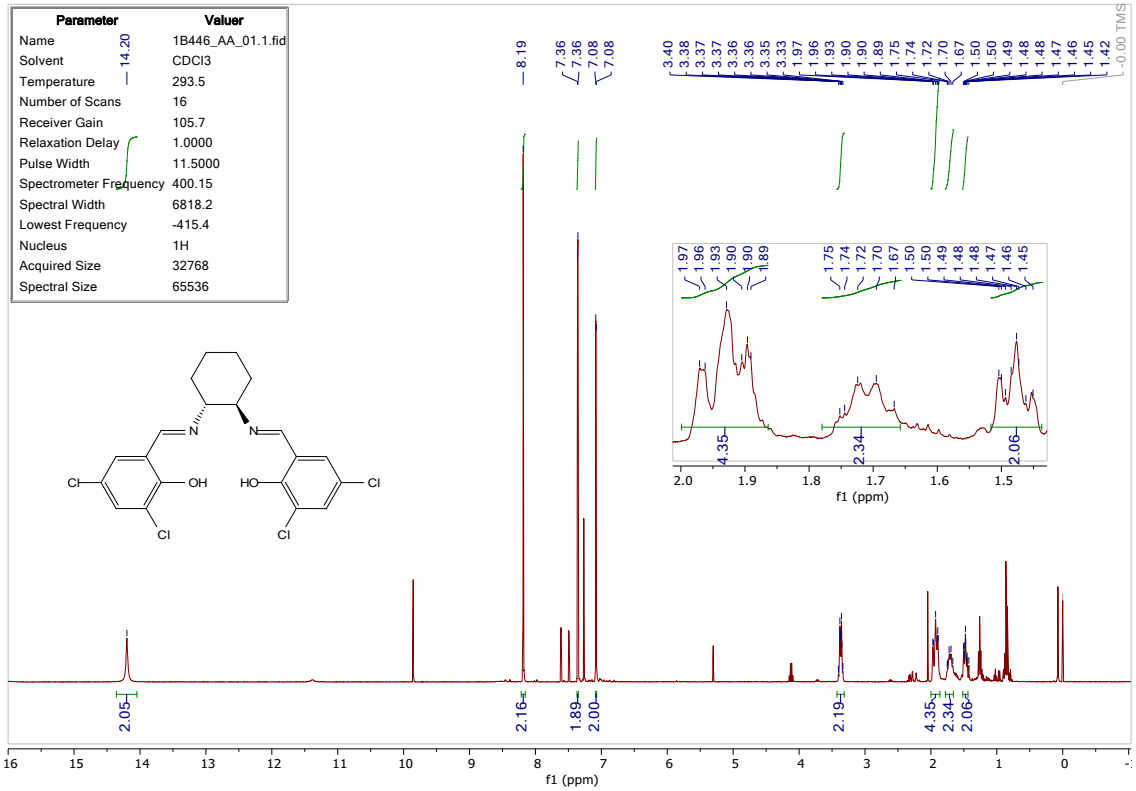

^{1}H NMR spectrum of **3l** (400 MHz, $CDCl_3$)

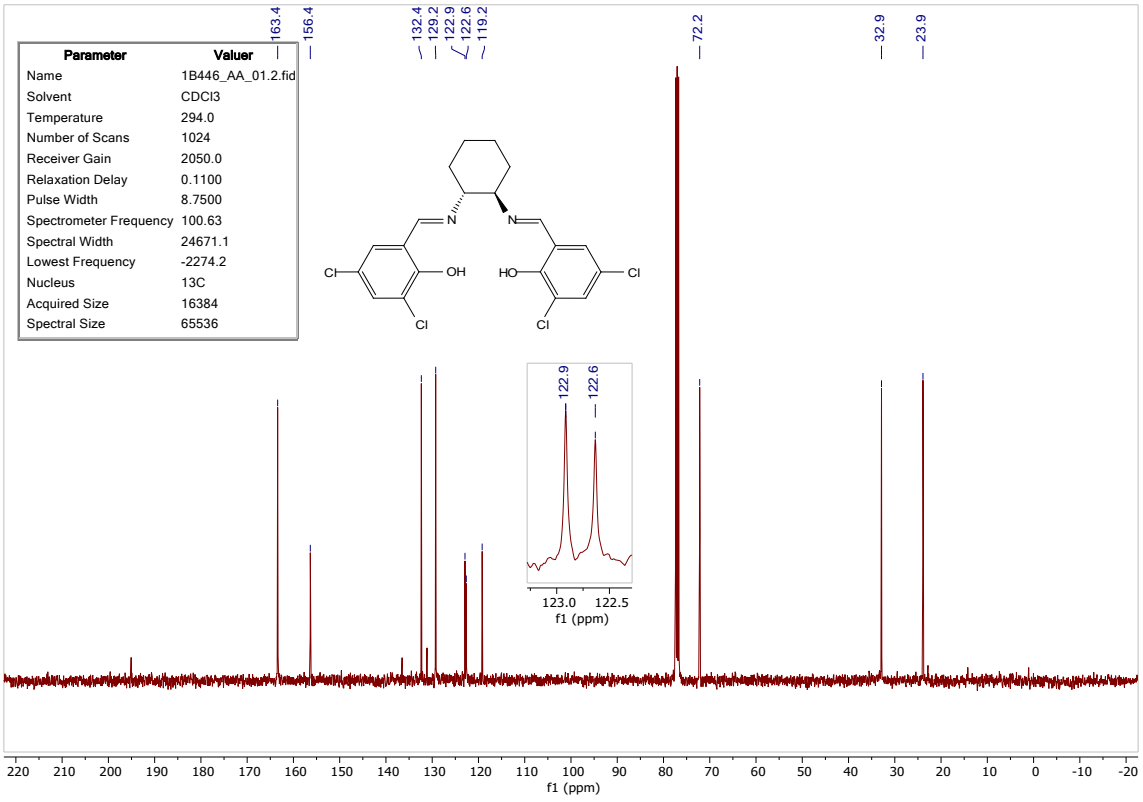

^{13}C NMR spectrum of **3l** (101 MHz, $CDCl_3$)

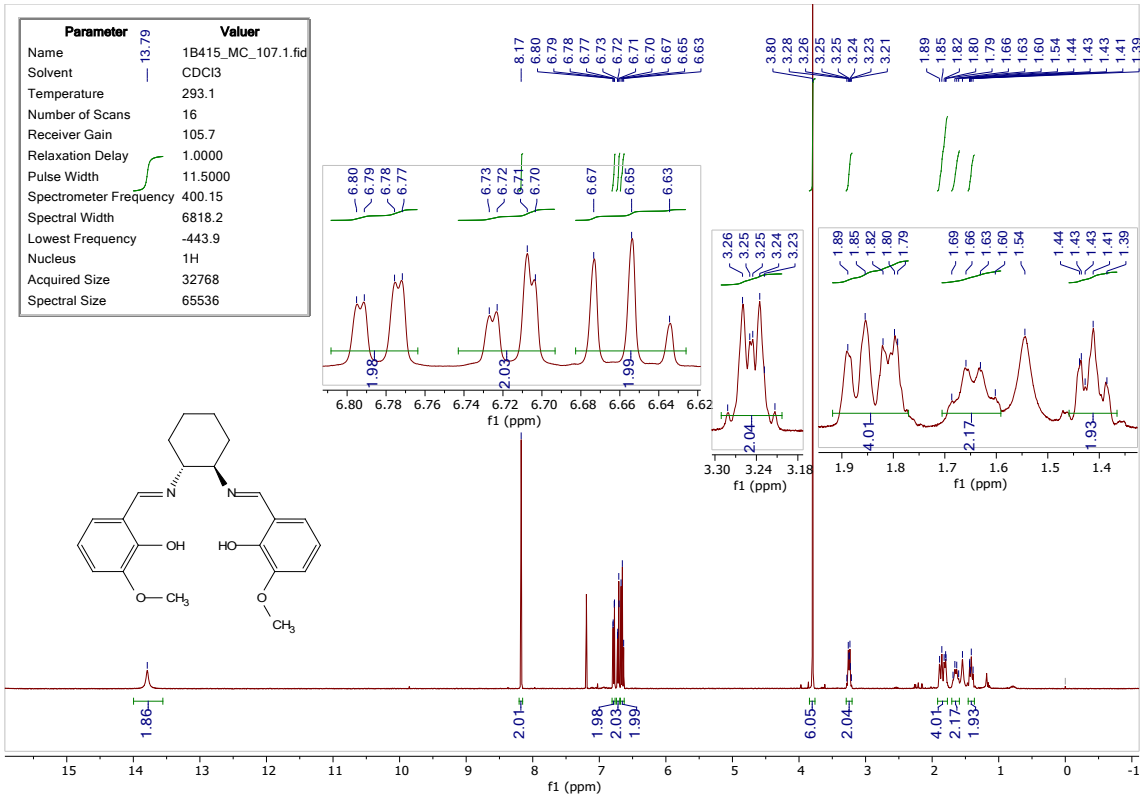

^{1}H NMR spectrum of **3m** (400 MHz, $CDCl_3$)

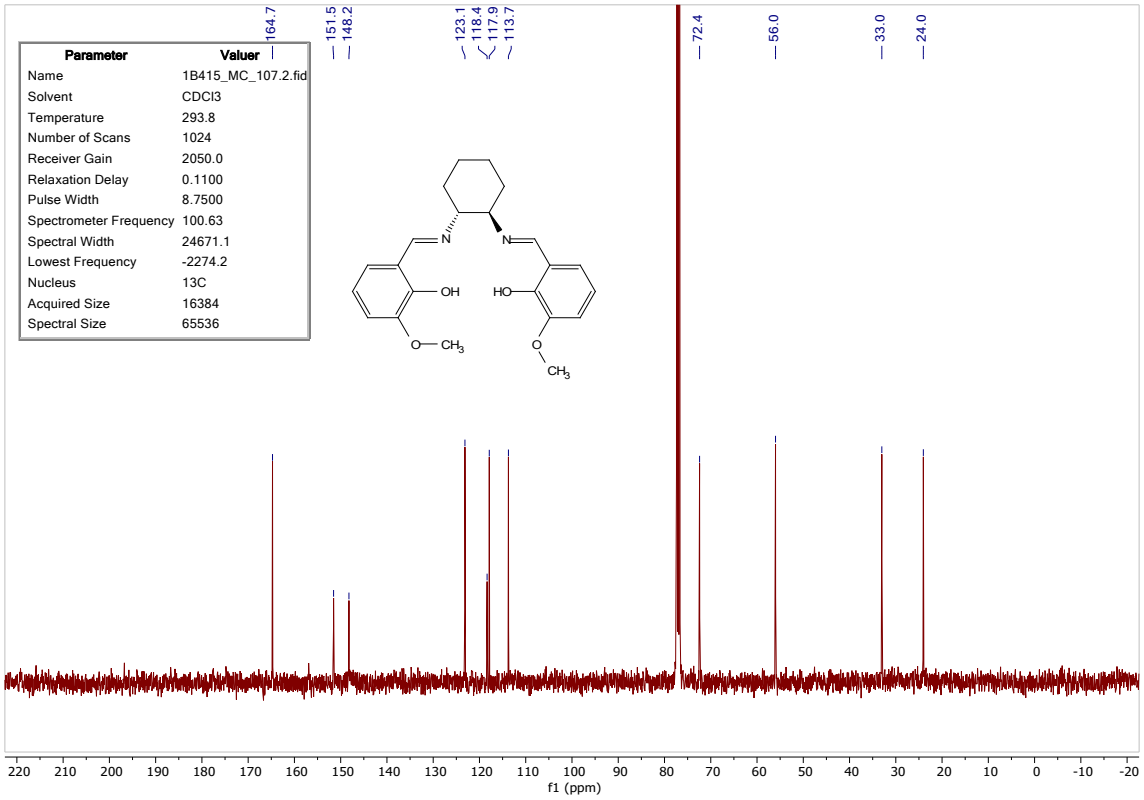

^{13}C NMR spectrum of **3m** (101 MHz, $CDCl_3$)

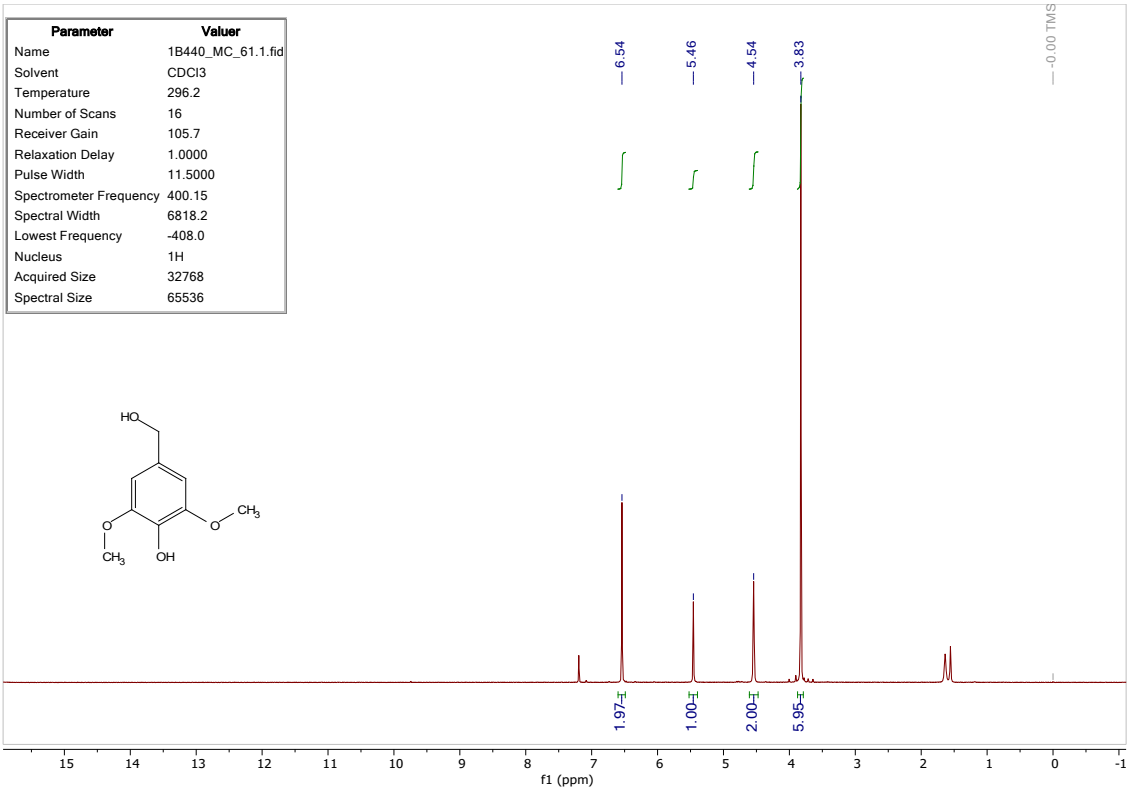

^{1}H NMR spectrum of **Syringyl Alcohol (5)** (400 MHz, $CDCl_3$)

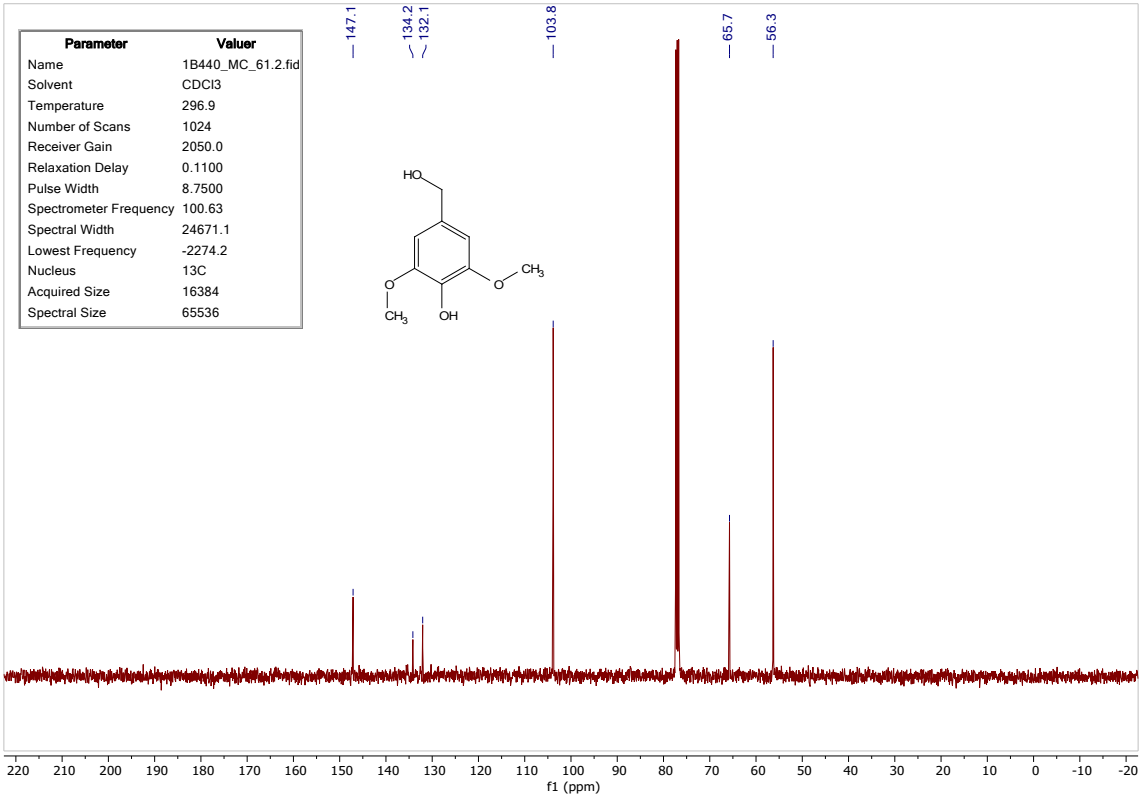

^{13}C NMR spectrum of **Syringyl Alcohol (5)** (101 MHz, $CDCl_3$)

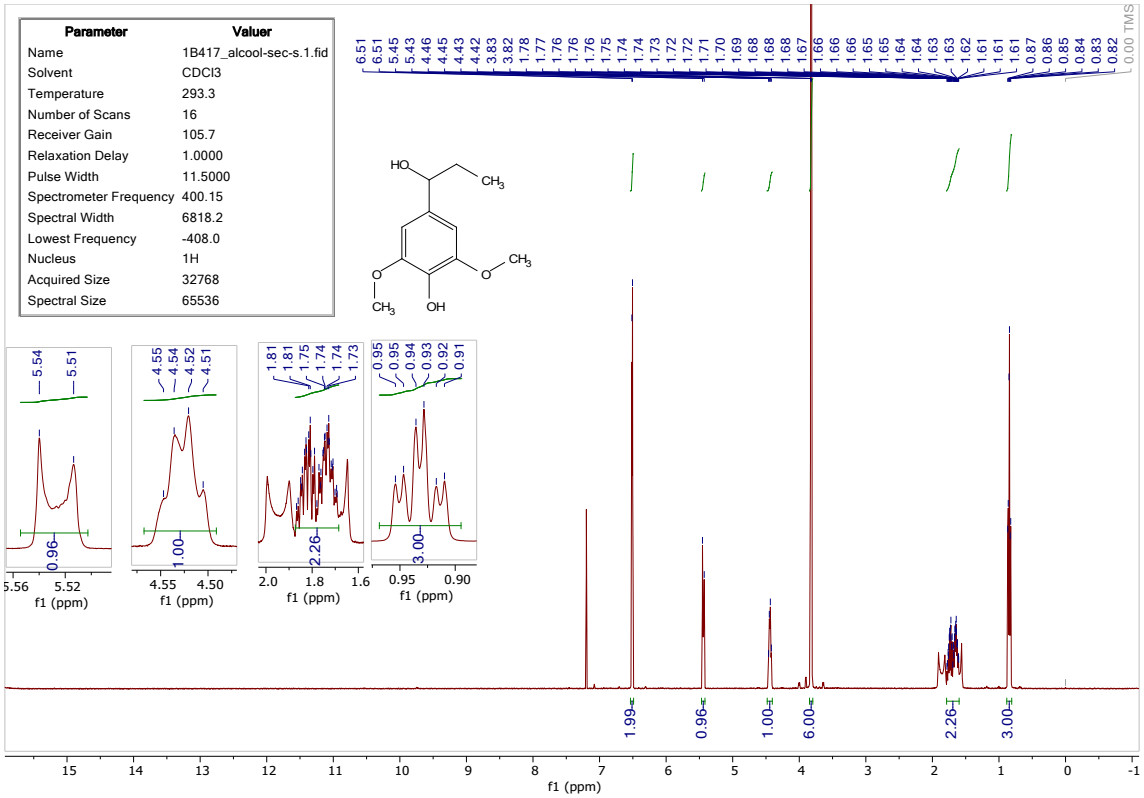

^{1}H NMR spectrum of **4-(1-Hydroxypropyl)-2,6-dimethoxyphenol (9)** (400 MHz, $CDCl_3$)

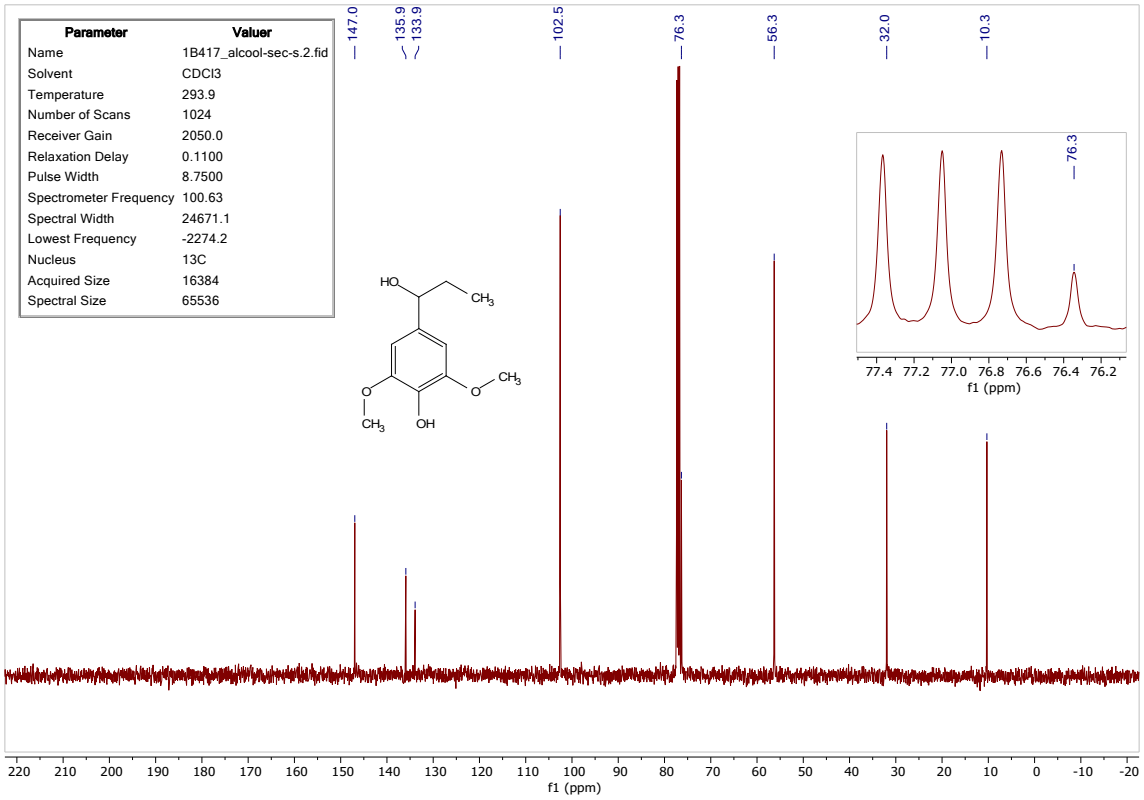

^{13}C NMR spectrum of **4-(1-Hydroxypropyl)-2,6-dimethoxyphenol (9)** (101 MHz, $CDCl_3$)

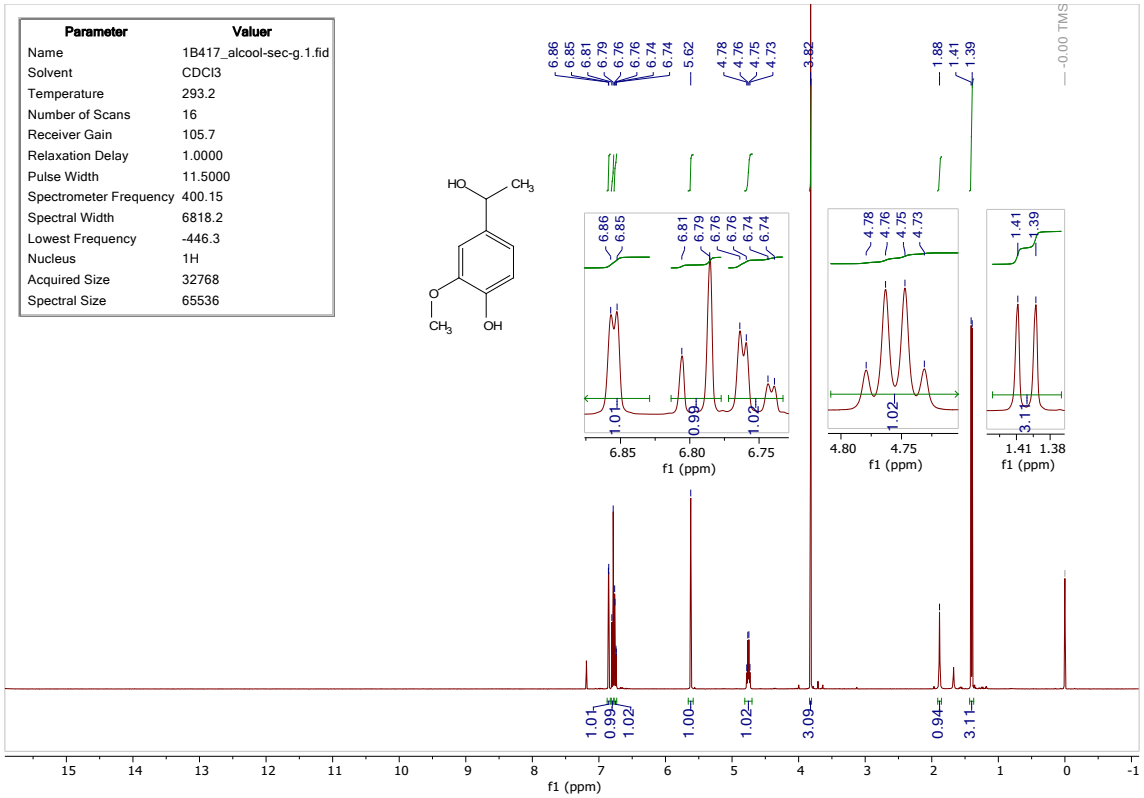

^{1}H NMR spectrum of **4-(1-Hydroxyethyl)-2-methoxyphenol (10)** (400 MHz, $CDCl_3$)

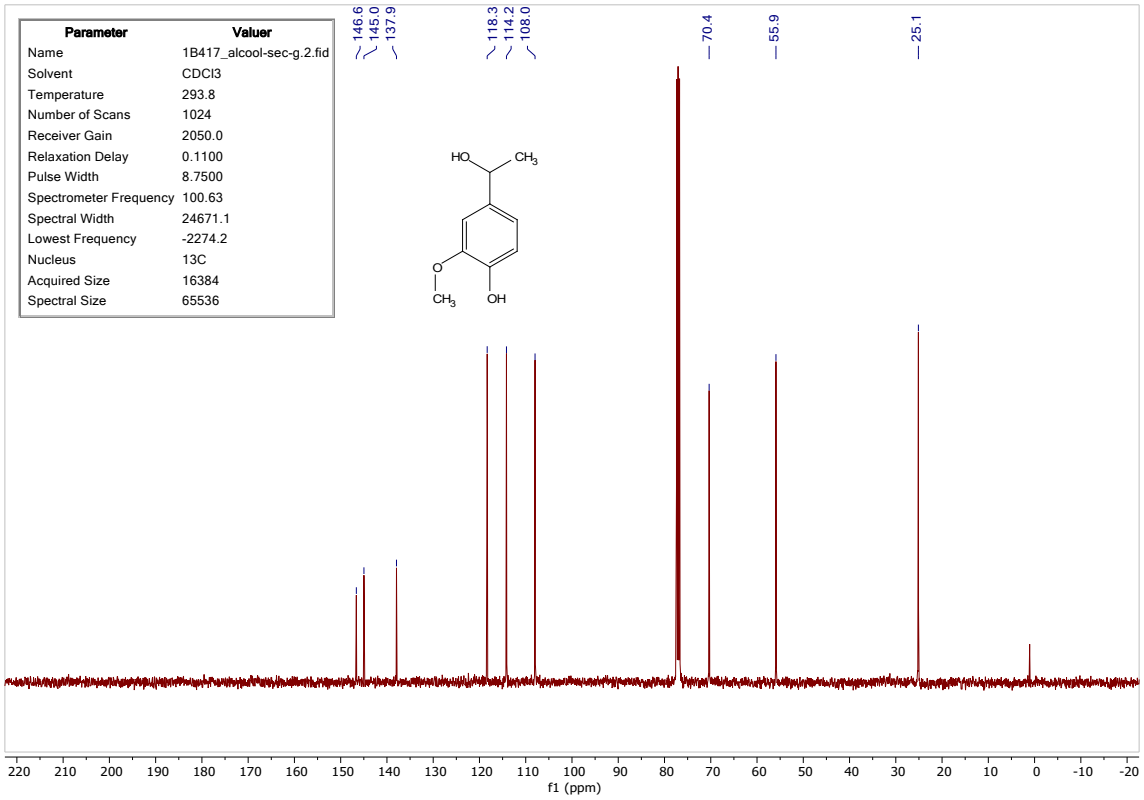

^{13}C NMR spectrum of **4-(1-Hydroxyethyl)-2-methoxyphenol (10)** (101 MHz, $CDCl_3$)

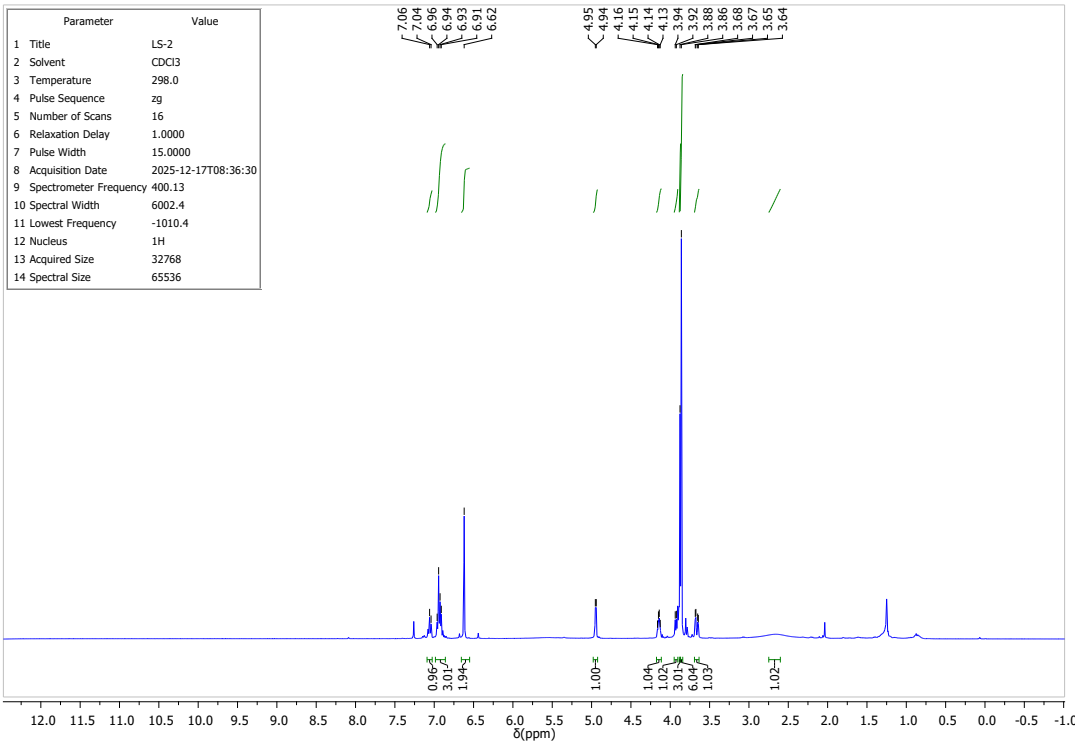

^{1}H NMR spectrum of **1-(4-Hydroxy-3,5-dimethoxyphenyl)-2-(2-methoxyphenoxy)propane-1,3-diol (12)** (400 MHz, $CDCl_3$)

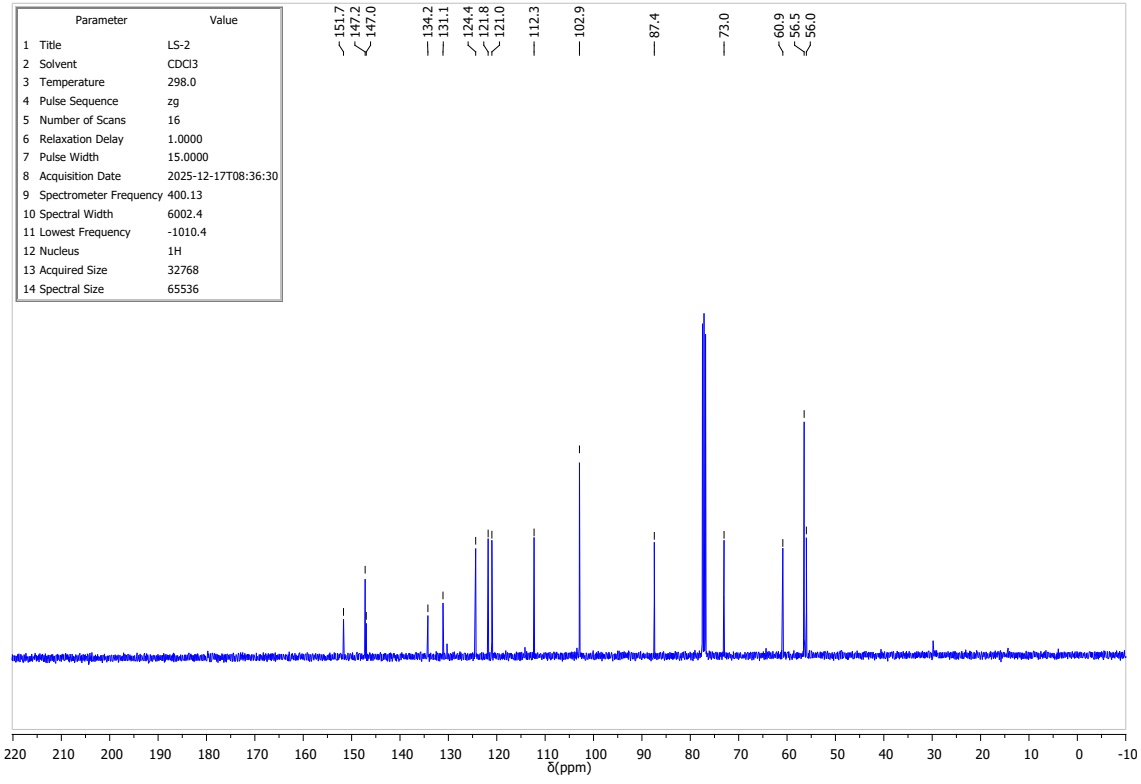

^{13}C NMR spectrum of **1-(4-Hydroxy-3,5-dimethoxyphenyl)-2-(2-methoxyphenoxy)propane-1,3-diol (12)** (101 MHz, $CDCl_3$)

S11. HRMS

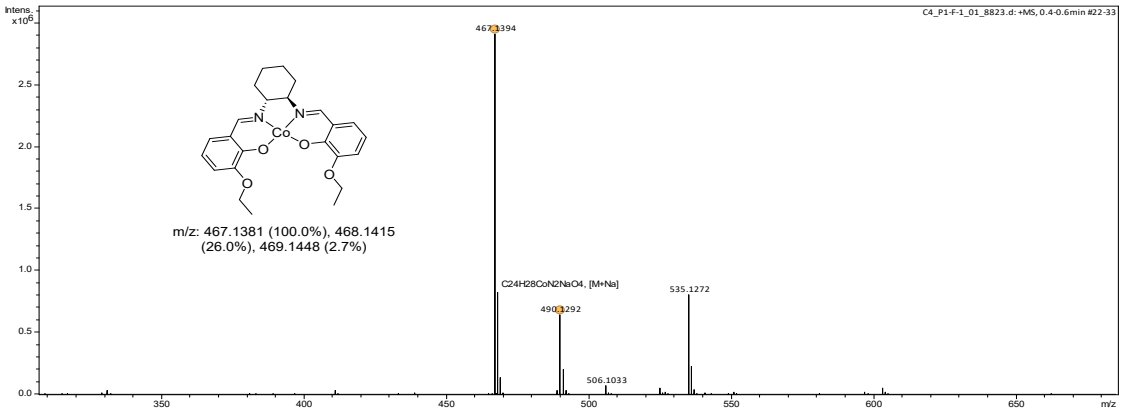

Mass spectra (ESI) of compound **4a**

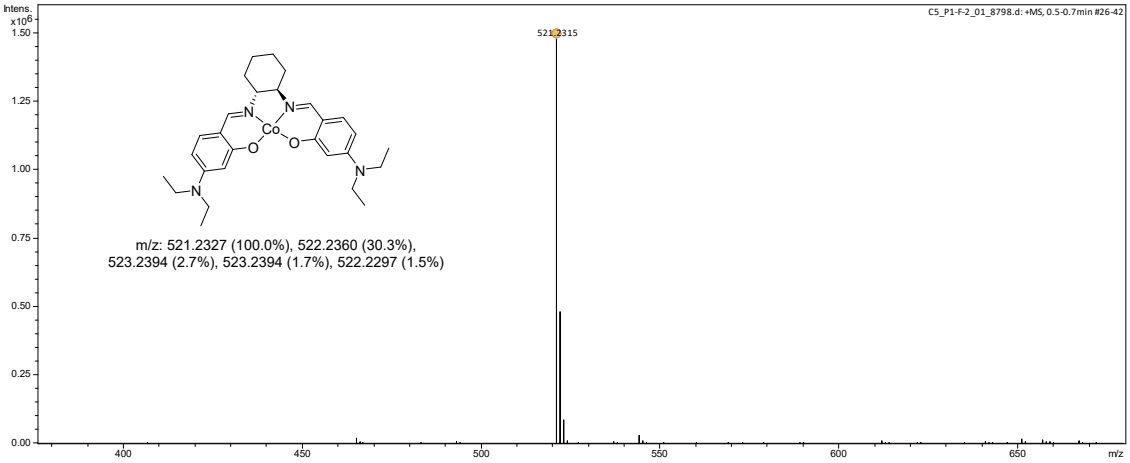

Mass spectra (ESI) of compound **4b**

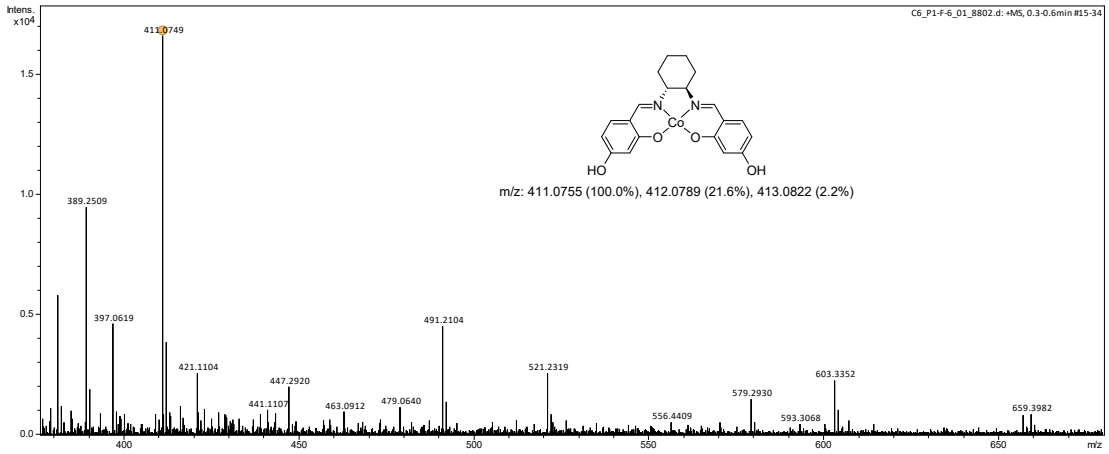

Mass spectra (ESI) of compound **4c**

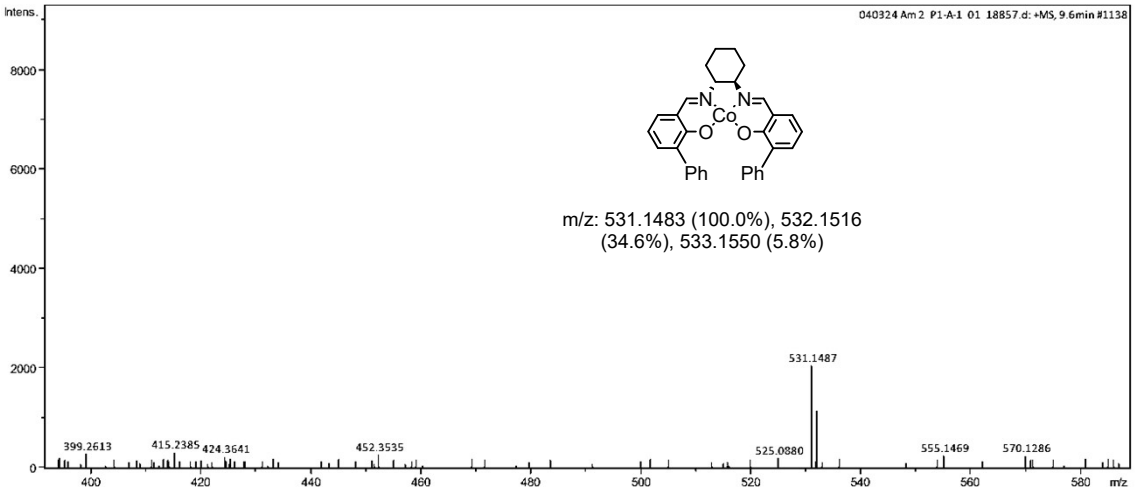

Mass spectra (ESI) of compound **4d**

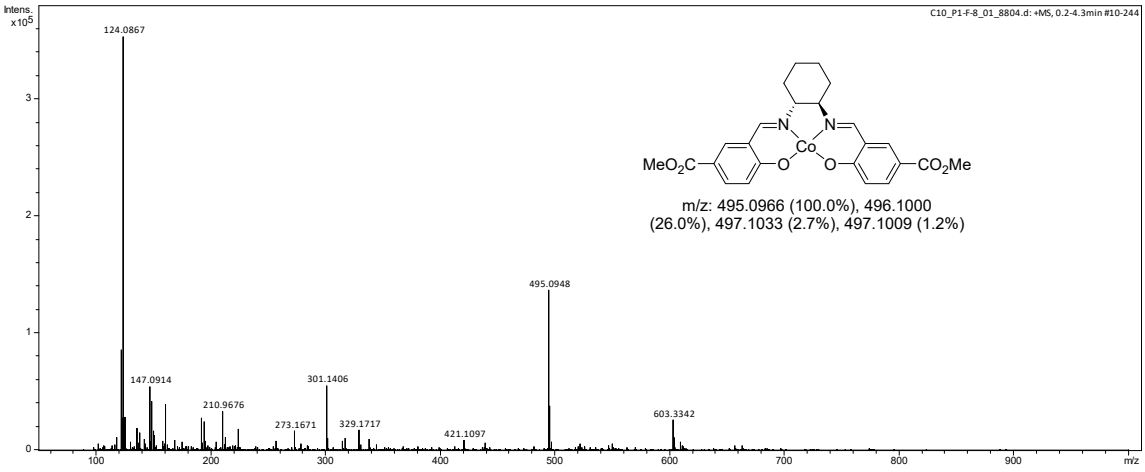

Mass spectra (ESI) of compound **4f**

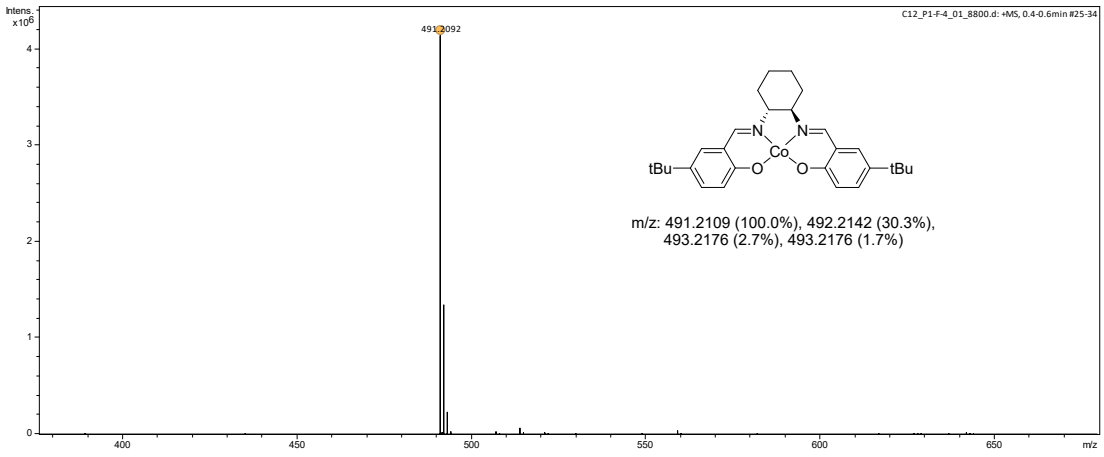

Mass spectra (ESI) of compound **4g**

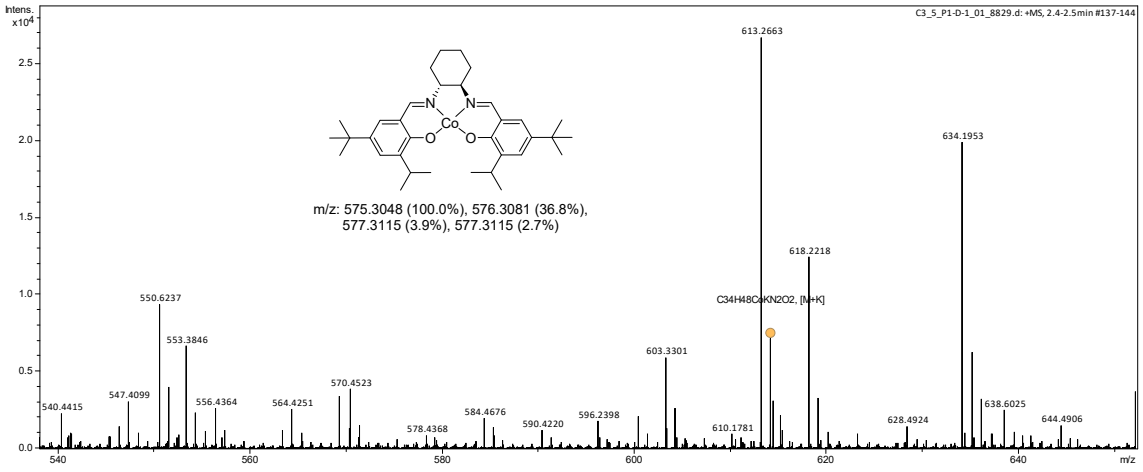

Mass spectra (ESI) of compound **4h**

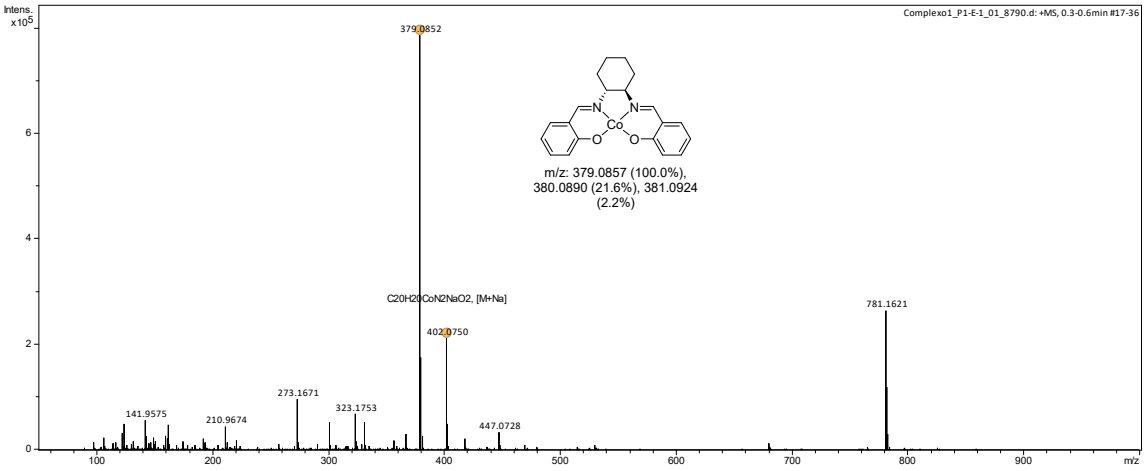

Mass spectra (ESI) of compound **4i**

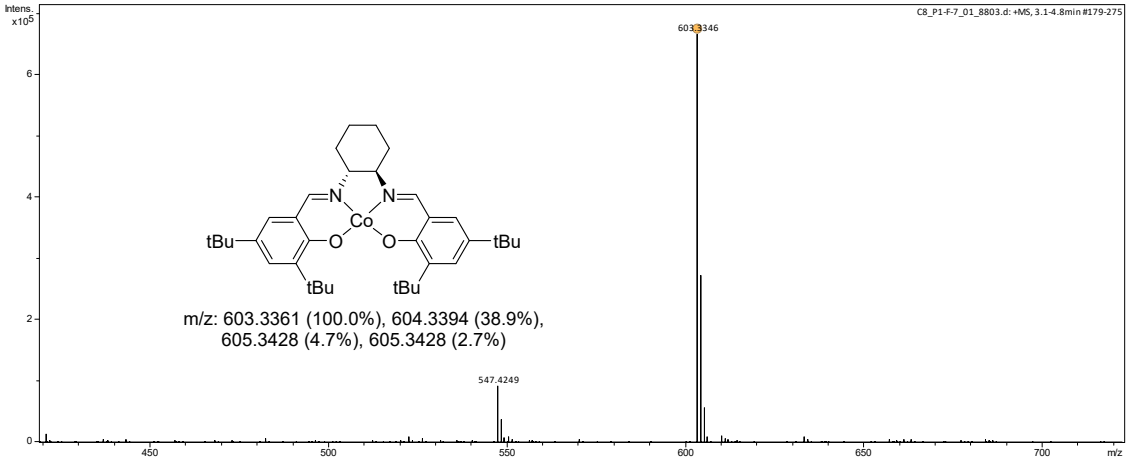

Mass spectra (ESI) of compound **4j**

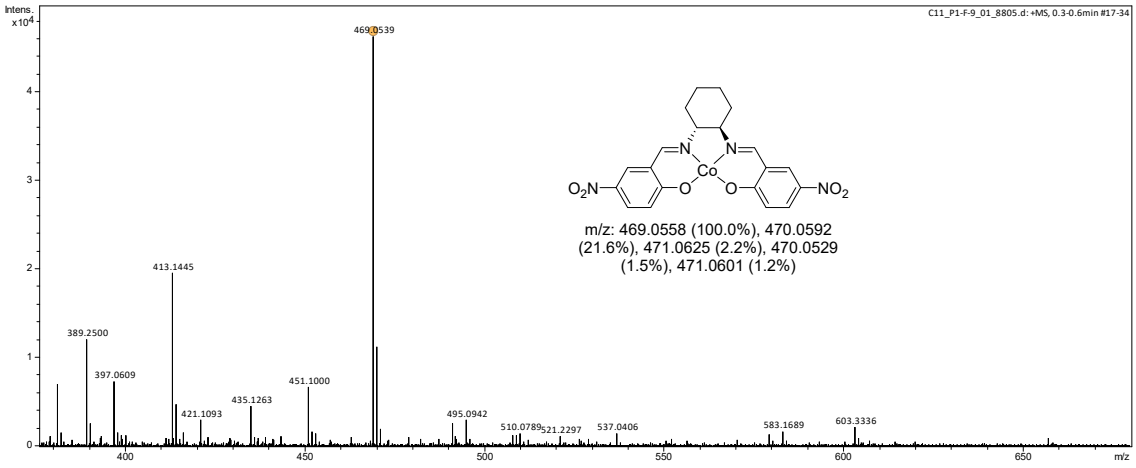

Mass spectra (ESI) of compound **4k**

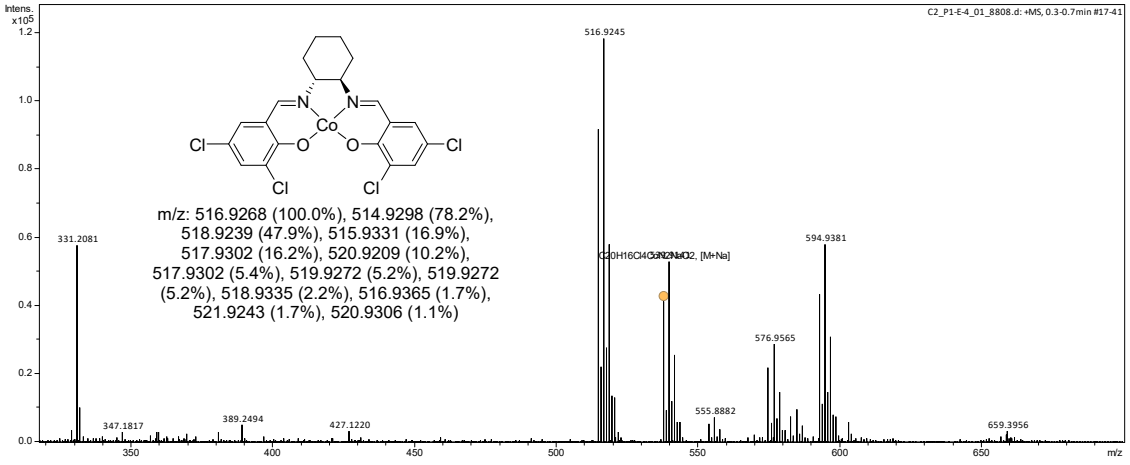

Mass spectra (ESI) of compound **4l**

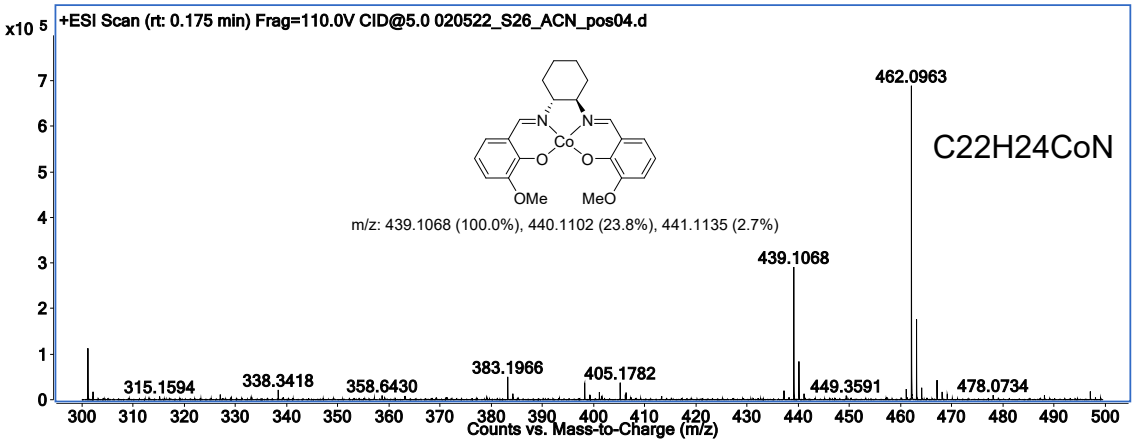

Mass spectra (ESI) of compound **4m**

S12. Infrared spectra

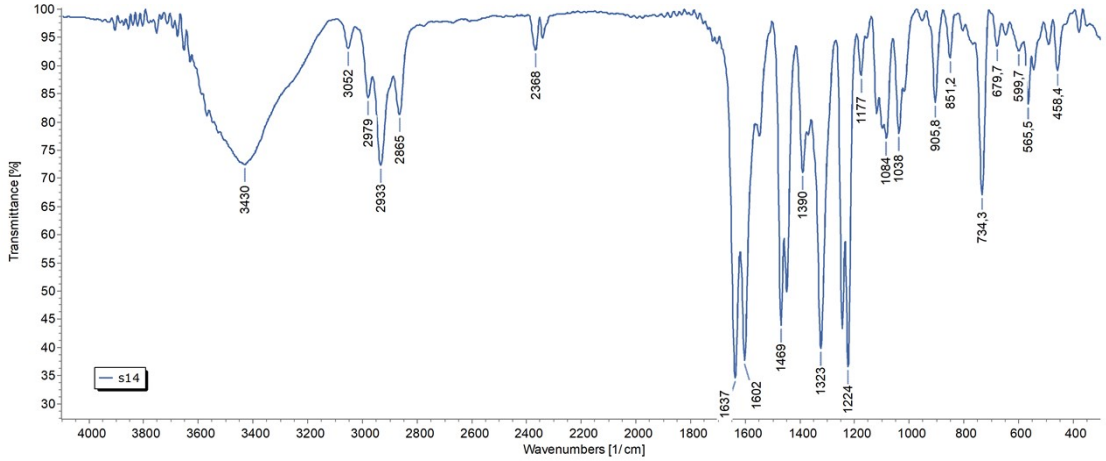

Infrared spectra of compound **4a**

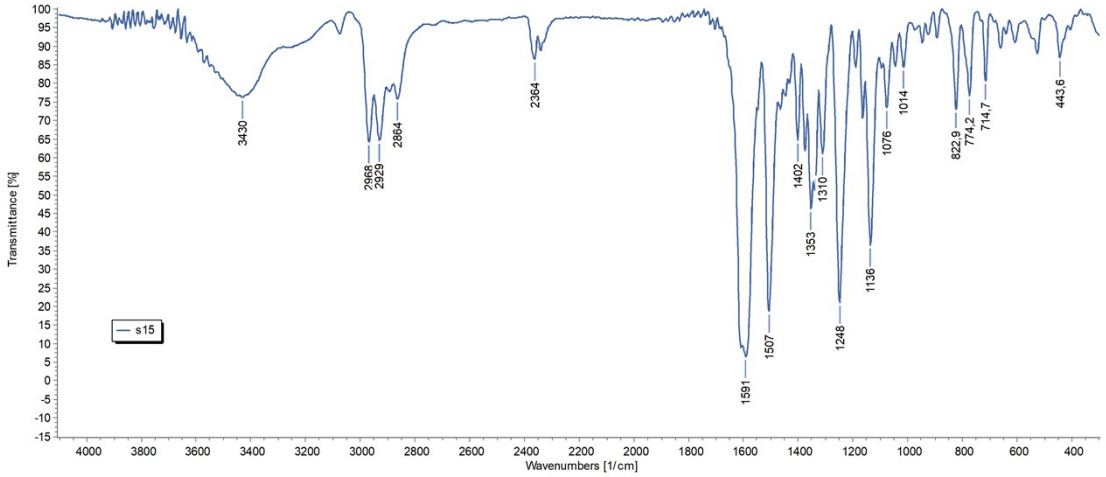

Infrared spectra of compound **4b**

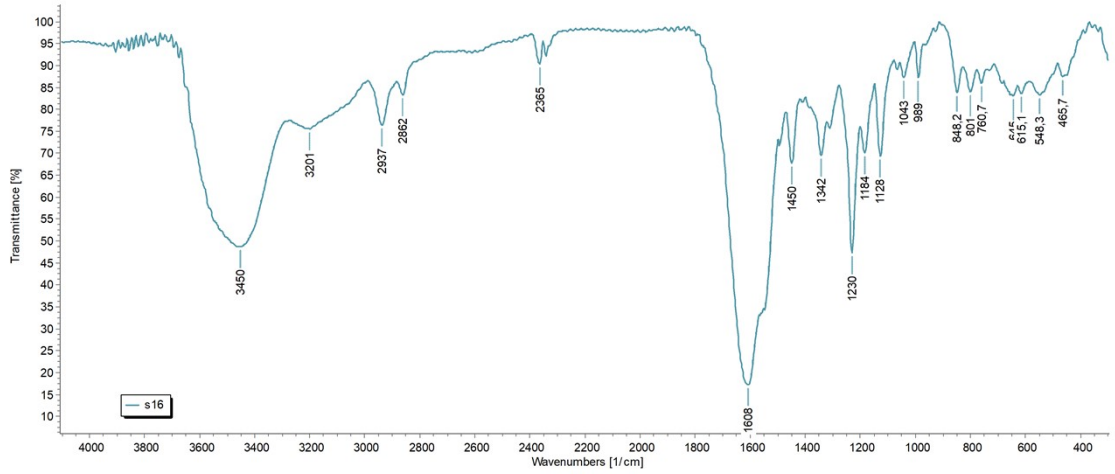

Infrared spectra of compound **4c**

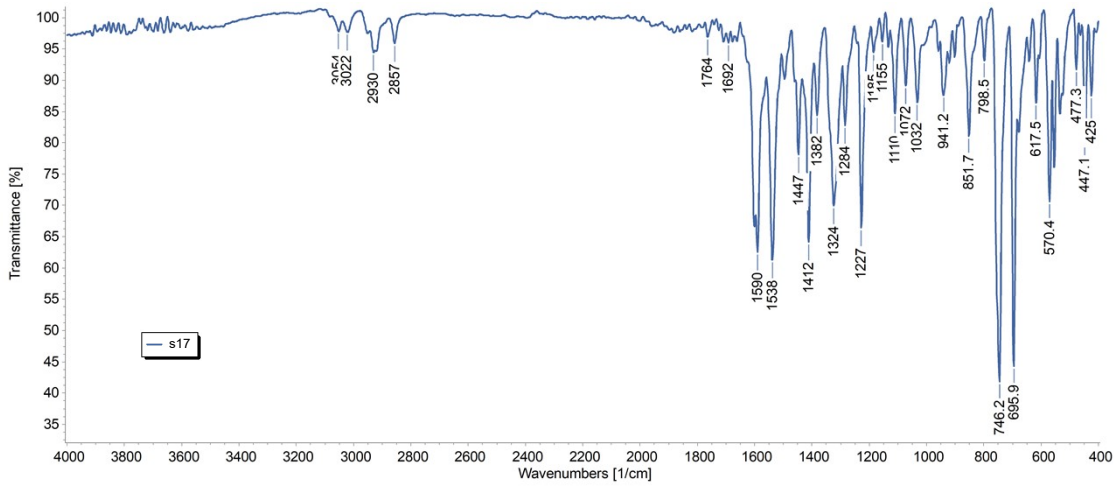

Infrared spectra of compound **4d**

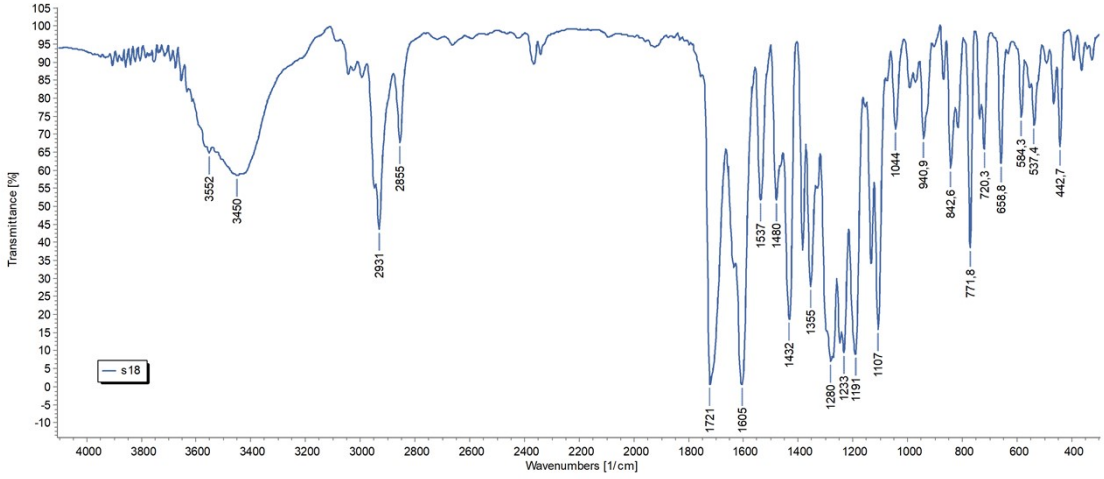

Infrared spectra of compound **4e**

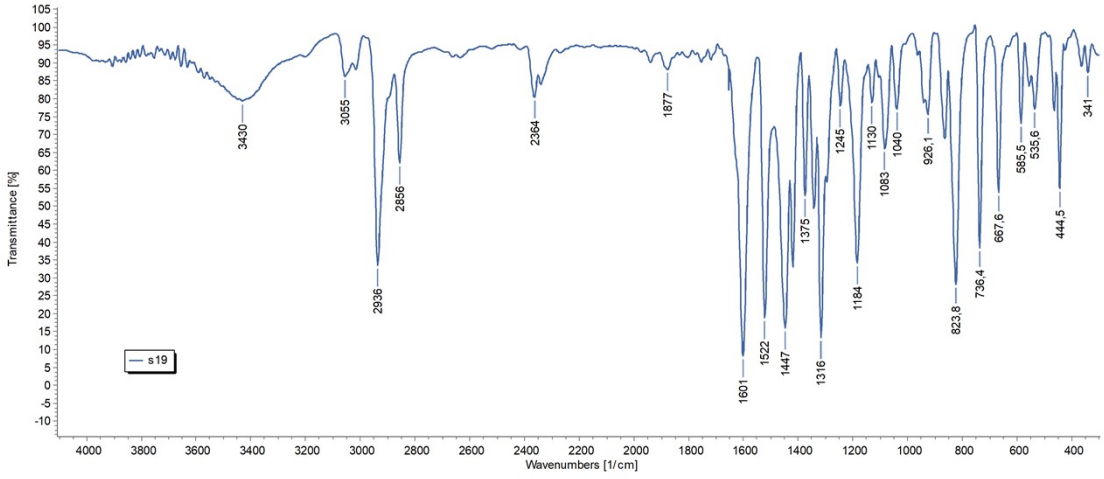

Infrared spectra of compound **4f**

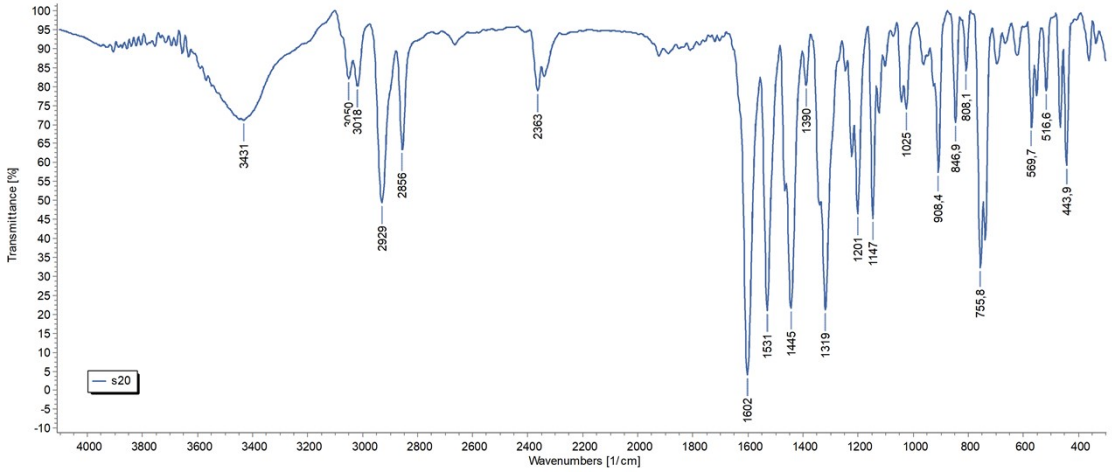

Infrared spectra of compound **4g**

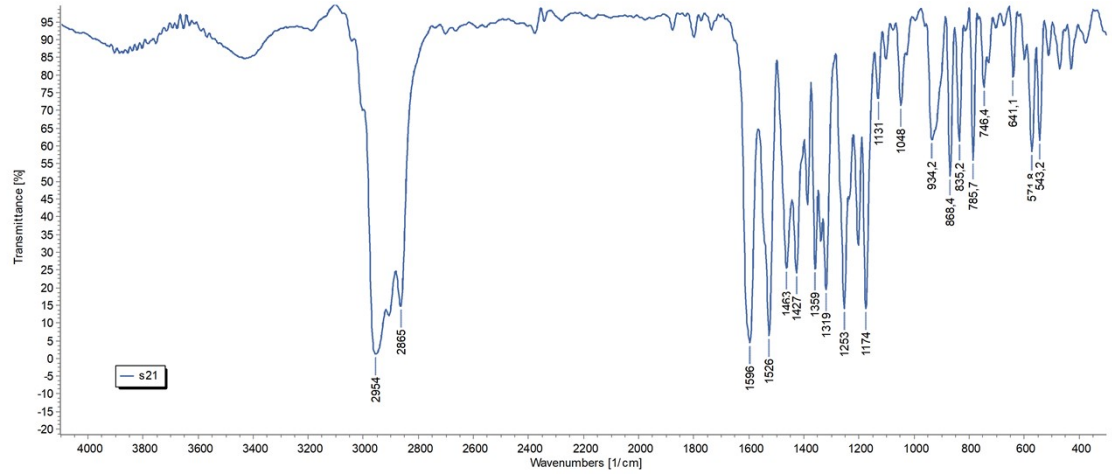

Infrared spectra of compound **4h**

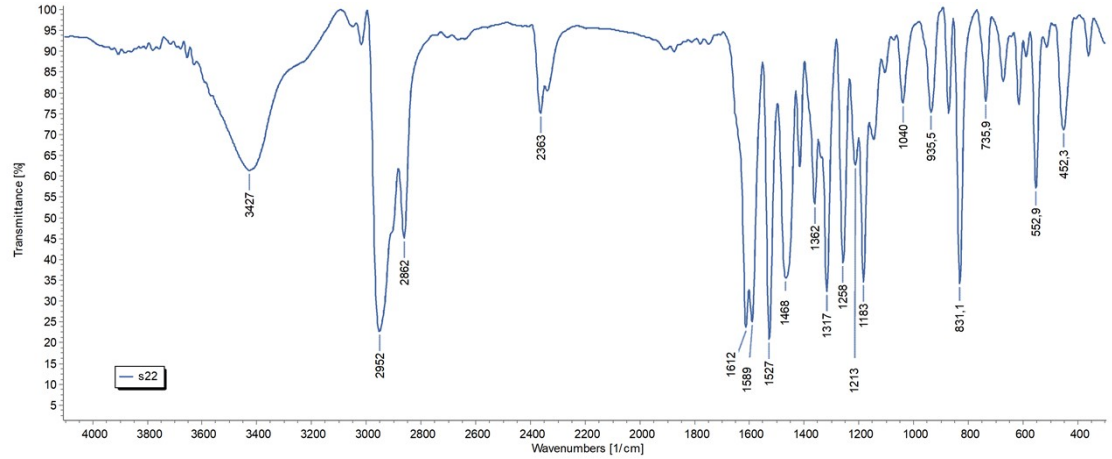

Infrared spectra of compound **4i**

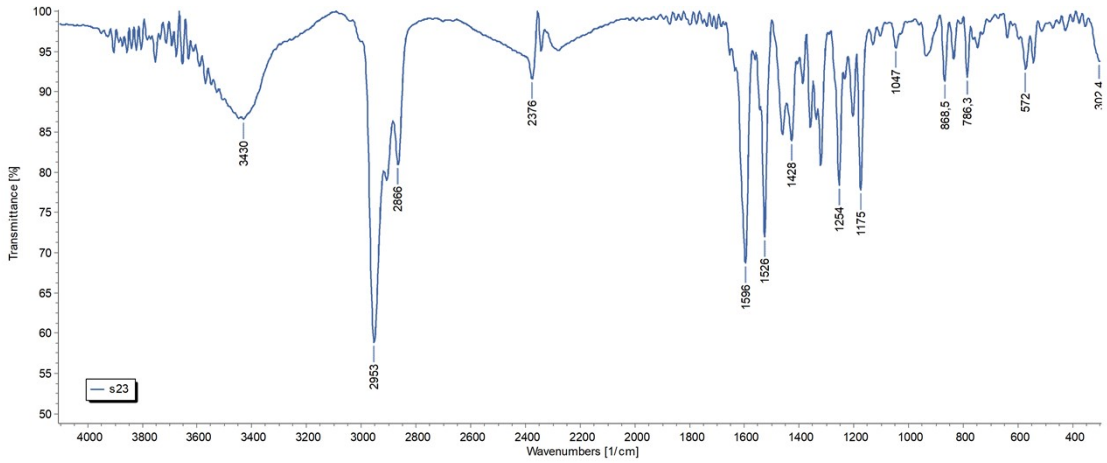

Infrared spectra of compound **4j**

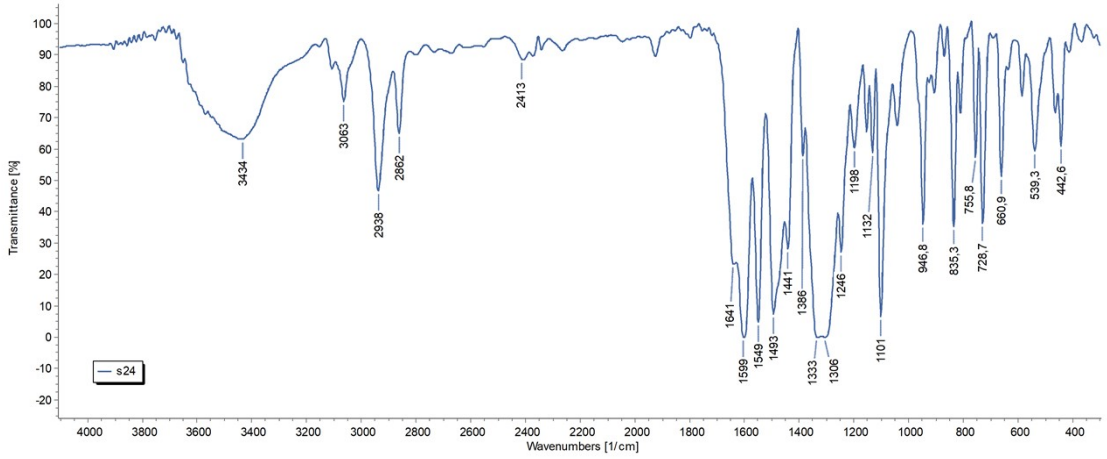

Infrared spectra of compound **4k**

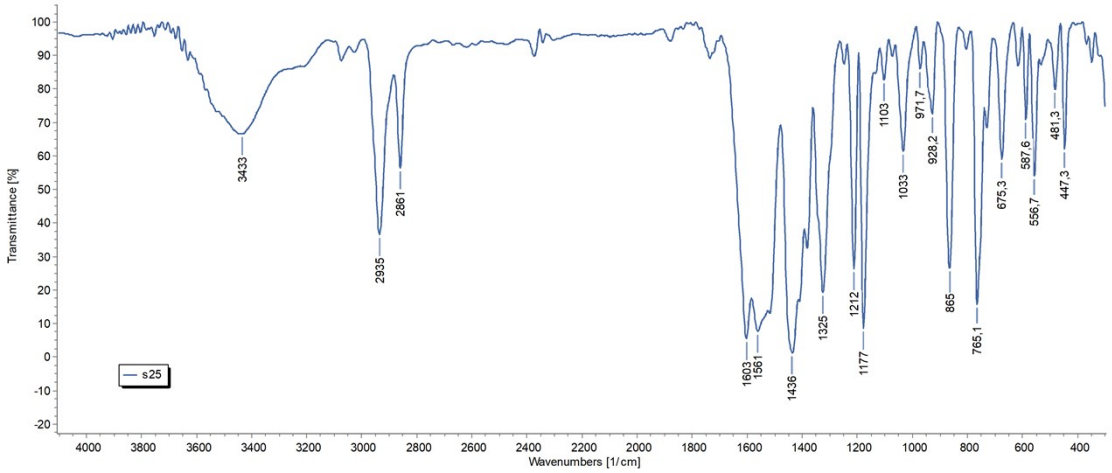

Infrared spectra of compound **4l**

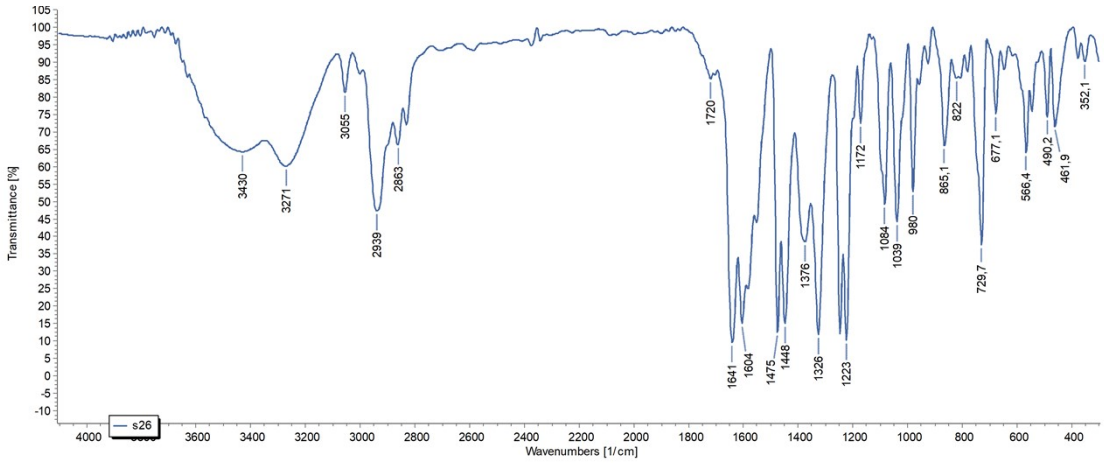

Infrared spectra of compound **4m**

S13. REFERENCES

[1]Biannic, B.; Bozell, J. J. Efficient Cobalt-Catalyzed oxidative conversion of lignin models to benzoquinones. *Organic Letters* **2013**, *15* (11), 2730–2733. https://doi.org/10.1021/ol401065r.

[2] Ting, C. P.; Tschanen, E.; Jang, E.; Maimone, T. J. Total synthesis of podophyllotoxin and select analog designs via C–H activation. *Tetrahedron* **2019**, *75* (24), 3299–3308. https://doi.org/10.1016/j.tet.2019.04.052.

[3] Biannic, B.; Bozell, J. J.; Elder, T. Steric effects in the design of Co-Schiff base complexes for the catalytic oxidation of lignin models to para-benzoquinones. *Green Chemistry* **2014**, *16* (7), 3635–3642. https://doi.org/10.1039/c4gc00709c.

[4] a) MacroModel, version 9.9, Schrödinger, LLC, New York, NY, 2012; b) N. G. J. Richards, W. C. Guida, R. Liskamp, M. Lipton, C. Caufield, G. Chang, T. Hendrickson, W. C. Still, *J. Comput. Chem.*, 1990, **11**, 440-467.

[5] Gaussian 16, Revisão B.01, Frisch, M. J.; Trucks, G. W.; Schlegel, H. B.; Scuseria, G. E.; Robb, M. A.; Cheeseman, J. R.; Scalmani, G.; Barone, V.; Petersson, G. A.; Nakatsuji, H.; Li, X.; Caricato, M.; Marenich, A. V.; Bloino, J.; Janesko, B. G.; Gomperts, R.; Mennucci, B.; Hratchian, H. P.; Ortiz, J. V.; Izmaylov, A. F.; Sonnenberg, J. L.; Williams-Young, D.; Ding, F.; Lipparini, F.; Egidi, F.; Goings, J.; Peng, B.; Petrone, A.; Henderson, T.; Ranasinghe, D.; Zakrzewski, V. G.; Gao, J.; Rega, N.; Zheng, G.; Liang, W.; Hada, M.; Ehara, M.; Toyota, K.; Fukuda, R.; Hasegawa, J.; Ishida, M.; Nakajima, T.; Honda, Y.; Kitao, O.; Nakai, H.; Vreven,

T.; Throssell, K.; Montgomery, J. A., Jr.; Peralta, J. E.; Ogliaro, F.; Bearpark, M. J.; Heyd, J. J.; Brothers, E. N.; Kudin, K. N.; Staroverov, V. N.; Keith, T. A.; Kobayashi, R.; Normand, J.; Raghavachari, K.; Rendell, A. P.; Burant, J. C.; Iyengar, S. S.; Tomasi, J.; Cossi, M.; Millam, J. M.; Klene, M.; Adamo, C.; Cammi, R.; Ochterski, J. W.; Martin, R. L.; Morokuma, K.; Farkas, O.; Foresman, J. B.; Fox, D. J. Gaussian, Inc., Wallingford CT, **2016**.

[6] Glendening, E. D.; Landis, C. R.; Weinhold, F. NBO 6.0: Natural bond orbital analysis program. *J. Comp. Chem.* **2013**, *34*, 1429.

[7] (a) Zhao, Y.; Truhlar, D. G. *Theor. Chem. Acc.* **2008**, *120*, 215. (b) Weigend, F.; Ahlrichs, R. *Phys. Chem. Chem. Phys.* **2005**, *7*, 3297.

[8] Brethomé, A. V.; Fletcher, S. P.; Paton, R. S. *ACS Catal.* **2019**, *9*, 2313.

[9] Kariofillis, S. K.; Jiang, S.; Zuranski, A. M.; Gandhi, S. S.; Alvarado, J. I. M.; Doyle, A. G. *J. Am. Chem. Soc.* **2022**, *2*, 1045.

[10] Jorner, K. MORFEUS: Molecular Features for Machine Learning, 2022.

[11] Luo, J.; Xue Z. Q.; Liu W. M.; Wu J. L.; Yang Z. Q. *J. Phys. Chem. A*. **2006**, *43*, 12005.

[12] Dotson, J. J.; Anslyn, E. V.; Sigman, M. S. *J. Am. Chem. Soc.* **2021**, *45*, 19187.

[13] Cedeno, D.; Bozell, J. J. Catalytic oxidation of para-substituted phenols with cobalt–Schiff base complexes/O2—selective conversion of syringyl and guaiacyl lignin models to benzoquinones. *Tetrahedron Letters*, **2012**, *53*, 2380.

[14] Aitken, H. R. M.; Furkert, D. P.; Hubert, J. G.; Wood, J. M.; Brimble, M. A. Enantioselective access to benzannulated spiroketals using a chiral sulfoxide auxiliary. *Org. Biomol. Chem.* **2013**, *11*, 5147.

[15] Rosevear, J.; & Wilshire, J. F. K. Preparation of some 2-(2'H-Benzotriazol-2'-yl) phenol ultraviolet absorbers: application of the transalkylation reaction. *Australian journal of chemistry*, **1985**, *38*, 1163.

[16] Rueda-Becerril, M.; Mahé, O.; Drouin, M.; Majewski, M. B.; West, J. G.; Wolf, M. O.; Sammis, G. M.; Paquin, J.-F. Direct C–F Bond Formation Using Photoredox Catalysis. *J. Am. Chem. Soc.* **2014**, *136*, 2637.

[17] Sun, M.; Xu, T.; Gao, W.; Liu, Y.; Wu, Q.; Mu, Y.; & Ye, L. Large ultra-high molecular weight polyethylene spherical particles produced by AlR 3 activated half-sandwich chromium (iii) catalysts. *Dalton Transactions*, **2011**, *40*, 10184.

[18] Sinitskii, A. S.; Abramova, V. V.; & Tretyakov, Y. D. Structural and optical properties of titania photonic crystal films prepared by a sol-gel method. *Mendeleev Communications*, **2007**, *17*, 1.

[19] Morandi, B.; Mariampillai, B.; & Carreira, E. M. Enantioselective Cobalt-Catalyzed Preparation of Trifluoromethyl-Substituted Cyclopropanes. *Angewandte Chemie International Edition*, **2011**, *50*, 1101.

[20] Hariharan, P. S.; & Anthony, S. P. Substitutional group dependent colori/fluorimetric sensing of Mn2+, Fe3+ and Zn2+ ions by simple Schiff base chemosensor. *Spectrochimica Acta Part A: Molecular and Biomolecular Spectroscopy*, **2015**, *136*, 1658.

[21] Nishioka, K.; Goto, H.; Sugimoto, H. Dual Catalyst System for Asymmetric Alternating Copolymerization of Carbon Dioxide and Cyclohexene Oxide with Chiral Aluminum Complexes: Lewis Base as Catalyst Activator and Lewis Acid as Monomer Activator *Macromolecules* **2012**, *45*, 8172.

[22] Yao, X.; Qiu, M.; Lü, W.; Chen, H.; Zheng, Z. Substituted salen–Ru (II) complexes as catalysts in the asymmetric cyclopropanation of styrene by ethyl diazoacetate: the influence of substituents and achiral additives on activity and enantioselectivity. *Tetrahedron: Asymmetry*, **2001**, *12*(2), 197-204.

[23] Zhang, G.; Constable, E. C.; Housecroft, C. E.; & Zampese, J. A. Assembling chiral salan–copper (II) complexes into a 2D-network with carboxylic acid functionalization. *Inorganic chemistry communications*, **2014**, *43*, 51-55.

[24] China. Yang, W.; Yang, Z.; She, M.; Liu, R.; Zhang, X.; Wang, H.; Ren, C.; Xihua University. *Diastereoselective synthesis of 1-aryl-1H-pyrido[3,4-b]indole derivatives.* **CN107417685A**, Dec 1, 2017.

[25] Awwadi, F. F.; Aldokh, M. K. M.; Alwahsh, M. I.; Hodali, H. A. Chirality and thermal stability of four salen complexes: Crystallographic, theoretical and TGA studies. *Polyhedron* **2023**, *244*, 116623. https://doi.org/10.1016/j.poly.2023.116623.

[26] Kwiatkowski, P.; Wojaczyńska, E.; Jurczak, J. (Salen)Co(II) complex—an efficient catalyst for the high-pressure Friedel–Crafts reaction of 2-methylfuran with alkyl glyoxylates. *Tetrahedron Asymmetry* **2003**, *14* (23), 3643–3645. https://doi.org/10.1016/j.tetasy.2003.08.012.

[27] Li, H.; Xi, D.; Niu, Y.; Wang, C.; Xu, F.; Liang, L.; Xu, P. Design, synthesis and biological evaluation of cobalt(II)-Schiff base complexes as ATP-noncompetitive MEK1 inhibitors. *Journal of Inorganic Biochemistry* **2019**, *195*, 174–181. https://doi.org/10.1016/j.jinorgbio.2019.03.022.

[28] Li, P.-T.; Mou, Q.; Yu, W. Regioselective 1,4-Hydroamination of 1,3-Dienes by Photoredox/Cobalt dual catalysis. *Organic Letters* **2025**.

https://doi.org/10.1021/acs.orglett.5c00281.

[29] Jacobsen, E. N.; Kakiuchi, F.; Konsler, R. G.; Larrow, J. F.; Tokunaga, M. Enantioselective catalytic ring opening of epoxides with carboxylic acids. *Tetrahedron Letters* **1997**, *38* (5), 773–776. https://doi.org/10.1016/s0040-4039(96)02414-8.

[30] Sun, W.; Xia, C.-G.; Zhao, P.-Q. Asymmetric borohydride reduction of aromatic ketones catalyzed by chiral salen–Co(II) complexes. *Journal of Molecular Catalysis a Chemical* **2002**, *184* (1–2), 51–55. https://doi.org/10.1016/s1381-1169(02)00035-3.

[31] Takeichi, T.; Arihara, M.; Ishimori, M.; Ttsuruta, T. Asymmetric cyclizations of some chlorohydrins catalyzed by optically active cobalt (salen) type complexes. *Tetrahedron* **1980**, *36* (23), 3391–3398. https://doi.org/10.1016/0040-4020(80)80189-x.

[32] Vlaminck, L.; Lingier, S.; Hufendiek, A.; Du Prez, F. E. Lignin inspired phenolic polyethers synthesized via ADMET: Systematic structure-property investigation. *European Polymer Journal* **2017**, *95*, 503–513. https://doi.org/10.1016/j.eurpolymj.2017.08.042.

[33] Yang, B.; Dong, K.; Li, X.-S.; Wu, L.-Z.; Liu, Q. Photoacid-Enabled Synthesis of Indanes via Formal [3 + 2] Cycloaddition of Benzyl Alcohols with Olefins. *Organic Letters* **2022**, *24* (10), 2040–2044. https://doi.org/10.1021/acs.orglett.2c00566.